ABSTRACT

Title of Dissertation: INTERACTIONS BETWEEN NITROGEN AND TEMPERATURE ON THE METABOLISM OF THE RED-TIDE MIXOTROPHIC DINOFLAGELLATE *KARENIA* SPP. IN SUPPORT OF PREDICTIVE MODELS: IMPLICATIONS FOR BLOOM DYNAMICS ON THE WEST FLORIDA SHELF

So Hyun (Sophia) Ahn,
Doctor of Philosophy, 2023

Dissertation directed by: Professor Patricia M. Glibert,
Marine Estuarine Environment Sciences

The toxic mixotrophic dinoflagellate *Karenia* spp. forms blooms almost annually in the Gulf of Mexico, especially on the West Florida Shelf (WFS). Blooms typically initiate in early fall but can persist from months to years. Daily, *Karenia* vertically migrates to the surface water during the day, possibly experiencing changes in temperature, light, nitrogen (N), and prey type and availability. Therefore, this dissertation aimed to examine the interplay between *Karenia*'s photo-autotrophic and phago-mixotrophic metabolism and the short-term fluctuations in environmental conditions to understand how these factors may relate to the conditions under which *Karenia* spp. are found in the WFS.

A culture of *K. mikimotoi* balanced photon flux pressure (light availability) with consumption in overall metabolism when pulsed with $^{15}N\text{-}NO_3^-$, $^{15}N\text{-}NH_4^+$, or ^{15}N-urea over the range of 15-25°C as shown by photosynthetic fluorescence. However, when shifted to 30°C, cells were significantly stressed, but urea-enriched cells showed a smaller decline in fluorescence, implying that urea might induce a photoprotective mechanism by increasing metabolic "pull." Studies conducted with natural *K. brevis* winter and summer populations during 2021 showed that thermal history played a critical role. Unusually, summer blooms had higher biomass but were stressed photosynthetically and nutritionally. However, ^{15}N-urea enriched summer cells had higher uptake rates as well as carbon (C) and N cell^{-1}, especially in warmer waters, showing differential thermal responses based on N forms.

Mixotrophy grazing measurements showed that *K. brevis* grazed both the picoplankter *Synechococcus* as well as the cryptophyte *Rhodomonas*. Grazing did not selectively target specific qualities of *Synechococcus* (based on differing N and P of the prey growth media), but ingestion rates were a function of prey-to-grazer ratios (R^2=0.76) as well as prey amounts (R^2=0.71). NanoSIMS confirmed ^{15}N incorporation from *Synechococcus* in *K. brevis*. In natural communities of *K. brevis*, ingestion rates were also significantly related to prey-to-grazer ratios ($p < 0.01$) and by temperatures ($p < 0.05$) to a lesser degree (R^2= 0.75) when incubated at ambient (24°C) and ambient temperature ± 5°C (19, 29°C). The grazer effects on the photosynthetic performance of grazer and prey were also examined. Grazing on *Synechococcus* indirectly reduce the photosynthetic performance of prey, especially at warmer temperatures but had little or no effect on the photosynthesis of *K. brevis* itself.

INTERACTIONS BETWEEN NITROGEN AND TEMPERATURE ON THE METABOLISM OF THE RED-TIDE MIXOTROPHIC DINOFLAGELLATE *KARENIA* SPP. IN SUPPORT OF PREDICTIVE MODELS: IMPLICATIONS FOR BLOOM DYNAMICS ON THE WEST FLORIDA SHELF

by

So Hyun Ahn

Dissertation submitted to the Faculty of the Graduate School of the
University of Maryland, College Park, in partial fulfillment
of the requirements for the degree of
Doctor of Philosophy
2023

Advisory Committee:
Professor Patricia M. Glibert, Chair
Dr. Cynthia Heil
Professor Diane Stoecker
Professor Ming Li
Associate Professor Yantao Li
Dean's Representative: Professor Sujay Kaushal

Acknowledgements

Without the help of everyone, I wouldn't be here. Thanks to Dr. Patricia M. Glibert, Dr. Cynthia Heil, Dr. Diane Stoecker, Dr. Ming Li, Dr. Yantao Li, Dr. Sujay Kaushal, Dr. Todd M. Kana, Dr. Chih-Hsien (Michelle) Lin, Dr. Samantha Gleich, Bruna Sobrinho, Dr. Nayani Vidyarathna, Dr. Tristyn Bercel, Sarah Klass, Chloe Manley, Amanda Muni-Morgan, Dr. Joaquín Martínez-Martínez, Dr. Anne Booker, Dr. Fei Cong, Dr. Shady Amin, Dr. Xavier Mayali, Dr. Mengmeng Tong, Dr. Stacie Flood, Dr. Sairah Malkin, Dr. Greg Silsbe, Dr. Fan Zhang, Dr. Jacob Cram & Pongo, Carin Starr, Pinky Liau, Dr. Lexy McCarty, Dr. Carol Kim, Yijun Guo, Dr. Wenfei Ni, Dr. Sang Lee, Dr. Jinwoo Ahn, Hyunjoo Shin, Taejun Ahn, Sylvia Kim, Yewon Kim, and Dr. Sueyoul Kim. Without them, my life would have been more challenging. I especially appreciate the time and effort of Dr. Glibert and also of my committee members, Dr. Heil, Dr. Stoecker, Dr. Ming Li, and Dr. Yantao Li.

I would like to thank to my funding sources: Explorers Club Washington group's exploration and field research grant, Ryan Saba Memorial student fellowship from Horn Point Laboratory (as well as Ellen and Kevin), Izaak Walton League of America scholarship, Paul C. Silva student grant from International Phycological Society, registration fee award for 19th International Conference on Harmful Algae (ICHA) from NOAA's National Centers for Coastal Ocean Science (NCCOS), student travel award for Joint Aquatic Science meeting from Association for the Sciences of Limnology and Oceanography, student travel award for 20th ICHA from NCCOS and Horn Point Laboratory travel awards and fellowship for 2 years. I also thank NOAA

grant NA19NOS4780183 (to PMG) and the Horn Point Laboratory for financial support. Finally, thanks to myself and Simba Ahn to bearing with me.

Table of Contents

List of Tables

List of Figures

Chapter 1: Introduction

The genus *Karenia* is a globally distributed bloom-forming dinoflagellate. Within this genus, *K. brevis* and *K. mikimotoi*, especially *K. brevis*, stand out as the predominant toxic species along the West Florida Shelf (WFS) and the broader expanse of the Gulf of Mexico. *Karenia* spp., which typically initiates blooms in late summer to early fall, is a slow-growing (~ 0.3 day^{-1}) mixotrophic dinoflagellate but can become dominant in Florida's water and persist for periods ranging from months to years (Brand et al., 2012; Heil et al., 2022). While physical mechanisms play important roles in large bloom initiation and expansion (Li et al., 2019), this eurythermal, euryhaline, wide light-tolerant taxon is capable of utilizing a broad spectrum of inorganic and organic nutrients, as well as ingesting prey (Glibert et al., 2009; Heil et al., 2014a; Huang et al., 2020), potentially contributing to its bloom development and maintenance. Nevertheless, many questions regarding the interplay between *Karenia*'s photoautotrophic and mixotrophic metabolism and the fluctuations in environmental conditions remain unanswered. Therefore, this dissertation aims to 1) Examine photosynthesis-irradiance responses and nutrient uptake rates of *Karenia* spp. to different forms and amounts of nutrients, especially nitrogen (N), and temperatures in laboratory and field experiments, and (2) Investigate if the prey quantity and nutritional quality could affect grazing and photo-physiological responses of *K. brevis*, under different temperatures in laboratory and field experiments to understand how these factors may relate to the conditions under

which *Karenia* spp. are found in the WFS. Given that the WFS is historically N-limited due to influence by phosphorous (P)-mining, overall studies focused on effects of N rather than P enrichment.

Typically, blooms of *K. brevis*–often mixed with *K. mikimotoi*–are initiated during the late summer to early fall (July to November), with the most frequent initiation in September in the WFS (Heil et al., 2022). These blooms tend to overwinter in typical years and are most likely to terminate in April, primarily due to physical factors. While natural populations of *K. brevis* (7-33°C) and *K. mikimotoi* (4-31°C) have been found across a wide temperature range, their optimal thermal range was narrower (e.g., 22-28°C) (Brand et al., 2012). Consequently, hot water temperatures (> 30°C) are considered significant barriers preventing robust blooms during the summer months (Magaña and Villareal, 2006; Vargo, 2009; Brand et al., 2012). However, in specific years such as 2005, 2018, and 2020, *Karenia* blooms have thrived extensively during these hot summer months leading to blooms of very long duration (Heil et al., 2022). Furthermore, daily, cells are likely to be exposed to thermal fluctuations of several degrees due to daylight surface aggregation behavior. These thermal fluctuations could be even more pronounced if cells vertically migrate (Heil et al., 2014b). This raises questions about how cells overcome and handle the thermal stress in both the short and long term.

Multiple nutrient sources (>12) have been identified to support *K. brevis* blooms on the WFS, including water column nitrification, estuarine flux, and mixotrophic consumption of prey (Heil et al. 2014a). The importance of each source differs depending on timing and location, and regenerated nutrient sources, such as

ammonium (NH_4^+), become increasingly important in supporting blooms in coastal and offshore environments (Heil et al., 2014a). Various chemical forms of nutrients, such as NH_4^+, nitrate (NO_3^-), urea, and amino acids, can be utilized by *Karenia* spp., but they prefer regenerated forms of N, such as NH_4^+ and urea (Heil et al., 2014a; Killberg-Thoreson et al., 2014; Bronk et al., 2014, Huang et al., 2020). In general, rising temperatures could increase enzyme activities related to N metabolism until the tolerance threshold (Ras et al., 2013; Shen et al., 2016; Kana et al., 1997). However, the key enzymes related to different forms of N could have differential thermal optimal ranges, regulating uptake rates of N, and consequently photosynthesis, influencing dynamics of *Karenia* spp. to different temperatures (Lomas and Glibert, 1999a; Glibert et al., 2016). Taken together, interactions of *Karenia* spp. between light, N forms, and temperature need to be better resolved to understand seasonal bloom dynamics and short-term effects on blooms on the WFS.

The common *Karenia* species, *K. brevis* and *K. mikimotoi*, are both dominant bloom-forming species in the WFS, exhibiting both photo-autrophy and phago-heterotrophy, i.e., mixotrophy, while the less common species, *K. bicuneiformis, K. papilionacea,* and *K. selliformis* appear to lack mixotrophic ability (Ok et al., 2023). Jeong et al. (2005) discovered that cultured *K. brevis* could graze on pico-cyanobacteria *Synechococcus* sp., and Glibert et al. (2009) confirmed higher grazing rates by cultured *K. brevis* with increasing *Synechococcus* amounts. In addition, enhanced growth rates under mixotrophic conditions in this species were shown (under low light conditions) (Glibert et al., 2009). Zhang et al. (2011; 2013) reported that cultured *K. mikimotoi* could ingest *Marinobacter* sp., fluorescent microspheres

(0.5 and 2μm), *Isochrysis galbana*, and *Hemiselmis virescens.* The presence of prey also increased growth rates in *K. mikimotoi*, implying that mixotrophy is a potentially significant nutrient source for *Karenia* spp. It is likely that *Karenia* spp., especially *K. brevis*, prefer small prey such as picocyanobacteria but may have a broader prey spectrum that has not yet been tested. Furthermore, grazing experiments with natural populations of *Karenia* spp. from the WFS have not been conducted. Therefore, this dissertation aimed to identify the grazing capacity of natural populations.

Mixotrophs may benefit from phagotrophy to supplement dissolved nutrients and/or carbon where their availability is limited (Stoecker et al., 2017). Specific nutrient deficiency can trigger mixotrophic grazing, while imbalances in nutrient ratios may lead mixotrophs to exhibit more heterotrophic behavior, thereby showing nutritionally controlled grazing activities as well as growth (e.g., Lundgren et al., 2016; Lin et al., 2017; Zhang et al., 2013). Lin et al. (2017) reported that low N:P *Karlodinium veneficum*, a member of the family *Kareniaceae* like the genus *Karenia*, showed the maximum grazing rates on N-rich *Rhodomonas salina* that were about 4-fold higher than those of high N:P predator feeding on N-rich prey. Additionally, Zhang et al. (2013) reported that their growth rates increased significantly when N-limited *K. mikimotoi* were fed with prey organisms. On the other hand, when *K. mikimotoi* was P-limited, no significant changes in growth were observed with prey addition, but the maximum cell density of grazers increased. While *K. brevis* may also show similar mixotrophic behavior, the role of both prey and predator's nutritional history on mixotrophy and growth remains unexplored yet.

The metabolic theory of ecology predicts higher temperature regulation in heterotrophic processes than autotrophic processes (Brown et al., 2004; Allen et al., 2005; Wilken et al., 2013). Mixotrophs can be more heterotrophic with rising temperatures (e.g., Wilken et al., 2013). Wilken et al. (2013) demonstrated a higher contribution of mixotrophic growth to photosynthesis with increasing temperature. Lin et al. (2018) reported higher grazing rates and biomass of *K. veneficum* at > 25°C, showing temperature regulation of mixotrophy. Furthermore, Lin et al. (2018) successfully applied a multi-element mechanistic model of mixotrophy under diverse N:P ratios and temperatures to experimental data of *K. veneficum*. The physiological data of both phototrophy and mixotrophy of *Karenia* spp. in a wide range of environmental factors, including temperatures and N forms and amounts, through this dissertation research, will be incorporated into an open-source physical (e.g., Regional Ocean Modeling System, ROMS) and biogeochemical model framework that stimulates water column biogeochemical cycling using a Row-Column Aesop (RCA) (Zhang et al., 2021). Such incorporation of nutritional physiology of *Karenia* spp. will improve the predictive power of a 3D-coupled model, especially on the long-term outlook of *Karenia* bloom on the WFS.

The overarching hypothesis of this dissertation research is that increasing temperature will enhance the metabolic rates (nutrient uptake, photosynthesis, mixotrophy, growth) of the dinoflagellate *Karenia* spp. and will do so to a greater extent with chemically reduced nitrogen and with heterotrophic process than autotrophic process. In particular, I hypothesize that (1) rates of N uptake and photosynthesis of *Karenia* spp. increase with rising temperature and will do so to a

greater extent with chemically reduced inorganic nitrogen, NH_4^+, and/or simple organic N, urea than with oxidized forms of N, NO_3^-; (2) Phago-mixotrophy is an important nutrient source for *K. brevis*, especially under warmer waters, and they can graze on diverse prey; (3) when inorganic nutrient supply ratio is imbalanced, rates of growth and grazing of *K. brevis* will nutritionally controlled by prey. These adaptations may allow *K. brevis* to thrive in summers when temperatures exceed their photosynthetic tolerance.

In order to address these hypotheses, (1) N uptake rates and photosynthesis-irradiance responses of cultured *K. mikimotoi* were investigated under different temperature (15, 20, 25, 30°C) and different N forms (NO_3^-, NH_4^+, urea) and amounts (1, 5, 10, 20, 50µM) in the short term (Chapter 2); (2) N uptake rates and photosynthesis-irradiance responses of natural *Karenia* spp. from winter and summer populations were determined under different temperature (15, 20, 25, 30°C or 15, 25, 30, 33°C) and different N forms (NO_3^-, NH_4^+, urea) and amounts (0-50µM) in the short term (Chapter 3 and 4); (3) Mixed culture experiments using varying proportions of *K. brevis* and several potential prey types with different nutritional quality were performed to establish rates of growth and feeding of *K. brevis* as well as associated changes in photophysiology of predator and prey (Chapter 5); (4) Grazing, growth, and photosynthetic responses by natural populations of *K. brevis* from the WFS on *Synechococcus* were examined under ambient (24°C) and ambient temperatures ± 5°C (19, 29°C) (Chapter 6). The overall conclusion and implication are presented at the end (Chapter 7).

The main chapters of the dissertation consisted of the following manuscripts:

1. Ahn, S.H., Glibert, P.M. (2022) Shining light on photosynthesis in the harmful dinoflagellate *Karenia mikimotoi*-Responses to short-term changes in temperature, nitrogen forms and availability. Phycology 2:30-44. https://doi.org/10.3390/phycology2010002 (Chapter 2).
2. Ahn, S.H. Glibert, P.M., Heil, C.A. (2022) Dynamic photo-physiological responses of the dinoflagellate *Karenia brevis* to short-term changes in temperature and nitrogen substrates. 19th International Conference on Harmful Algae, La Paz, B.C.S., Mexico. International Society for the Study of Harmful Algal Blooms. https://doi.org/10.5281/zenodo.7034896 (Chapter 3).
3. Ahn, S.H. Glibert, P.M., Heil, C.A. (2023) In hot water: Interactions of temperature, nitrogen form and availability and photosynthetic and nitrogen uptake responses in natural *Karenia brevis* populations. Harmful Algae 129:102519. https://doi.org/10.1016/j.hal.2023.102519 (Chapter 4).
4. Ahn, S.H, Glibert, P.M., Xavier, M. (2023) *Karenia brevis* grazing on *Synechococcus* and on *Rhodomonas*: Effects of food quantity and quality and photophysiological responses of predator and prey (Chapter 5).
5. Ahn, S.H. and Glibert, P.M. Temperature-dependent mixotrophy in natural populations of the toxic dinoflagellate *Karenia brevis* (Chapter 6).

Chapter 2: Shining light on photosynthesis in the harmful dinoflagellate *Karenia mikimotoi*-Responses to short-term changes in temperature, nitrogen form, and availability[1]

Abstract

Karenia mikimotoi is a toxic bloom-forming dinoflagellate that sometimes co-blooms with *Karenia brevis* in the Gulf of Mexico, especially on the West Florida Shelf where strong vertical temperature gradients and rapid changes in nitrogen (N) can be found. Here, the short-term interactions of temperature, N form, and availability on photosynthesis–irradiance responses were examined using rapid light curves and PAM fluorometry in order to understand their interactions, and how they may affect photosynthetic yields. Cultures of *K. mikimotoi* were enriched with either nitrate (NO_3^-), ammonium (NH_4^+), or urea with varying amounts (1, 5, 10, 20, 50 µM-N) and then incubated at temperatures of 15, 20, 25, 30 °C for 1 h. At 15–25 °C, fluorescence parameters (Fv/Fm, rETR) when averaged for all N treatments were comparable. Within a given light intensity, increasing all forms of N concentrations generally led to higher photosynthetic yields. Cells appeared to dynamically balance the "push" due to photon flux pressure and reductant generation, with consumption in overall metabolism ("pull" due to demand). However, at 30 °C, all fluorescence parameters declined precipitously, but differential responses were observed

[1] Ahn, S.H., Glibert, P.M. (2022) Shining light on photosynthesis in the harmful dinoflagellate *Karenia mikimotoi*–Responses to short-Term changes in temperature, nitrogen form, and availability. Phycology 2(1):30-44.

depending on N form. Cells enriched with urea at 30 °C showed a smaller decline in fluorescence parameters than cells treated with NO_3^- or NH_4^+, implying that urea might induce a photoprotective mechanism by increasing metabolic "pull".

Introduction

Karenia mikimotoi, the close relative of the harmful dinoflagellate *Karenia brevis* that forms massive annual blooms mostly in the Gulf of Mexico, is a hemolytic and cytotoxic dinoflagellate found in coastal waters around the world, including Asia (e.g., Japan, China, Korea, Hong Kong), Europe (e.g., Norway, United Kingdom, Denmark, Spain), Oceania (e.g., Australia, New Zealand), and America (e.g., United States, Chile) (Brand et al., 2012; Li et al., 2019). Several *Karenia* species co-exist and often co-bloom with *K. brevis* in the Gulf of Mexico, especially on the West Florida Shelf (Brand et al., 2012; Haywood et al., 2004). Although highly variable from year-to-year, *Karenia* spp. blooms on the West Florida Shelf commonly occur from early fall through winter and only rarely persist as substantial blooms throughout the summer (Lenes and Heil, 2010).

Temperature is an important variable in understanding the physiological success of phytoplankton taxa, but due to its effect on key enzymes and the different temperature optima of enzymes involved in photosynthesis and metabolism of different forms of nitrogen (N), temperature may have different effects on physiological status depending on growth N form. Seasonal temperature changes on the West Florida Shelf range from lows of ~15 °C in winter when *K. brevis* blooms are more common, to highs of >30 °C in mid-summer. Sharp vertical gradients in temperature may also exist. For example, Weisberg et al. (2014) reported, for the

West Florida Shelf for the month of July 2010, that temperatures changed from near 29 °C at the surface to near 17 °C near the bottom, where waters are influenced by upwelling. The near-bottom waters are also more enriched in nitrate (NO_3^-) relative to the surface waters in which regenerated forms of N (e.g., ammonium (NH_4^+) or urea), are proportionately more abundant. Even when strong upwelling is not present, strong vertical gradients in temperature may be commonly found (Weisberg and He, 2003). Any vertically migrating cells would be subject to sharp changes in temperature and possibly to co-occurring changes in N form and concentration. Here, the short-term interactions of temperature, light, and N form, and amounts were examined in *K. mikimotoi,* with an aim of understanding how these responses may relate to the fluctuating conditions, under which *K. mikimotoi* is found on West Florida Shelf.

Temperature effects on photosynthesis and N nutrition are complex, but the interactions between temperature, photosynthesis, and different N forms in phytoplankton metabolism are not well understood. The biophysical light reactions of photosynthesis are relatively temperature-insensitive, while the biochemical reactions (e.g., Calvin Cycle reactions and non-photochemical reactions in the thylakoid) are temperature sensitive leading to reduced rates of carbon (C) assimilation at low temperatures (Glibert et al., 2016). Temperature also affects enzymes associated with NO_3^- and NH_4^+ (Gao et al., 1983). The enzyme involved in NO_3^- reduction, nitrate reductase (NR), typically has an inverse relationship with temperature (generally between 12 °C and 25 °C) (Gao et al., 1983; Kristiansen, 1983; Lomas and Glibert 1999a, 1999b) while the enzymes involved in NH_4^+ assimilation, glutamine

synthetase–glutamate synthase (GS-GOGAT), are positively related to temperature across the same range (e.g., Clayton and Ahmed, 1986). The assimilation of NO_3^- would thus be expected to be higher at lower temperatures (10–15 °C), and indeed, over the temperature range 5–25 °C, NO_3^- uptake by both diatom-dominated and dinoflagellate-dominated natural communities typically show an inverse relationship with temperature, while NH_4^+ uptake typically shows a positive relationship (Lomas and Glibert 1999a, 1999b). Urease, the enzyme involved in urea metabolism, also appears to have a positive relationship with temperature for many phytoplankton taxa, and at least for one dinoflagellate, *Prorocentrum minimum*, rates of activity remain elevated up to temperatures of 50 °C (Fan et al., 2003). Taken together, the assimilation of NO_3^-, NH_4^+, and urea are regulated differently by temperature, a factor that can influence phytoplankton dynamics in an environment in which N forms may be variable.

Light is a fundamental source for photoautotrophs, however, if light energy absorbed by pigments in photosystem II (PSII) exceeds its utilization in C assimilation, PSII can experience oxidative or other damage (Genty et al., 1989; Murchie and Lawson, 2013; Kana et al., 1997). The reaction center chlorophyll (Chl) in PSII, which is aggregated on the thylakoid membrane, absorbs quanta of photosynthetically active radiation (PAR) and generates electrons and protons from water molecules that, in turn, contribute to the generation of chemical energy (ATP, NADPH) that is used to drive diverse metabolic processes such as C and N assimilation. However, the supply of chemical energy must be matched to its use in metabolism to protect PSII from over-reduction (e.g., Kana et al., 1997). One of the

important mechanisms to rapidly regulate excess light energy is non-photochemical quenching (NPQ) (of fluorescence) (Glibert et al., 2016; Murchie and Lawson, 2013). This process mainly dissipates the absorbed energy that exceeds the capacity of electron transport over demand of metabolism as non-radiative harmless heat. There are multiple mechanisms contributing to photoprotection, and photoregulation, and the actual relationship between NPQ and photoprotection is complex. Light, nutrients, and temperature are among the main factors affecting the capacity of electron transport and the demand for metabolism (Kana et al., 1997; Ras et al., 2013). When photosynthetic organisms experience nutrient deficiency, metabolism may be resource limited, but not necessarily energy limited. Thus, reduced metabolic use of absorbed light energy may result in over-excitation, altering cellular energy balance (Kana et al., 1997; Ras et al., 2013). In such a case, the reduced demand for metabolism decreases the energy utilization capacity, and it might accelerate photoinhibition. One pathway by which NPQ in algae is triggered is via the accumulation of Light Harvesting Complex Stress Related Proteins (LHCSRs; e.g., Peers et al., 2009), and recent work (Perozoni et al., 2020) has characterized these proteins for the green alga *Chlamydomonas reinhardtii*. Here, these interactions were studied using pulse-amplitude modulation (PAM) fluorometry.

As with other *Karenia* species, *K. mikimotoi* is a relatively slow-grower but has a strong adaptive capacity to fluctuating environments (Brand et al., 2012; Li et al., 2019). Although differences have been found between subspecies, *K. mikimotoi* is a eurythermal (4–31 °C) and euryhaline (salinity of 9–35) species (Brand et al., 2012). While generally thought to be a low-light specialist, *K. mikimotoi* is also

capable of growing well in a wide range of light intensities (Brand et al., 2012; Li et al., 2019) and is positively phototactic. Nutritionally, *Karenia* spp. are flexible, utilizing various inorganic and organic nutrients and showing phago-mixotrophy (Brand et al., 2012; Zhang et al., 2011, 2013; Heil et al., 2014a; Glibert et al., 2009; Jeong et al., 2005). On the West Florida Shelf, diverse nutrient sources (e.g., land-derived nutrient inputs, microbially regenerated nutrients, regenerated nutrients from decaying fish during toxic blooms, nitrification) may be available to be taken up by *Karenia* spp. (Heil et al., 2014a). While *Karenia* spp. are primarily photo-autotrophic, they may also consume prey, and higher growth rates of *K. brevis* (Glibert et al., 2009; Jeong et al., 2005) and *K. mikimotoi* (Zhang et al., 2011, 2013) have been observed when they have ingested prey organisms compared to growth on inorganic nutrient sources.

In this study, the objective was to analyze photosynthesis in *K. mikimotoi,* in response to short-term exposures to varying combinations of temperature, N form, and concentration. We focused on short-term (hour time scale) exposure to different temperatures, bracketing the temperatures most commonly experienced on the West Florida Shelf, simulating how cells may respond to environmental changes that may be experienced near coastal fronts, in vertical gradients, or near nutrient sources. Photosynthesis-irradiance responses were examined using rapid light curves. We hypothesized that photosynthetic efficiency in *K. mikimotoi* will increase with temperature and with increasing N concentrations (all forms), but that with increasing temperatures, photosynthetic efficiency—the relative amount of absorbed light energy that can be used to drive photosynthesis—will increase to a greater extent,

with increasing concentrations of chemically reduced forms of N compared to changes with increasing concentrations of NO_3^-.

Materials and methods

Algal Culture

A culture of non-axenic *K. mikimotoi* (ARC165, originally isolated from Venice, Florida in 2006) was obtained from Mote Marine Laboratory, Sarasota, FL, USA. The *K. mikimotoi* were grown in semi-batch cultures using L1-silicate media with N added as NO_3^- (Guillard, 1975). All culture media were prepared with 0.2 µm filtered nearshore west Florida waters and sterilized by autoclaving. Cultures were grown over 12 h light:12 h dark cycle under 40 µmol photons m^{-2} s^{-1} at salinity 32~34 and 20 °C.

Specific growth rate, nutrient analysis

While maintaining the stock culture, changes in cell number over time were monitored by counting cells with light microscopy using a hemocytometer after fixing with 5% Lugol's solution. The specific growth rate (µ) of *K. mikimotoi* was calculated according to

$$\mu = (\ln X_2 - \ln X_1)/(t_2 - t_1) \quad (1)$$

where X_1 and X_2 are the cell numbers at time t_1 and t_2, respectively. At the start of the experiment, samples for cell counts and ambient nutrients were collected. Aliquots of culture were filtered through precombusted (450 °C for 2 h) Whatman GF/F filters (Florham Park, NJ, USA) were stored in a −20 °C freezer for further analysis. The

filtrates were reserved for ambient nutrient analysis, which was later done via autoanalysis at the Mote Marine Laboratory.

Experimental Setup

To initiate the experiment, the culture was first diluted to a final concentration of 6200 cells ml^{-1} with autoclaved filtered seawater in order to reduce the concentrations of residual nutrients. Aliquots of the diluted culture were then transferred to 60, 50 mL polypropylene tubes. The tubes were divided into 12 batches of five tubes (Fig. 2.1). Within each batch, tubes received an enrichment of either NO_3^-, NH_4^+ or urea at the following concentrations: 1, 5, 10, 20, 50 μM-N, as ^{15}N (99% enriched). One batch of each substrate enrichment gradient (NO_3^-, NH_4^+ or urea) was then incubated for 1 h at each of four different temperatures. To do so, tubes were placed in temperature-controlled water baths maintained at 15, 20, 25, 30 °C. Tubes were illuminated continuously by LED lights with 350–400 μmol photons m^{-2} s^{-1} as measured with QSL-100 quantum scalar irradiance meter (Biospherical Instruments Inc., San Diego, CA, USA). At the end of the incubation period, tubes were subsampled for photosynthesis measurements and ^{15}N incorporation as described below.

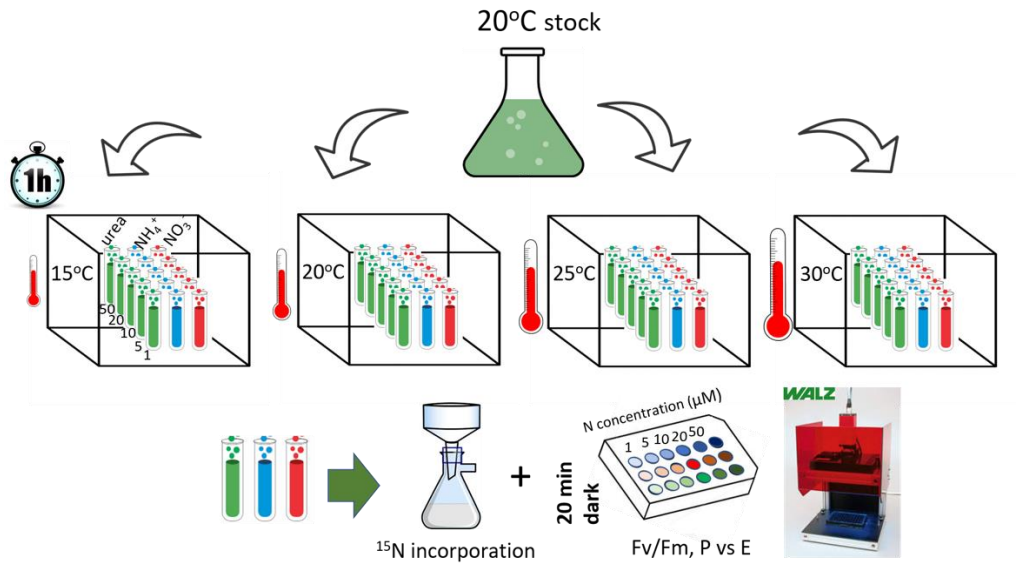

Figure 2.1. Schematic of the experimental design to measure ^{15}N incorporation and photosynthesis-irradiance responses of *K. mikimotoi* exposed to different temperature, N forms, and concentrations. Green tubes represent those enriched with urea; blue tubes—those enriched with NH_4^+; and red tubes—those enriched with NO_3^-.

Chl fluorescence measurements

After the 1 h incubation at the designated temperature, black multiwell plates (24 wells each) were filled with *K. mikimotoi* cells from the various tubes (3 mL in each well) and were dark acclimated for 20 min to fully open (i.e., oxidize) the PSII reaction center Chl and to minimize non-photochemical energy dissipation. Fluorescence emissions from PS II were monitored by a MAXI-Imaging PAM M-Series (Heinz Walz GmbH, Effeltrich, Germany), equipped with 44 blue LED lamps. Light intensities were calibrated with a ULM-500 Light Meter & Logger equipped with a micro quantum sensor (Heinz Walz GmbH, Effeltrich, Germany). Rapid light curves were run to monitor PS II fluorescence emissions as a function of rapid changes in irradiance (12 steps for 20 s at each step: 0, 4, 10, 28, 53, 86, 128, 178,

236, 377, 460, 671 µmol photons m^{-2} s^{-1}). The data were exported from the ImagingWin software (Heinz Walz GmbH, Effeltrich, Germany) and fluorescence parameters were calculated. For the dark-adapted cells, the maximum quantum yields of PSII photochemistry were calculated as the ratio of variable fluorescence (Fv) to maximum fluorescence (Fm), Fv/Fm (Murchie and Lawson, 2013; Scheriber et al., 1994). Subsequently, the effective quantum yield of PSII photochemistry at each light step was calculated as

$$YII = (F'm - Ft)/F'm \quad (2)$$

where F'm is light-acclimated maximum fluorescence and Ft is the steady-state value of fluorescence immediately prior to a flash for a light-adapted sample, respectively (Genty et al., 1989; Kramer et al., 2004). The quantum yield of non-regulated non-photochemical energy dissipation (YNO) and the quantum yield of regulated non-photochemical energy dissipation (YNPQ) were further calculated to analyze the allocation of PSII excitation energy at each light step (Kramer et al., 2004). The sum of these three yields equals 1.

The relative electron transfer rate (rETR) of PS II in units of µmol electrons m^{-2} s^{-1} was calculated as

$$rETR = 0.5 \times YII \times PAR \times 0.84 \quad (3)$$

which is the product of the effective quantum yield (YII) and photosynthetically active radiation (PAR), adjusting the product by a factor of 0.5, which takes into account that half of the absorbed light energy is directed to PSII, and by the factor 0.84, which is the presumed PAR absorptivity (e.g., Genty et al., 1989). Photosynthesis-irradiance curves were fitted using the formula of Platt et al. (1980)

and rETR parameters were calculated using the R package ‘phytotools’ (https://cran.r-project.org/package=phytotools (accessed on April 12, 2021).

The photosynthetic quenching parameter, qP, was calculated according to

$$qP = (F'm - Ft)/(F'm - F'o) \quad (4)$$

in which minimum fluorescence level of illuminated sample is F’o. In order to convert this to a measure of excitation pressure, the value 1-qP was calculated. This value is also interpreted as the number of photosynthetic reaction centers that are closed (Maxwell and Johnson, 2000). Thus, whereas Fv/Fm is a measure of quantum efficiency of PSII and the efficiency of non-photochemical quenching (when all reaction centers are considered open and the cells are dark-adapted), any change in qP reflects the degree of reaction center closures under varying light conditions.

^{15}N Isotope Analysis

After incubation, and immediately after the filling of the microwell plates for photosynthetic measurements, the remaining volumes in each of the experimental tubes were filtered through precombusted (450 °C 2 h) Whatman GF/F filters. The filters were immediately frozen, then subsequently dried and transferred to tin capsules. Isotope analysis was then undertaken by the UC Davis Stable Isotope Facility. Values are reported as ^{15}N atom percent enrichment of samples at the end of the incubation periods (Glibert et al., 2019).

Statistical Analysis

All statistical analyses were performed with R. The normality of data was checked with Shapiro–Wilks test and the homogeneity of variance was assessed with

Levene's test in R package 'car'. Differences between different temperature (15, 20, 25, 30 °C) and N forms (NO_3^-, NH_4^+, urea) of fluorescence data (e.g., Fv/Fm, rETR parameters) were tested using one-way analysis of variance (ANOVA), followed by Tukey's HSD test for pairwise comparisons.

Results

Initial cell and nutrient conditions

The specific growth rate of the initial undiluted culture at the time of the experiment was 0.23 day^{-1}. The cells were not nutrient-depleted and the measured concentrations of nutrients after dilution with filtered seawater were 289 µM ± 2.8 and 1.1 ± 0.5 µM for $NO_3^-$and NH_4^+, respectively, and 7.7 ± 0 µM for PO_4^{3-}. Urea concentrations were negligible.

PSII quantum efficiency and quantum yields

Over the range of 15–25 °C, the maximum quantum yields of PSII photochemical efficiency, Fv/Fm, did not differ significantly between the N treatments when the different N concentrations for each temperature were averaged (ANOVA, $p > 0.05$) (Tables 2.1 and 2.2). The Fv/Fm averaged 0.44 ± 0.03 for the 15–25 °C treatments when all N forms and concentrations are taken into account. However, within each N form, Fv/Fm tended to increase with temperature (ANOVA, $p < 0.05$) (Table 2.2) and concentrations (Fig. 2.2). In contrast, at 30 °C, the Fv/Fm of all the N-enriched samples dropped precipitously. The Fv/Fm of samples enriched with NO_3^- and NH_4^+ and incubated at 30 °C dropped to <0.1, while those with urea enrichment fell to a range of 0.1–0.2. The Fv/Fm values of the urea-treated samples

(0.17 ± 0.04) were 2-fold higher than those of the NH_4^+-treated samples (0.07 ± 0.03) (Tukey's HSD, $p < 0.01$) and 9-fold higher than those of the NO_3^--treated samples (0.02 ± 0.03) (Tukey's HSD, $p < 0.001$) (Fig. 2.2 and Table 2.2). At 30 °C, the Fv/Fm values also showed a general decline when enriched at concentrations >5 µM-N (Fig. 2.2). This trend was most apparent for samples enriched with urea.

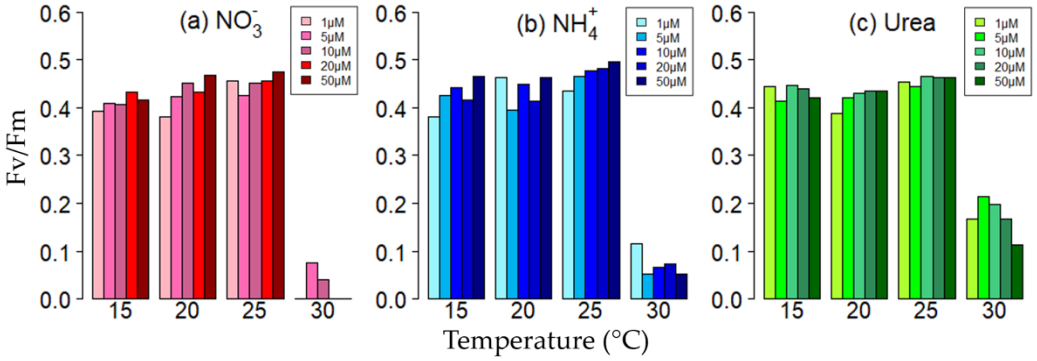

Figure 2.2. Maximum photosystem II photochemical efficiency, Fv/Fm, of *K. mikimotoi* exposed to different temperatures (15, 20, 25, 30 °C) when pulsed with different nitrogen forms (NO_3^-, NH_4^+, urea) and amounts (1, 5, 10, 20, 50 µM-N). Within each depicted temperature, the darker the color of the bars, the higher the enrichment with added N.

Table 2.1. Analysis of variance (ANOVA) results testing N form effects at each temperature

	ANOVA (N form effects)			
	Fv/Fm		$rETR_{max}$	
	F(df=2)	P-value	F (df=2)	P-value
15°C	1.329	0.301	4.901	**0.028**
20°C	0.329	0.726	3.942	0.048
25°C	1.361	0.293	3.238	0.075
30°C	25.58	**<0.001**	12.85	**0.001**

Table 2.2. The averaged Fv/Fm and $rETR_{max}$ (Note that only the statistical results for the ANOVA at 15, 20, 25ºC are shown here). Significant results are shown in bold.

	NO_3^-		NH_4^+		Urea	
	Fv/Fm	$rETR_{max}$	Fv/Fm	$rETR_{max}$	Fv/Fm	$rETR_{max}$
15°C	0.41±0.01	11.2±2.0	0.43±0.03	15.6±3.0	0.43±0.02	14.1±1.6
20°C	0.43±0.03	11.6±1.4	0.44±0.03	14.0±1.7	0.42±0.02	14.1±1.7
25°C	0.45±0.02	10.1±2.2	0.47±0.02	13.0±2.0	0.46±0.01	12.7±1.8
30°C	0.02±0.03	0.9±0.8	0.07±0.03	2.4±0.7	0.17±0.04	3.1±0.6
ANOVA (temperature effects at 15-25°C)						
F (df=2)	3.935	0.856	3.368	1.613	7.485	1.192
P-value	**0.049**	0.449	0.069	0.240	**0.008**	0.337

At 15–25 °C, the quantum yields of the effective photochemical efficiency of PSII, YII, of *K. mikimotoi* declined with increasing transient light intensities (Fig. 2.3a–i). The rates of decline were similar for all N treatments (ANOVA, $p > 0.05$). At 30 °C, all values of YII were much reduced, but values for samples enriched with urea were significantly higher than values for those samples enriched with either NO_3^- or NH_4^+ (Tukey's HSD, $p < 0.001$) (Fig. 2.3j–l). For a given light intensity, most values of YII increased with increasing N concentrations at 15–25 °C (Fig. 2.3a–i), while no consistent N concentration effects were found at 30 °C (Fig. 2.3j–l).

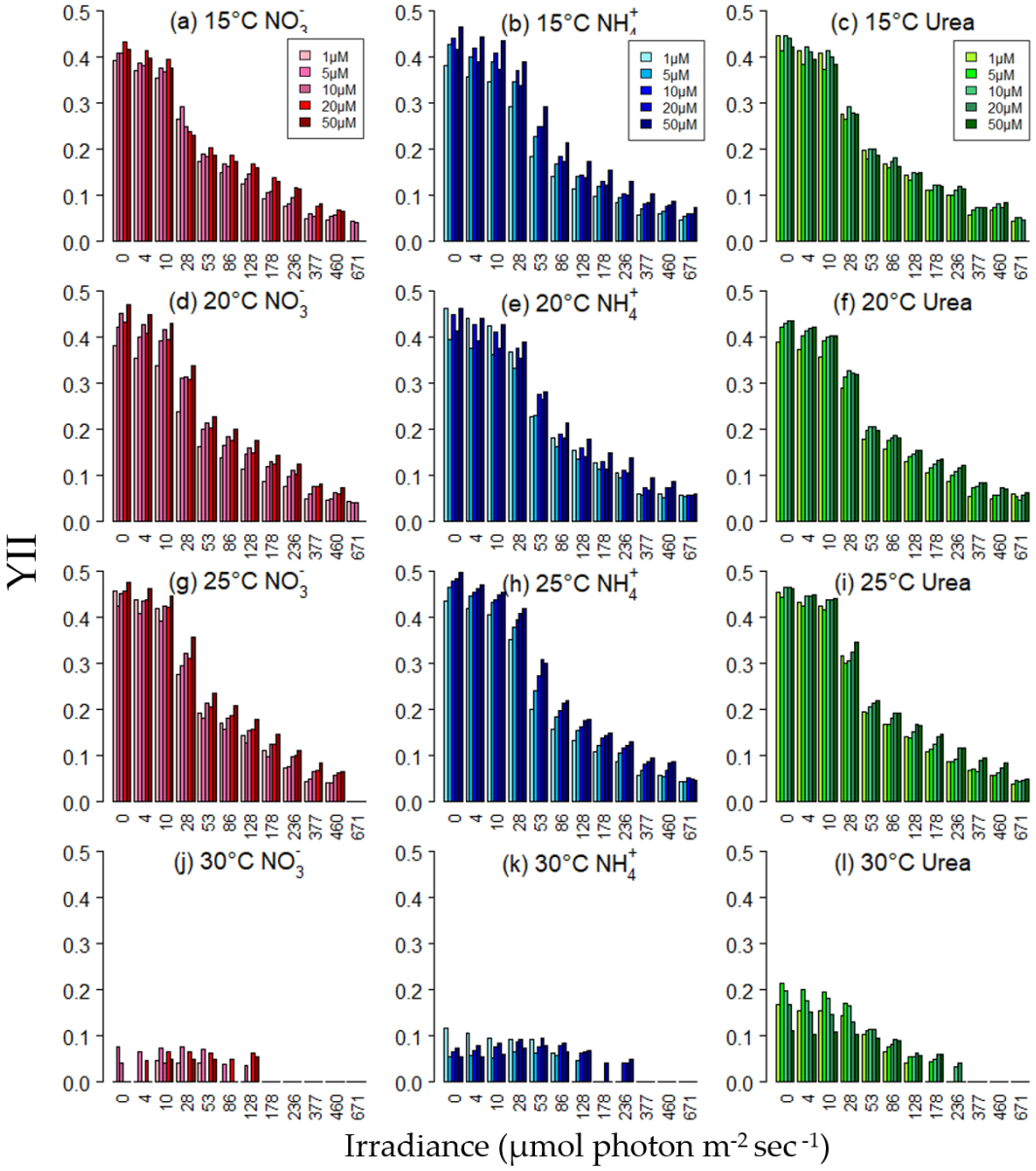

Figure 2.3. Effective Photosystem II photochemical efficiency, YII, as a function of irradiance for *K. mikimotoi* exposed to different temperatures (15, 20, 25, 30 °C) when pulsed with different nitrogen forms (NO_3^-, NH_4^+, urea) and amounts (1, 5, 10, 20, 50 µM-N). Within each depicted irradiance level, the darker the color of the bars, the higher the enrichment with added N.

Relative electron transfer rate

The rapid light response curves of rETR showed a typical saturating response with little evidence of photoinhibition at 15–25 °C at all N forms and concentrations (Fig. 2.4a–i). Only a few treatments showed down-regulation of photochemical reactions, thus exhibited reduction in rETR values at the highest light intensity (e.g., 20 and 50 µM-N of urea at 25 °C). As with values of Fv/Fm and YII, values of rETR were reduced significantly at 30 °C across the light range, but the extent of reduction differed depending on the form of N (ANOVA, $p < 0.01$) (Fig. 2.4j–l). Both light-limited and light-saturated parts of the rETR versus irradiance curves responded to changes in N concentrations with stronger effects on the light-saturated regions at 15–25 °C (Fig. 2.4a–i). For example, the light-limited rETR of the 1 µM-N NH_4^+ treatment at 15 °C (0–178 µmol photons m^{-2} s^{-1}) increased 43% compared to the 50-µM-N NH_4^+ treatment at 15 °C, and the light-saturated rETR of the 1µM-N NH_4^+ treatment at 15°C (236–460 µmol photons m^{-2} s^{-1}) increased 63% compared to the 50 µM-N NH_4^+ treatment at 15 °C.

No significant temperature effects on $rETR_{max}$ were found at 15–25°C at each N source (ANOVA > 0.05) (Table 2.2) while N source effects were found at two temperatures (Tukey's HSD, $p < 0.05$) (Table 2.1). The $rETR_{max}$ values of the NH_4^+-enriched cultures (15.6 ± 3.0) were significantly higher than those of samples enriched with NO_3^- (11.2 ± 2.0) at 15°C (Tukey's HSD, $p < 0.05$) and $rETR_{max}$ values of the NO_3^--enriched cultures (0.9 ± 0.8) were markedly lower than those of

the NH_4^+-enriched samples (2.4 ± 0.7) (Tukey's HSD, $p < 0.05$), and the urea-treated samples (3.1 ± .0.6) at 30°C (Tukey's HSD, $p < 0.01$) (Fig. 2.5, Table 2.2).

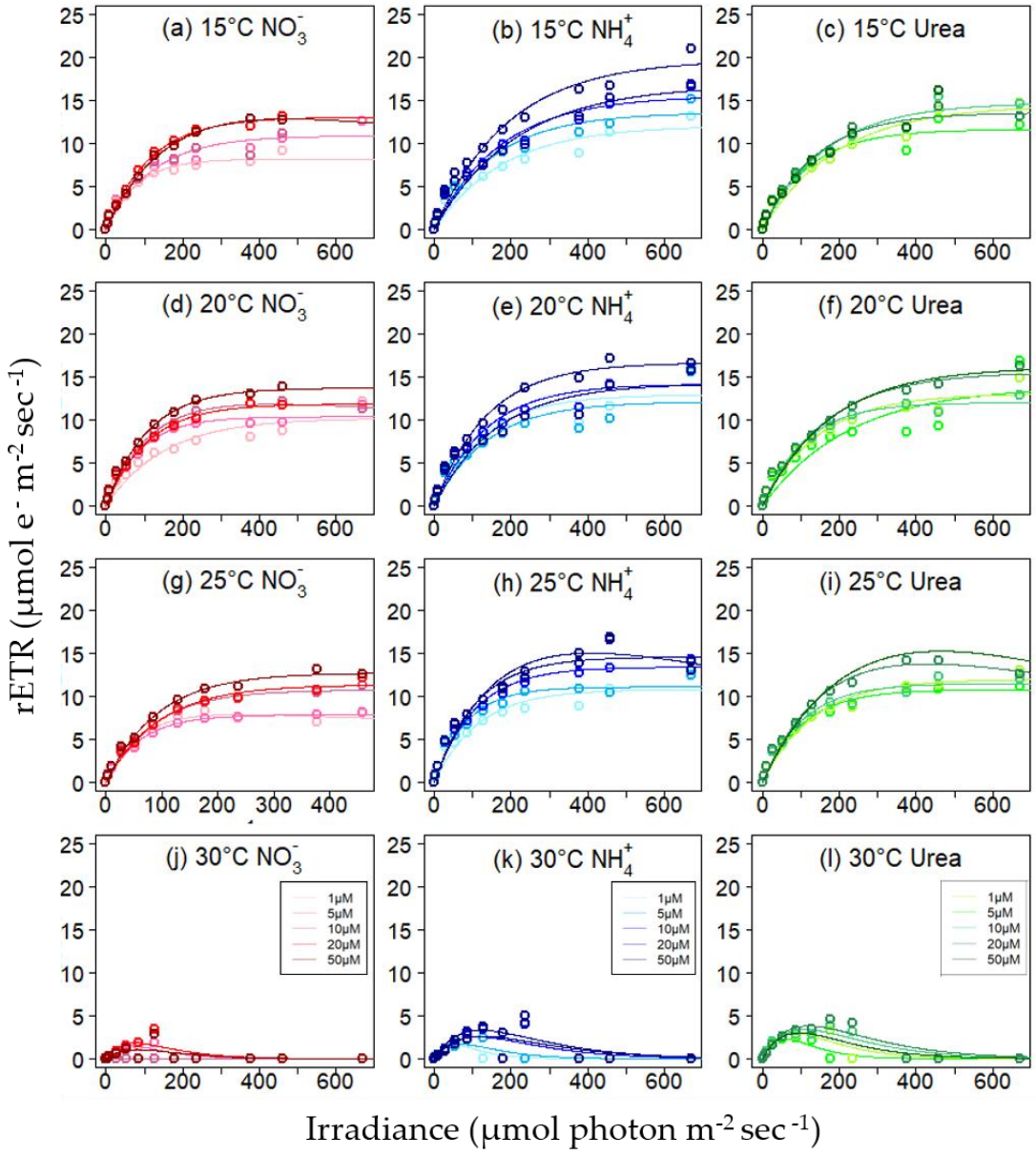

Figure 2.4. The rapid light responses of rETR of *K. mikimotoi* exposed to different temperatures (15, 20, 25, 30 °C) when pulsed with different nitrogen forms (NO_3^-, NH_4^+, urea) and amounts (1, 5, 10, 20, 50 µM-N). For each depicted ETR curve, the darker the color of the lines, the higher the enrichment with added N.

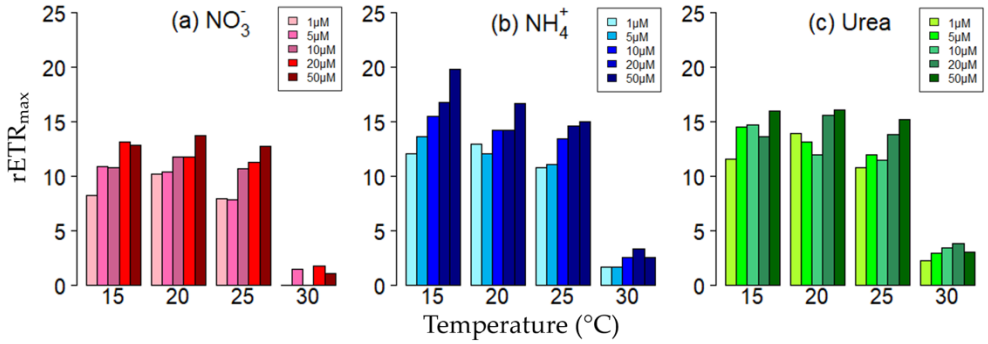

Figure 2.5. The $rETR_{max}$ of *K. mikimotoi* exposed to different temperatures (15, 20, 25, 30 °C) when pulsed with different nitrogen forms (NO_3^-, NH_4^+, urea) and amounts (1, 5, 10, 20, 50 µM). Within each depicted temperature, the darker the color of the bars, the higher the enrichment with added N.

Excitation pressure

The excitation pressure, 1-qP, increased with increasing transient light intensities at 15–25 °C (Fig. 2.6a–i). When cells were fully dark-adapted (I = 0 µmol photons m^{-2} s^{-1}), reaction centers were all open and 1-qP values were low, but by 10 µmol photons m^{-2} s^{-1}, an increasing fraction of reactions centers were closed. At each light intensity, excitation pressure decreased with increasing concentrations of N forms (Fig. 2.6a–i). However, cells exposed to 30 °C exhibited closed reaction centers across all nearly all irradiance levels for samples enriched with NO_3^- and NH_4^+, while for samples enriched with urea, full reaction center closure was observed only for samples exposed to >100 µmol photons m^{-2} s^{-1} (Fig. 2.6j–l). Measures of the quantum yields of regulated and non-regulated non-photochemical energy dissipation (YNPQ and YNO) for all experimental treatments are provided in the in Supplementary Materials (Figs. S2.1 and S2.2).

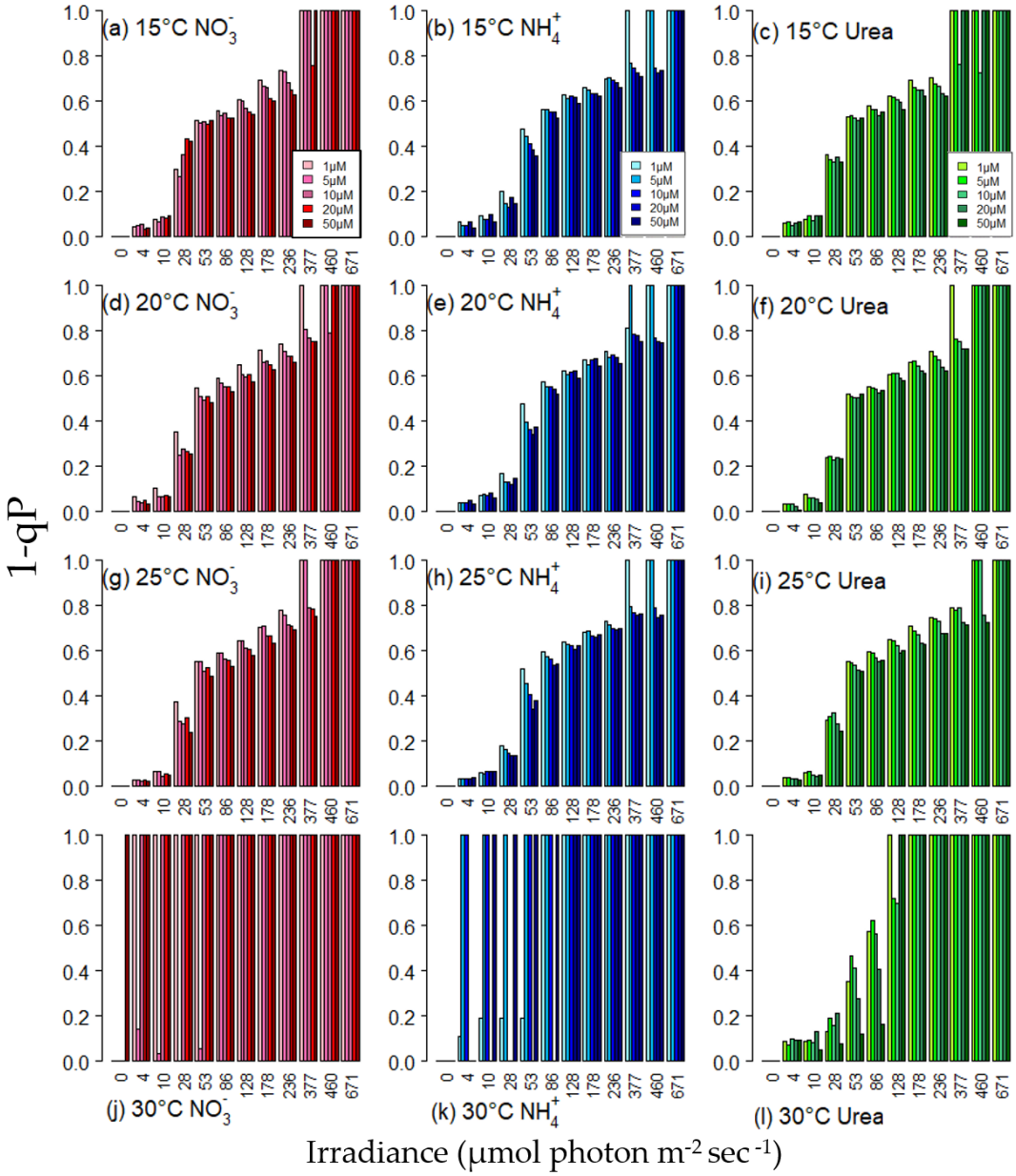

Figure 2.6. The extent of PSII reaction center closures, 1-qP, as a function of irradiance for *K. mikimotoi* exposed to different temperatures (15, 20, 25, 30 °C) when pulsed with different nitrogen forms (NO_3^-, NH_4^+, urea) and amounts (1, 5, 10, 20, 50 µM-N). Within each depicted irradiance level, the darker the color of the bars, the higher the enrichment with added N.

^{15}N isotope incorporation

The incorporation of ^{15}N (as ^{15}N atom percent) varied with substrate, and temperature. Over the concentration range, the ^{15}N enrichment of NO_3^- was linear for each temperature, and only a slight, but not significant, increase in ^{15}N incorporation was noted at 30 °C compared to the other temperatures (Fig. 2.7a). Isotopic enrichment levels were highest for NH_4^+, and all temperatures indicated a saturating response across the concentration gradient. At saturation, the atom % enrichment levels at 25 °C and 30 °C were significantly higher than those measured at 15 °C and 20 °C (Fig. 2.7b). For urea, there was no saturation in the response, but the ^{15}N atom% values across all concentrations were significantly higher at 30 °C than atom% enrichment values at the other temperatures, which did not differ from each other (Fig. 2.7c).

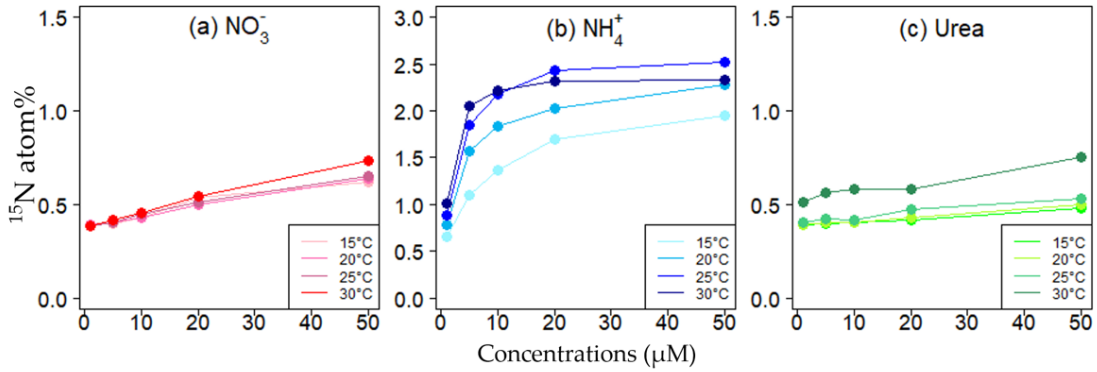

Figure 2.7. Atom percent enrichment of ^{15}N for *K. mikimotoi* exposed to different temperatures (15, 20, 25, 30 °C) when pulsed with different nitrogen forms (NO_3^-, NH_4^+, urea) and amounts (1, 5, 10, 20, 50 µM-N). For each depicted curve, the darker the color of the lines, the higher the enrichment with added N. Note that the scale of Y-axis is different.

Discussion

Light, nutrients, and temperatures drive different rates of metabolism within the cell, and the challenge for the cell is to balance energy and reductant generation with that of its consumption. Here, varying each of these factors in short-term exposures, the dynamic balance between the "push" due to photon flux pressure and the metabolic "pull" of diverse metabolic reactions of *K. mikimotoi* was investigated (Fig. 2.8). These results are complementary to the dynamic balance theory of photosynthetic regulation (Kana et al., 1997), which articulated the notion that the concentration of photosynthetic pigments in algae could be explained by the opposing forces of excitation pressure on PSII and degree of reduction of the plastoquinone pool of PSII. Therefore, acclimated pigment concentrations balance the light energy input and biochemical energy use in response to environmental conditions, demonstrating the sensitivity of PSII to metabolic feedback. Once an excitation event occurs in PSII, the downstream redox state determines the electron sink capacity. The redox state around PSII responds rapidly to changes in light availability (and Calvin cycle activity), N reduction and assimilation. Whereas pigment changes with multiple environmental changes were emphasized by Kana et al. (1997), in their description of the dynamic balance theory, various fluorescent parameters, including the excitation pressure on PSII, were measured directly herein with changes in light, temperature, and N availability.

The initial hypothesis, that photosynthetic efficiency in *K. mikimotoi* will increase with temperature and with increasing N concentrations, and that with increasing temperatures, photosynthetic efficiency will increase to a greater extent

with increasing concentrations of chemically reduced forms of N, compared to changes with increasing concentrations of NO_3^-, was largely borne out, but the highest temperature tested yielded differential stresses depending on N form. Here, the interactions of the different physiological processes measured are described, as well as implications for growth of *Karenia* on the West Florida Shelf.

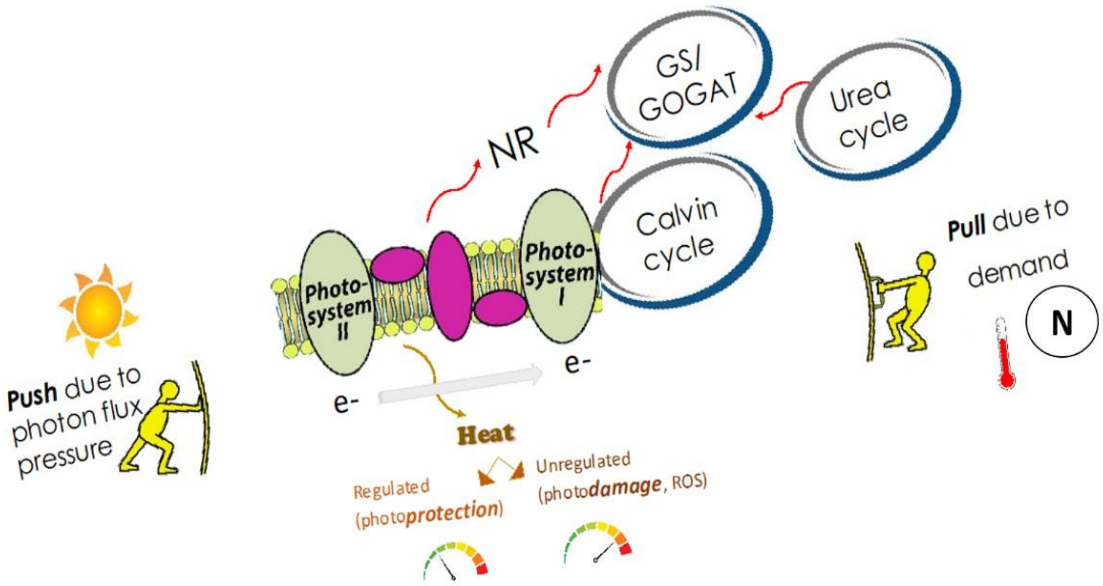

Figure 2.8. Conceptual figure representing push and pull of energy during photosynthesis and metabolic reactions associated with C and N assimilation.

Temperature, Energy (Light) and Material (N) Addition Effects on Photosynthesis

The biochemical reactions of photosynthetic metabolism are generally considered to be more sensitive to temperature than the light reactions, and increase with temperature up to an optimum temperature, above which they decline rapidly (Glibert et al., 2016; Padfield et al., 2015). Shen et al. (2016) reported for *K.*

mikimotoi that the effective quantum yield, YII (pulsed with 70 µmol photons m^{-2} s^{-1}), and $rETR_{max}$ increased from 16–28 °C although only estimates from 16 °C were statistically lower than those measured at 20, 24, and 28 °C. In this study, generally the maximum quantum yield, Fv/Fm, increased with temperature at each N form (e.g., 0.41 ± 0.01, 0.43 ± 0.04, 0.45 ± 0.02 at 15, 20, 25 °C, respectively, when cells were NO_3^--enriched) although differences were statistically not significant in the case of NH_4^+-enriched cells (Table 2.2). However, when cells were light saturated, no clear temperature effects were found in $rETR_{max}$ in the range of 15–25 °C (Table 2.2). The cultures from Shen et al. (2016) were acclimated to each temperature while our cultures were adapted to 20 °C and exposed to new thermal environments for 1 h. The optimal temperature for maximum photosynthetic rate can increase with increasing growth temperature (Hikosaka et al., 2006). At 30 °C, all photosynthetic parameters dropped significantly, suggesting that even a 1 h exposure to this temperature was stressful for *K. mikimotoi*. Note that herein additional cultures incubated at 30 °C overnight (no extra N addition) did not survive (data not shown).

At all but the highest temperature tested, with increasing light intensity, i.e., increasing "push" due to photon flux pressure (Fig. 2.8), rETR increased progressively until the PSII was saturated with light (Ik) (Fig. 2.4). Although the efficiency of photochemical light capture, YII, decreased with increasing irradiance (Fig. 2.3), enhanced photon flux pressure on PSII increased the quantity of energy channeling to photochemistry, thus, increasing the rETR until Ik. At a given irradiance, rETR increased further with increasing N concentrations. Even though cultures were N-sufficient, photosynthetic activity increased with all forms of N

addition when temperature was not at a stressful level (Fig. 2.4). The increased supply of material (N in this case) enhanced metabolic activity, thus raising the demand for energy to run diverse metabolism ("pull" due to demand) (Fig. 2.8). This enhancement was stronger when cells were light saturated. The $rETR_{max}$ clearly responded to increasing N addition with little variations at 15–25 °C (Fig. 2.5). The dark-adapted fluorescence parameter, Fv/Fm, was also generally increased with all forms of N addition (Fig. 2.2).

N Form Effects on Photosynthesis at 30 °C

When temperature was not at a stressful level, *K. mikimotoi* was able to operate its photosynthetic apparatus efficiently with all forms of N tested in this study. However, at 30 °C, cells were dissipating most of their absorbed light energy non-photochemically, but at different degrees depending on N form. At the highest temperature, reaction centers were fully closed for the NO_3^- and NH_4^+ treatments across most irradiance levels (Fig. 2.6j, k). The NO_3^--enriched culture showed the strongest stress (Fv/Fm = 0.02, $rETR_{max}$ = 0.9), and then NH_4^+-enriched cells (Fv/Fm = 0.07, $rETR_{max}$ = 2.4; Table 2.2). Fluorescence parameters were still significantly lower at this high temperature compared to those at 15–25 °C, but when cells were treated with urea, *K. mikimotoi* experienced less stress than those cells enriched with NO_3^- and NH_4^+ (Fv/Fm = 0.17, $rETR_{max}$ = 3.1), implying that urea might induce certain photoprotective mechanisms.

The ^{15}N isotope enrichment trends confirmed the differential effects of temperature with the different forms of N (Fig. 2.7). Little effect of temperature was observed with $^{15}NO_3^-$ incorporation, but with $^{15}NH_4^+$, incorporation increased as

temperatures rose, and for urea, the highest temperature uniquely yielded the highest isotopic incorporation. Such trends would support the different responses seen in Fv/Fm and rETR with the different N enrichments.

Although *K. mikimotoi* has been known to use diverse forms of N, the underlying mechanisms for metabolizing each N form are complex with respect to temperature. The inhibition of NR activity at higher temperatures might hinder the first step of NO_3^- metabolism, reduction to NO_2^- (Glibert et al., 2016), thereby decreasing subsequent intracellular N supply. Dai et al. (2014) reported that *K. mikimotoi* grown on NO_3^- could not survive at 30 °C and NR activity was significantly inhibited at this temperature compared to 15–25 °C. On the other hand, the metabolic flux of reduced forms of N such as NH_4^+ and urea is expected to be higher at higher temperatures (Glibert et al., 2016). For example, at higher temperatures, the activity of GS that adds NH_4^+ to glutamate by using ATP to produce glutamine increases. Moreover, the activity of GOGAT that combines glutamine to 2-oxoglutarate using electrons can be higher at 30 °C compared to activity rates at lower temperatures (Glibert et al., 2016, Dagenais-Bellefeuille and Morse, 2013). All energy-consuming metabolism will increase the energy demand, thereby enhancing the capacity of photochemical use of absorbed light energy. This might partly explain why NH_4^+-treated sample showed four times higher Fv/Fm and three times higher $rETR_{max}$ compared to NO_3^--treated cells at 30 °C (Figs. 2.2 and 2.5, Table 2.2). However, cells enriched with urea showed even higher estimates, implying that energy demand for metabolism could be relatively higher. Dinoflagellates have a urea cycle that helps reallocation of intracellular C and N (Dagenais-Bellefeuille and

Morse, 2013) and several enzymes involved in the urea cycle have been identified in *K. mikimotoi*, suggesting that this species could also have a complete urea cycle (Shi et al., 2021). The increased intracellular recycling of C and N from protein catabolism and photorespiration through the urea cycle could enhance overall metabolic flux, thus increasing the demand for chemical energy. To balance this demand, a higher proportion of absorbed light energy could be funneled into photochemistry, therefore increasing Fv/Fm and rETR. Moreover, generally, urease, which catalyzes the hydrolysis of urea, has a positive relationship with temperature (Fan et al., 2003, Solomon et al., 2010).

Implications of Temperature Effects for Natural Assemblages

In the field, *K. mikimotoi* has been observed over a wide range of temperatures, 4–31 °C although some subspecies have narrower temperature ranges (e.g., Norway isolate: 10–25 °C) (Brand et al., 2012; Li et al., 2019; Gentien, 1998). In culture experiments, it has been shown that *K. mikimotoi* cells can survive and grow well at 16, 20, 24, 28 °C (Shen et al., 2014, 2016), but not at 10 and 30 °C (Dai et al., 2014), suggesting that *K. mikimotoi* would have a relatively narrow optimum temperature for their growth (Brand et al., 2012; Shen et al., 2014). In general, rising temperatures accelerate enzymatic reactions by increasing the proportions of molecules that have sufficient kinetic energy to react, thus increasing overall metabolic flux (the "pull" due to demand) (Figure 2.8) (Eppley, 1972; Marañón et al., 2018). Indeed, the maximum specific growth rates were observed at 24 °C and 25 °C in the previously cited studies (Shen et al., 2016; Dai et al., 2014).

Karenia blooms that primarily occurs in the fall months rarely persist throughout hot summer months on the West Florida Shelf. The summers—during which water can >30 °C—may represent a thermal barrier for large blooms to be maintained. However, *Karenia* cells are occasionally found to sustain substantial blooms in extremely hot surface waters (>30°C). Generally, West Florida Shelf is characterized by low ambient dissolved inorganic nutrients, but elevated nutrients, especially dissolved organic nutrients (e.g., urea) can occur nearshore (Heil et al., 2014a). Urea has been widely used as a fertilizer within Florida and some of this nutrient can be delivered to nearshore (Glibert et al., 2006). This raises the possibility that high temperature stress might be alleviated when urea is available because more photons can be processes photochemically, thus cells can operate photosynthesis more efficiently in very warm conditions with reduced organic nitrogen. Therefore, increased availability of urea might be able to support maintaining *Karenia* blooms under short-term heat stress.

Appendix I: Supplementary Material

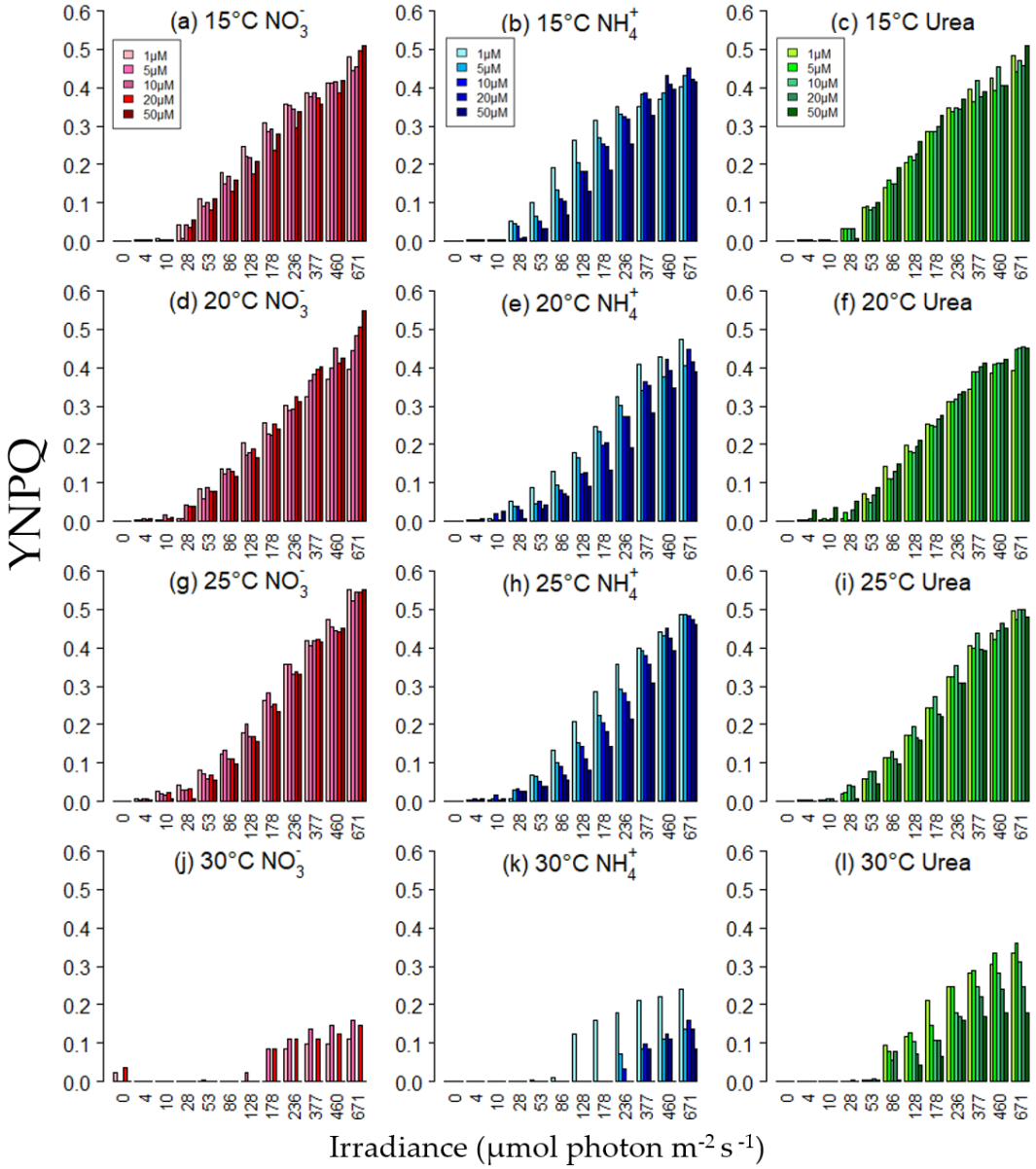

Figure S2.1. Quantum yield of regulated non-photochemical energy dissipation, YNPQ, as a function of irradiance for *K. mikimotoi* exposed to different temperatures (15, 20, 25, 30°C) when pulsed with different nitrogen forms (NO_3^-, NH_4^+, urea) and amounts (1, 5, 10, 20, 50 µM). Within each depicted irradiance level, the darker the color of the bars, the higher the enrichment with added N. YNPQ represents energy loss of excitation energy thorough harmless heat dissipation related to non-photochemical quenching. Within each depicted temperature, the darker the color of the bars, the higher the enrichment with added N.

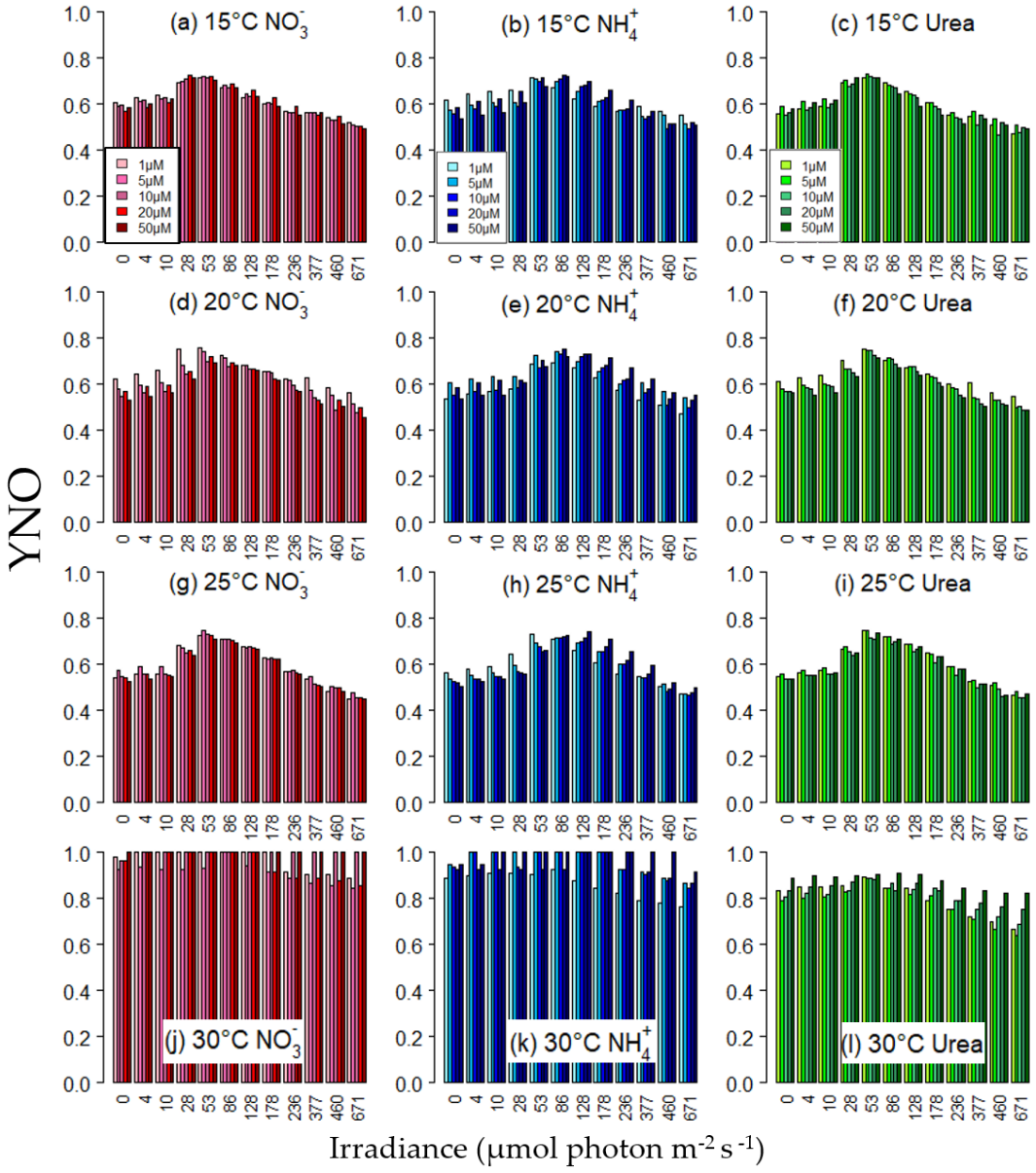

Figure S2.2. Quantum yield of non-regulated non-photochemical energy dissipation, YNO as a function of irradiance for *K. mikimotoi* exposed to different temperatures (15, 20, 25, 30°C) when pulsed with different nitrogen forms (NO_3^-, NH_4^+, urea) and amounts (1, 5, 10, 20, 50 µM). Within each depicted irradiance level, the darker the color of the bars, the higher the enrichment with added N. YNO represents the sum of non-regulated heat dissipation and fluorescence emission ("primarily constitutive losses"). Within each depicted temperature, the darker the color of the bars, the higher the enrichment with added N.

Chapter 3: Dynamic photo-physiological responses of dinoflagellate *Karenia brevis* to short-term changes in temperature and nitrogen substrates[2]

Abstract

On the West Florida Shelf, annual blooms of the neurotoxin-producing harmful dinoflagellate, *Karenia brevis* (and other *Karenia* species) cause negative effects on the environment, the economy, and on human health. Blooms primarily occur in the fall months and may overwinter into winter and spring, but they rarely persist throughout the hot summer months when water temperatures are > 30°C. During 2020 and 2021, an unusually prolonged *K. brevis* presence occurred. During the early phase of this bloom (January, 2021) when *K. brevis* were present in low-moderate abundances in southwest Florida, experiments on rates of photosynthesis were conducted on surface samples from two offshore stations within the bloom. Photosynthesis-irradiance responses were examined using PAM fluorometry to assess responses to varying nitrogen conditions and temperatures. Treatments included controls and exposures to temperatures of 15, 20, 25, 30°C with and without 10 µM additions of three nitrogen forms (nitrate, ammonium, and urea). Although there were variations between stations, in general decreasing trends of fluorescence parameters with increasing temperature from 15°C to 30°C were observed, suggesting that 30°C

[2]Ahn, S.H., Glibert, P.M, Heil, C.A. Dynamic photo-physiological responses of the dinoflagellate *Karenia brevis* to short-term changes in temperature and nitrogen substrates, In: Band-Schmidt, C.J. and Rodríguez-Gómez, C.F. (eds.) (2022) Proceedings of the 19th International Conference on Harmful Algae, La Paz, B.C.S., Mexico. International Society for the Study of Harmful Algal Blooms. pp. 52-57.

might be physiologically stressful for *Karenia*. However, when cells were treated with urea, this reduction was substantially less. These results suggest *K. brevis* dependence on nitrogen form may change with temperature, and availability of chemically-reduced organic forms of nitrogen may be favored at the highest temperatures that *Karenia* may experience.

Introduction

On West Florida Shelf (WFS), the toxic dinoflagellate *Karenia brevis* forms red tides almost annually (e.g., Heil et al., 2014a). The location, magnitude, and duration of blooms vary every year and are linked to environmental factors in a complex manner. While both state monitoring and focused research efforts have led to considerable understanding about the ecology and physiology of *K. brevis* (Kusek et al., 1999; Heil et al., 2014b and references therein). Many critical questions regarding the physiology of *K. brevis* under different environmental conditions remain unanswered.

Temperature, nutrients, and light are three critical environmental factors regulating the physiology of *K. brevis* (Heil et al., 2014a, 2014b). Temperature has long been considered a significant factor affecting *Karenia* bloom dynamics on WFS. Although factors underlying bloom initiation interact in a complicated manner, temperature is considered an important factor in determining whether blooms are likely to occur (Kusek et al., 1999). Blooms rarely persist throughout the summer months, when water temperatures can be > 30^{o}C. In that laboratory experiments have shown a temperature optimum of 22-28^{o}C (e.g., Vargo, 2009), the lack of summer blooms has been suggested to be due, at least in part, to high temperatures.

Temperature not only affects growth, but it also affects the metabolism of different forms of nitrogen (N) differently (e.g., Glibert et al., 2016). These patterns could be species-specific but, in general, the enzyme involved in nitrate (NO_3^-) metabolism, NO_3^- reductase, has an inverse relationship with temperature over the range from 15-30ºC (Lomas and Glibert, 1999a, 1999b) while enzymes involved in the assimilation of chemically reduced nitrogen, ammonium (NH_4^+), glutamine synthetase and glutamate synthase, and urea, urease, tend to show a positive relationships with temperature over this same temperature range (Lomas and Glibert, 1999a, 1999b; Fan et al., 2003; Glibert et al., 2016). Although it is an obligate autotroph, *K. brevis* can use many different forms of N, including NO_3^-, NH_4^+, and urea (Glibert et al., 2009; Bronk et al., 2014). Therefore, multiple N sources available on WFS such as nutrients from freshwater and estuarine flows, and regenerated nutrients from dead fish could support *K. brevis* blooms simultaneously (Heil et al., 2014a). This dinoflagellate can also obtain nutrition via mixotrophy (Glibert et al., 2009).

Blooms of *K. brevis* initiate offshore and may be transported to the WFS via upwelling (Weisbeg and He 2003; Weisberg et al., 2014). Generally, *K. brevis* densities on the WFS starts to increase in late summer and can remain high during fall and winter when surface water temperatures can be low as ~15°C. Cell densities tend to decrease during late spring and rarely persist through the hot summer when temperatures are higher than 30°C (Brand and Compton, 2007). Vertical gradients in temperatures of > 5-10°C may also exist throughout the year on WFS (Weisberg and He, 2003; Weisberg et al., 2014). Thus, *K. brevis*, which vertically migrates, can be

subject to abrupt changes in temperature and possibly to co-occurring changes in N forms and light conditions. Here, the short-term interactions of temperature, N forms, and light on photosynthetic performance of the winter *Karenia* community were examined to understand how these responses may relate to the conditions under which the *Karenia* community is found on WFS.

Material and methods

Bloom sampling and experimental setup

Near-surface water samples were collected from two offshore stations (15S, 26.3896N, -81.9800W and 19S, 26.28625N, -82.34284W) on January 22, 2021. Ambient water temperature was measured using Seabird 19 plus V2 package. Water was returned to the lab within 2 h and manipulation experiments were immediately initiated. Water from each station was first transferred to 50 mL polypropylene tubes. Nutrient additions (10 µM of NO_3^-, NH_4^+, or urea) were added to four tubes from each station and four unamended tubes from each station served as controls. Subsequently, one set of tubes from each station, including a control, and one each enriched with either NO_3^-, NH_4^+, or urea, were placed in four different temperature-controlled water baths (15, 20, 25, 30°C) and incubated for 1 h under 100 µmol photons m^{-2} s^{-1}.

Chlorophyll a, nutrient and *K. brevis* cell concentrations

Immediately upon return to the laboratory, water samples were filtered through pre-combusted (450°C, 2-3 h) Whatman GF/F filters for chlorophyll *a* (Chl *a*) determination. The filtrates were frozen in brown bottles for subsequent

measurements of NO_3^- + nitrite (NO_2^-). NH_4^+, urea, and phosphate (PO_4^{3-}) via autoanalyzer at the Mote Marine Laboratory. Additionally, 5 mL of each bloom water was fixed with acidic Lugol's solution and *K. brevis* concentrations were determined by light microscopy.

Experimental photosynthetic responses

To assess the photosynthetic response of the samples exposed to different nutrient and temperatures, *in vivo* Chl *a* fluorescence was measured using a Phyto-PAM-II multi-excitation wavelength chlorophyll fluorometer (Heinz Walz GmbH, Effeltrich, Germany). With appropriate calibration and deconvolution of fluorescence signals, this instrument can measure photosynthetic responses of four different major classes of algae, including cyanobacteria, green algae, brown algae, and phycoerythrin-containing cells with single measurements. The brown algal signal includes both diatoms and dinoflagellates, but microscopic analyses confirmed that the dominant organism present in this category was *K. brevis*.

After 1 h of incubation, samples were dark-adapted for 20 min and Rapid Light Curves were conducted using twelve incremental irradiance steps (0, 6, 24, 42, 73, 109, 188, 227, 334, 489, 591, 719 µmol photons m^{-2} s^{-1}). The maximum photochemical efficiency of photosystem II (PS II) was calculated as Fv/Fm = (Fm-Fo)/Fm where Fv is the variable fluorescence, Fo is the minimal fluorescence, and Fm is the maximum fluorescence**.** The maximum relative electron transport rates ($rETR_{max}$) were calculated from rETR versus irradiance curves using the Platt et al. (1980) equation. Statistical analysis of fluorescence parameters was performed using R.

Results and discussion

Both stations were characterized by low inorganic nutrient concentrations (Table 3.1). The Chl *a* concentration was 4-fold lower and the phaeophytin/Chl *a* (Phaeo/Chl *a*) ratio was higher at station 19S compared to station 15S (Table 3.1). Ambient temperature at the time of sampling was 20°C.

Table 3.1. Concentrations of Chl *a* (µg L^{-1}) and nutrients (µM). Urea was not detectable.

	Station 15S	Station 19S
Chl *a*	10.5	2.4
Phaeo/Chl *a*	0.23	0.4
NO_3^-+NO_2^-	< 0.07	< 0.07
NH_4^+	0.23	0.15
PO_4^{3-}	0.20	0.05

Both stations had a mixed phytoplankton community composition, with substantial *K. brevis* abundance. Station 15S was dominated by dinoflagellates (220,000 cell L^{-1}) and 94% of the dinoflagellate population was *K. brevis.* At station 19S, approximately 30% of algae were dominated by dinoflagellates (20,000 cell L^{-1}) (Fig. 3.1), of which 75% were *K. brevis*. Neither station had more than a small percentage of diatoms (6 %). Therefore, it is reasonable to assume that most of the fluorescence signals of the brown algae originated from *K. brevis* during this study.

In general, decreasing trends of the maximum quantum yields of PSII photochemical efficiency, Fv/Fm, were observed in each N treatment as temperature increased from 15°C to 30°C although only estimates from station 15S were significantly different (ANOVA, $p < 0.5$) (Figs. 3.2a-b). However, this trend was less

consistent when cells were treated with urea. The $rETR_{max}$ also showed similar trends with Fv/Fm (Figs. 3.2c-d). Although the differences were less at station 19S, generally $rETR_{max}$ also decreased with increasing temperature except for the urea-treated samples.

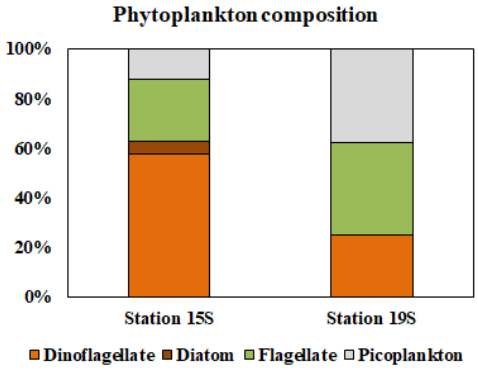

Figure 3.1. Phytoplankton composition at two stations during January 22, 2021 on WFS.

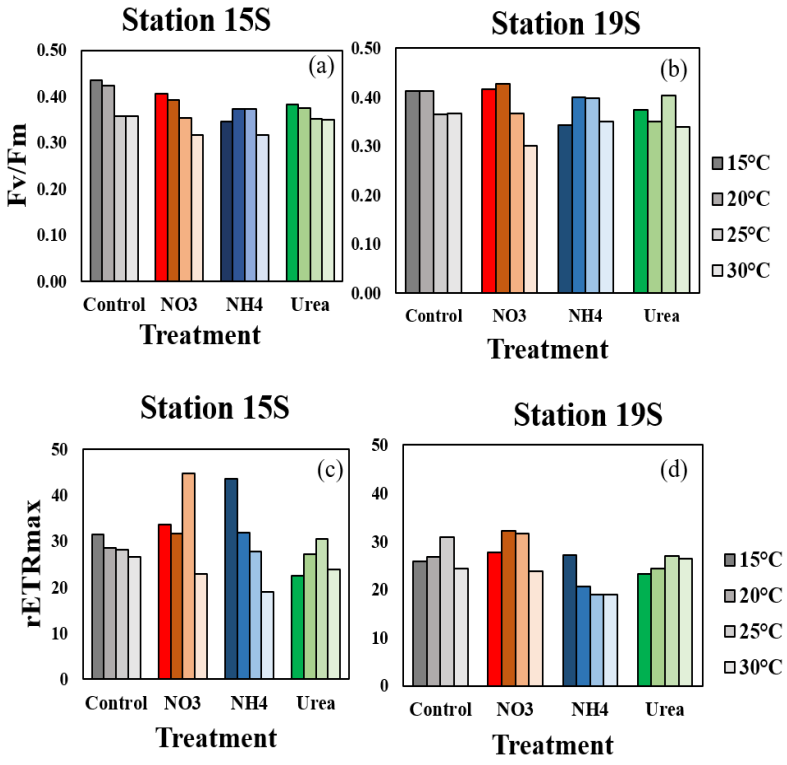

Figure 3.2. Fv/Fm and $rETR_{max}$ (µmol electrons m^{-2} s^{-1}) of *K. brevis* exposed to different temperatures (15, 20, 25, 30°C) and nitrogen (10 µM NO_3^-, NH_4^+ or urea) additions. The color bars increase in brightness from 15°C to 30°C at each treatment.

In both field and laboratory cultures, *K. brevis* has been observed in the range of 7-33°C, but the optimum temperature range has previously been reported to be relatively narrow, 22-28°C (Kusek et al., 1999). The decline of fluorescence parameters after even 1 h exposure to 30°C in this study suggests that this high temperature is stressful for the winter *Karenia* community. However, when bloom water was enriched with urea, fluorescence parameters were less reduced (Fig. 3.2), implying that urea might induce a photoprotective mechanism. Dinoflagellates have a urea cycle that helps reallocation of intracellular carbon (C) and N (Dagenais-Bellefeuille and Morse, 2013) and in *Karenia mikimotoi*, several enzymes involved in the urea cycle have been identified (Shi et al., 2021). The increased recycling of C and N from catabolism and photorespiration through the urea cycle could enhance overall metabolic flux, thus increasing the demand for chemical energy to run metabolism. To match this demand, a higher proportion of absorbed light energy may be channeled to photochemical reactions, therefore increasing Fv/Fm and rETR. In addition, urease, the enzyme involved in urea metabolism, generally has a positive relationship with temperature (Fan et al., 2003). Therefore, when urea is available at 30°C, high temperature stress might be partly alleviated by balancing light energy demand.

At 15°C, which is lower than the optimal temperature range for *K. brevis*, the photosynthetic performance of winter *Karenia* communities was not significantly reduced compared to those temperatures close to or at optimal temperatures and some fluorescence parameters (e.g., Fv/Fm) were even higher at this cool temperature (Fig. 3.2). The winter *Karenia* community, which was adapted to cool ambient water temperatures at the time of sampling, were able to operate their photosynthetic apparatus efficiently at 15°C. Compared to station 15S populations, cells at station 19S did not respond significantly to N pulses, even though ambient N concentration was very low. However, the *K. brevis* cells from this station may have been physiologically less active, as indicated by the higher Phaeo/Chl *a* ratio, suggesting that *K. brevis* at station 19S would be less photosynthetic active.

Overall, these results indicate the photosynthetic response of *K. brevis* to changes in N supply may vary with temperature and suggest that the pull of metabolism may buffer the stress of high light, but that the extent of this photoprotection mechanism depends on N form.

Chapter 4: In hot water: Interactions of temperature, nitrogen from and availability and photosynthetic and nitrogen uptake responses in natural *Karenia brevis* population[3]

Abstract

During 2020-2021, an unusually prolonged bloom of the toxigenic dinoflagellate *Karenia brevis* persisted for more than 12 months along the Gulf coast of Florida, resulting in severe environmental effects. Motivated by the possibility that unusual nutrient conditions existed during summer 2021, the short-term interactions of temperature, nitrogen (N) forms (ammonium (NH_4^+), nitrate (NO_3^-), and urea) and availability on photosynthesis-irradiance responses and N uptake rates were examined in summer 2021 and compared to such responses from the earlier winter. Winter samples were exposed to temperatures of 15, 20, 25, 30°C while summer samples were incubated at 15, 25, 30, 33°C, representing the maximum range the cells might experience throughout the water column due to daytime surface heating or extreme weather events. Depending on thermal history of the cells, photosynthetic performance differed when cells were exposed to the same temperature, showing a capacity for thermal acclimation in this species. Although blooms generally do not persist throughout the summer, bloom biomass was remarkably higher in summer than during the winter. However, most of the photosynthetic parameters and N uptake

[3] Ahn, S.H., Glibert, P.M., Heil, C.A. (2023) In hot water: Interactions of temperature, nitrogen form and availability and photosynthetic and nitrogen uptake responses in natural *Karenia brevis* populations. Harmful Algae 129:102519.

rates, as well as total carbon (C) and N cell^{-1} were significantly lower in the summer populations, showing that the summer populations were photosynthetically and nutritionally stressed. When the summer cells were treated with urea, however, uptake rates and total C and N cell^{-1} were higher than with the other N substrates, especially in warmer waters, showing differential thermal responses depending on N forms.

Introduction

During 2020-2021, the west coast of Florida experienced an unusually prolonged neurotoxic dinoflagellate *Karenia brevis* bloom that lasted more than 12 months. The bloom began in October 2020 and ended in early December 2021. In typical years, blooms of *K. brevis*–often mixed with other *Karenia* species such as *K. mikimotoi*–are initiated in the late summer to early fall with the most frequent initiations in September after the wet season (Heil et al., 2022). Blooms typically overwinter but rarely last throughout the summer months (Brand and Compton, 2007; Lenes and Heil, 2010; Turley et al., 2022) with the most frequent terminations in April due to physical factors such as bloom dispersal to offshore or other regions (Heil et al., 2022). It has been presumed that summer water temperatures, which can exceed 30^{o}C, are at the upper limit of the thermal niche for *K. brevis* thereby preventing blooms from persisting at that time (Magaña and Villareal, 2006; Vargo, 2009). Nevertheless, in several recent years (e.g., 2005, 2018) and including 2020, blooms did persist throughout the summer, raising questions about how such blooms overcame the thermal stress.

Karenia brevis is a eurythermal species and has been found in a wide range of temperatures from 7-33°C in the field (Brand et al., 2012). The optimal temperature for this species has been reported to be narrower, 22-28°C (Vargo, 2009; Brand et al., 2012), but acclimation to lower and higher temperatures can occur (Kusek et al., 1999). Considering the daylight surface aggregation behavior of *K. brevis* (Heil et al., 2014b), these cells are likely to be exposed to several degree temperature fluctuations on a daily basis, and if cells vertically migrate, their daily temperature fluctuations may be greater. Ahn and Glibert (2022) found that when *K. mikimotoi*, acclimated to 20°C, was exposed to 30°C, significant stress on photosynthetic properties ensued. However, when subjected to N enrichment—especially with chemically reduced forms of N—the stress level on photosynthesis was mitigated.

An important factor that may have contributed to the unusually prolonged bloom of 2021 is nutrient enrichment that occurred due to the discharge of nutrients from a former phosphate (PO_4^{3-}) processing operation (Piney Point Facility) into lower Tampa Bay (Beck et al., 2022; Chen et al., 2023). The facility, although non-operational in 2021, stored PO_4^{3-} mining waste in large, open, above ground phosphogypsum stacks. In March 2021, leaks were discovered and the reservoir's wastewater was discharged into lower Tampa Bay. This wastewater had concentrations of PO_4^{3-} and ammonium (NH_4^+) at several orders higher concentrations compared to the historical median in the area (Beck et al., 2022; Morrison et al., 2023). In all, the Piney Point spill discharged an estimated 186 metric tons of nitrogen (N) directly into lower Tampa Bay over 10-days, yielding a nutrient load equivalent to that normally received by the lower Tampa Bay annually (Beck et

al., 2022). While these nutrients were dispersed, diluted, and consumed during the spring months and decreased to background levels within weeks, pathways of nutrient recycling are presumed to have been sustained for months in and near the mouth of Tampa Bay, potentially contributing to this bloom (Morrison et al., 2023; Chen et al., 2023). The availability of nutrients, directly or indirectly, from this discharge may be one mechanism by which *K. brevis* overcame thermal stress of the summer (e.g., Thomas et al., 2017).

Key questions related to over-summering *K. brevis* populations are: Do summer populations in the very warm waters of the Gulf of Mexico, which can exceed 30°C at mid-day, experience physiological stress, and to what extent does nutrient availability alleviate this stress? How do temperature responses of photosynthesis under different temperatures compare to known thermal responses? Do winter populations experience the same thermal stresses as summer populations? It was hypothesized that, although the summer *K. brevis* populations were able to form massive blooms during the summer of 2021, these cells were photosynthetically and nutritionally stressed compared to late winter populations but overcame some of this stress when provided with chemically reduced forms of N. Thus, the main objective of this study was to examine rates of photosynthesis and N uptake rates of the summer *K. brevis* bloom under varying temperature and nutrient conditions and to compare responses to those from a more typical, over-wintering bloom when both populations are enriched with N. Given that the West Florida Shelf is historically N-limited, this study focused on effects of N rather than P enrichment.

Materials and methods

Field sampling and environmental parameters

Sampling was conducted at four sites in January 2021 and at one site over four dates in July 2021 (Table S4.1; see also Ahn et al., 2022). At each site, near-surface water samples (0.5 m) were collected. While collecting the waters, a 153 μm mesh was used to remove large zooplankton. The January sites included three coastal stations (13S, 15S, 19S) sampled from the R/V Mote, and Sanibel Island water sampled from a shore site. Summer samples were collected from the Mote Institute dock at New Pass, Sarasota, on July 21, 27, 28, 29, 2021 (Fig. 4.1B and Table S4.1). Bloom locations were chosen based on the Red Tide Status maps (Statewide *Karenia brevis* concentrations) produced by the Florida Fish and Wildlife Research Institute (https://myfwc.com/research/redtide/statewide/; Fig. 4.1A). Ambient temperature and salinity were measured using a Seabird 19 plus V2 package for the coastal stations and with a YSI (YSI Inc., Ohio, USA) for the Sanibel Island and New Pass land-based sampling. Water samples from each location were returned to the lab within 30-45 min (from the land sites) to 2 h (from the coastal sites) and held under shade and at near ambient temperatures during transport.

Upon return to the laboratory, samples were first filtered onto Whatman GF/F filters (Whatman, Maidstone, United Kingdom) for chlorophyll *a* (Chl *a*) in duplicate except for the July 28 and 29 samples. Filters and filtrates were immediately frozen. Analysis of Chl *a* was subsequently undertaken using a 10-AU Fluorometer (Turner Designs, California, USA) according to the method of Holm-Hansen et al. (1965). The filtrates were later analyzed at the Mote Marine Laboratory for NH_4^+, nitrate +

nitrite (NO_3^- + NO_2^-), and PO_4^{3-} via a segmented flow autoanalyzer 3 (SEAL Analytical, Wisconsin, USA) and for urea using a UV/VIS Scanning UV-3100PC spectrometer (VWR, Pennsylvania, USA) according to Solomon et al. (2007). Samples for NH_4^+, NO_3^- + NO_2^-, and PO_4^{3-} were not duplicated, except those from January 22 and July 28, but urea samples collected on January 22 were duplicated. Nutrient samples for station 13S were not available. A subsample (~ 5 mL) from each sampling site was preserved with acidified Lugol's iodine solution for taxonomic identification. Counts were made with a Sedgewick-Rafter chamber (1 mL) on preserved samples using Zeiss PrimoStar microscopy (Zeiss, Oberkochen, Germany).

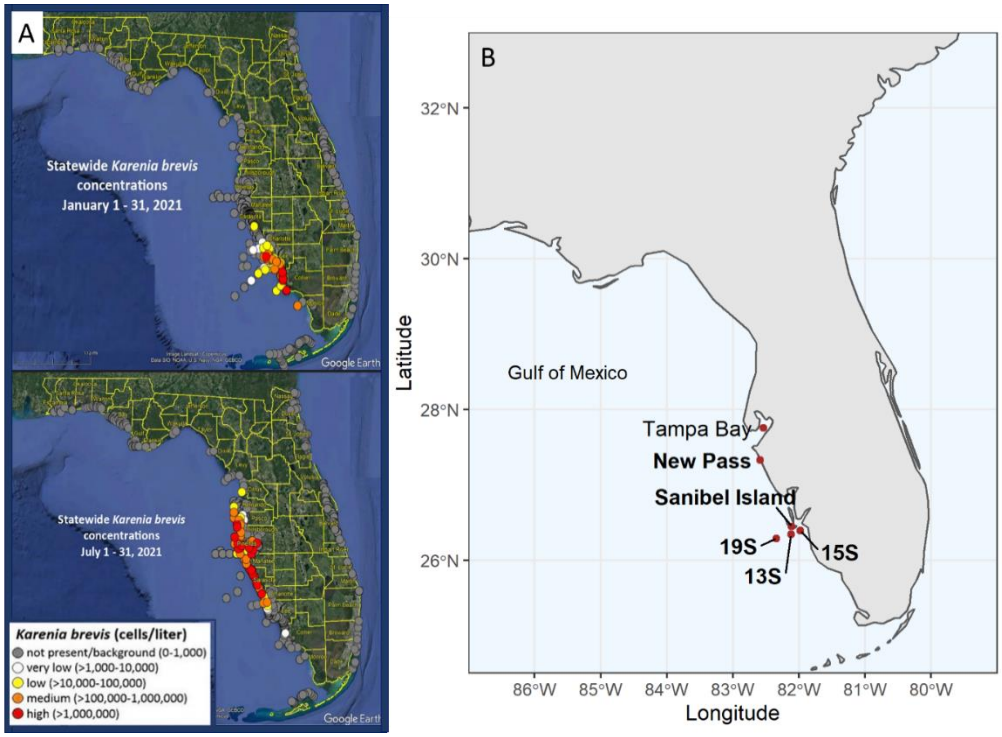

Figure 4.1. Locations of (A) the *Karenia brevis* bloom in January and July 2021 (Red Tide Status Maps produced by the Florida Fish and Wildlife Research Institute) and

(B) the study area during January and July 2021. Sampling locations are shown in bold. See Table S4.1 for details.

Experimental plan

Overview

Upon return to the laboratory and processing for ambient dissolved nutrients and Chl *a*, samples from all sites were exposed to a range of temperatures, N substrates and concentrations to assess photosynthetic performance and rates of N uptake (Fig. 4.2 and Table S4.1). Temperature variations were intended to both bracket and exceed the natural and extreme daily temperature fluctuations cells might experience due to diel vertical migration or surface water temperature warming. Concentrations of N were added over a range from sub-saturating to saturating. Although the saturating concentrations were above those normally experienced by the dinoflagellates, the unusual conditions such as the Piney Point spill or accumulations of decaying fish could provide elevated, if not sustained, pulses of nutrient.

Due to varying cell concentrations of the different samples, not all manipulations were undertaken on all samples (Table S4.1). Samples were held in either angled neck flasks (Corning, New York, USA) or polypropylene tubes. Also, due to the differences in ambient temperatures between the summer and winter assemblages, the specific range of temperatures to which samples were exposed experimentally varied, but all experiments included treatments ranging from 15^{o}C to $\geq$ 30^{o}C. Incubations were conducted in custom-made temperature-controlled water baths (Bay Instruments LLC, Maryland, USA), illuminated by LED lights with 100-150 μmol photons m^{-2} s^{-1}.

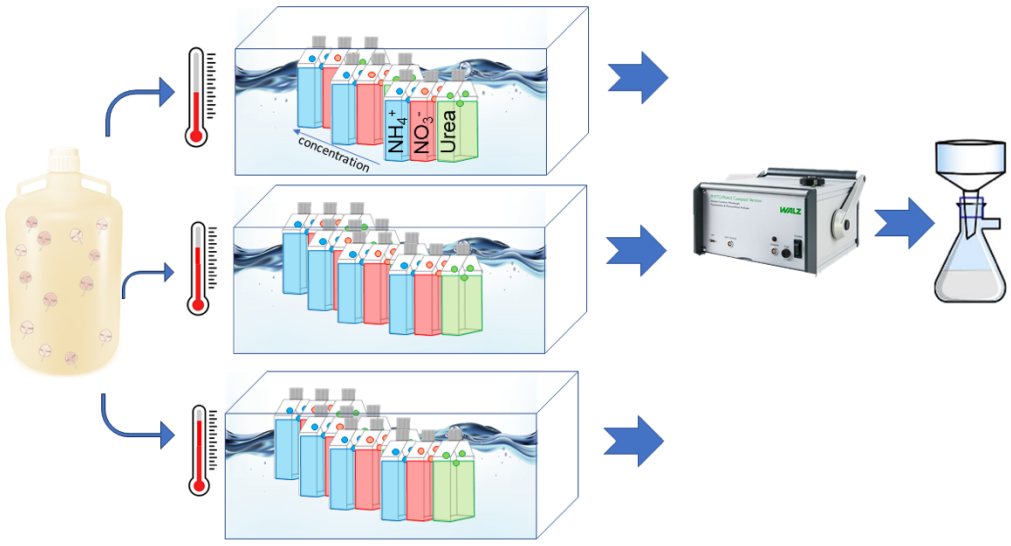

Figure 4.2. Experimental design to measure photosynthetic performance and ^{15}N uptake rates of the natural samples containing *K. brevis* collected during January and July 2021. Samples were enriched with different N substrates (symbolized here as different colors) and at different concentrations and incubated at different temperatures. After incubations, subsamples were taken for analysis by PAM fluorometry, and the remaining sample was filtered for ^{15}N uptake. See Table S4.1 for details.

Photosynthesis

After incubation, rates of photosynthesis were determined using Pulse-Amplitude-Modulation (PAM) fluorometry. Samples were dark acclimated for at least 20 min, and then fluorescence parameters were measured using a Phyto-PAM-II (Heinz Walz GmbH, Effeltrich, Germany). Based on appropriate calibration of algae-specific reference spectra, this fluorometer can measure photosynthetic responses and biomass of four different major classes of algae, including cyanobacteria, green algae,

brown algae, and phycoerythrin-containing algae, with a single measurement. In all samples, the brown algal signal dominated due to the dominance of *K. brevis* in each sample, as verified by microscopy. Rapid light curves were generated to monitor photosystem II (PSII) fluorescence emissions as a function of rapid changes in irradiance (20 s at each step from 1 to 500-700 μmol photons m^{-2} s^{-1}). Light intensities were calibrated with an ULM-500 Light Meter and Logger equipped with a micro quantum sensor (Heinz Walz GmbH, Effeltrich, Germany).

The following fluorescence parameters were analyzed by PAM fluorometry: maximum quantum yield of PSII photochemistry of dark-adapted samples, $F_v/F_m = (F_m - F_o)/F_m$; effective quantum yield of PSII photochemistry of illuminated samples, $YII = (F_m' - F)/F_m'$; quantum yield of regulated non-photochemical quenching, $YNPQ = (F/F_m') - (F/F_m)$; and quantum efficiency of non-regulated non-photochemical quenching, $YNO = F/F_m$, where F_m is the maximal fluorescence of dark-adapted samples, F_o is the minimal fluorescence of dark-adapted samples, F_v is the variable fluorescence of dark-adapted samples, F_m' is the light-acclimated maximum fluorescence, and F is the momentary fluorescence (Schreiber et al., 1994; Klughammer and Schreiber, 2008). It is generally assumed that YII + YNPQ + YNO sum to 1 (Klughammer and Schreiber, 2008). The relative electron transport rate (rETR) of PSII was calculated according to Schreiber et al. (1994). Rapid light curves were fitted to the models of Platt et al. (1980) to calculate $rETR_{max}$, maximum relative electron transport rate and I_k, the minimum saturating irradiance. All parameters were calculated and exported from the PhytoWin-3 Software (Heinz Walz GmbH, Effeltrich, Germany).

Nitrogen uptake

Samples were enriched with $^{15}NH_4^+$, $^{15}NO_3^-$ or ^{15}N-urea (Cambridge Isotope Laboratories, Inc., Massachusetts, USA), in a gradient of 4-6 concentrations from 0 to 50 µM-N per temperature (Table S4.1). No samples for N uptakes were collected at the January coastal sites. After incubation (1-2 h), samples were filtered onto pre-combusted (450°C, 2h) GF/F filters (Whatman, Maidstone, United Kingdom) to measure ^{15}N incorporation. Sample filters were first frozen, and subsequently dried overnight at 50°C and transferred into tin capsules (Costech Analytical Technologies, Inc., California, USA). Samples were analyzed by mass spectrometry at the University of California, Davis Stable Isotope Facility to yield isotope enrichment and carbon (C) and N content. Rates of N uptake were calculated according to Glibert and Capone (1993). The N uptake data were fitted to the Michalis-Menten formula using R Software to calculate the maximum absolute uptake rate per cell (ρ_{max}, pmol-N cell^{-1} h^{-1}) (package 'drc').

Statistical analysis

The photosynthetic parameters were compared between N substrates, seasons and temperatures using two approaches. First, comparisons were made for all samples for which N was enriched at a level of 10 µM-N. Second, comparisons were made using the averages of all N enrichments. This included the summer samplings (except July 29) and the coastal sites sampled in January.

N uptake rates were calculated as a function of N concentrations and only maximum absolute uptake rates per cell extracted from each curve were compared herein between different N treatments, temperatures, and seasons. Total C and N cell$^-$

[1] were averaged for different N concentrations at each temperature. These comparisons included all the summer stations and the Sanibel Island site in January.

All statistical analyses were performed using R software (R core team, 2022). The data were tested for two assumptions: normality (Shapiro-Wilk) and homoscedasticity (Levene's). The significance between different temperatures (15, 20, 25, 30°C (winter) or 15, 25, 30, 33°C (summer)) of the fluorescence and N uptake data were tested using one-way analysis of variance (ANOVA) with Tukey's honestly significant differences (HSD) *post hoc* comparisons. If data did not satisfy the normality assumption, a non-parametric Kruskal-Wallis's analysis of variance with Dunn's *post hoc* test was applied. The *p*-values were adjusted with the Benjamini-Hochberg method. For the data from January 22, and 27 and July 28, when different forms of N (NH_4^+, NO_3^- or urea) were tested in the same day, the significance between different N forms was also tested. Comparisons between coastal stations and Sanibel Island or between winter and summer were done using a *t*-test. If data did not satisfy the normality assumption, the Wilcoxon signed-rank test was applied.

Results

Environmental conditions

In January, surface water temperature was 20°C at the coastal stations and 23°C at the Sanibel Island site. In July, surface water temperature at the time of sampling was 27°C but warmed to > 30°C during the daytime.

Surface concentrations of $NO_3^- + NO_2^-$ and urea at all sites and samplings were < 1 µM-N, and were somewhat higher for NH_4^+, up to 3.01 µM-N, in July (Table 4.1).

The highest PO_4^{3-} concentration, 1.35 µM-P was observed in July, but ranged from 0.05 to 0.46 µM-P at all other times (Table 4.1).

Concentrations of Chl *a* varied substantially between times of sampling, both within and between seasons (Table 4.1). In January, Chl *a* was lower at the coastal stations than at Sanibel Island ($p < 0.05$). Due to the dense aggregation of cells that were sampled in July, Chl *a* was nearly 400 µg L^{-1} (Table 4.1).

In winter, the density of *K. brevis* was lower in the coastal stations compared to the Sanibel Island station. Cell abundance of *K. brevis* accounted for 67% (± 10%) of the total protist plankton community at the coastal stations, while it accounted for 76% at the Sanibel Island station (Table S4.2). Some diatoms were present in the January coastal (11% ± 8%, e.g., *Guinardia flacida*) and Sanibel Island samples (10%; e.g., *Pseudo-nitzschia* spp.). The contribution of other protists, such as unidentified flagellates, in the January samples ranged from 11% for the Sanibel Island sample to 21% (± 7%) for the coastal stations (Table S4.2).

In July 27 and 28, 95% of the total protist plankton were *Karenia* spp. (98% was *K. brevis* on July 27 and virtually all *Karenia* spp. were *K. brevis* on July 28). On July 29, *K. brevis* accounted for 89% of total algae with a small percentage of diatoms present (4-11%; e.g., *Skeletonema costatum*) (Table S4.2). Paired *K. brevis* cells were observed on July 28 and 29.

Table 4.1. Environmental parameters at sampling site. Values were averaged if duplicated samples were collected in duplicated (± standard deviation). NO_3^- + NO_2^-, NH_4^+, PO_4^{3-}, Chl *a*, and n.d. stand for nitrate + nitrite, ammonium, phosphate, chlorophyll *a* and no data.

		NO_3^- + NO_2^- (µM)	NH_4^+ (µM)	Urea (µM)	PO_4^{3-} (µM)	Chl *a* (µg L^{-1})	*Karenia* density (cells L^{-1})
	13S	n.d.	n.d.	n.d.	n.d.	4.0 ± 0.2	88,000
Coastal stations	15S	< 0.07*	0.23	0.67 ± 0.34	0.20	10.5 ± 0.0	206,667
Jan 22	19S	< 0.07*	0.15	0.69 ± 0.31	0.05	2.4 ± 0.0	30,000
	mean**	< 0.07*	0.19 ± 0.06	0.68 ± 0.27	0.13 ± 0.11	5.6 ± 3.8	108,222 ± 90,053
Sanibel Island Jan 27		0.11 ± 0.06	1.76 ± 1.03	0.27	0.30 ± 0.01	24.0 ± 2.2	520,000
New Pass July 21		0.74 ± 0.07	0.98 ± 0.29	0.09	0.24 ± 0.00	24.4 ± 1.2	n.d.
New Pass July 27		0.67 ± 0.25	2.58 ± 0.26	0.30	0.22 ± 0.01	75.9 ± 1.0	3,460,000
New Pass July 28		< 0.07*	2.08	0.02	1.35	397.0	15,000,000
New Pass July 29		< 0.07*	3.01 ± 0.95	0.01	0.46 ± 0.07	387.6	7,300,000

*If concentration of NO_3^- + NO_2^- was lower than detection limit, it is marked as < 0.07.
**Mean values were averaged from 15S and 19S values for nutrient concentrations.

Maximum photosynthetic yield

With the exception of the coldest treatment in the summer samples, F_v/F_m for all samples and treatments was maintained within the relatively narrow range of 0.28-0.48. Nevertheless, within this narrow range there were differences with temperature (Figs. 4.3, S4.1).

In the winter coastal station samples, F_v/F_m decreased significantly with increasing temperature when cells were enriched with NO_3^- ($p < 0.05$) (Fig. 4.3B, Table S4.3). For cells enriched with NH_4^+, those exposed to 30°C showed significantly reduced F_v/F_m compared to those exposed to 20°C ($p < 0.05$) (Fig. 4.3A) while no significant differences were found in the comparable urea-enriched cells ($p > 0.05$) (Fig. 4.3C). No differences between different N forms were found at each temperature except at 15°C in the winter coastal populations. The F_v/F_m of NH_4^+-treated cells were lower than those enriched with NO_3^- at 15°C ($p < 0.05$) (Table S4.3).

Regardless of whether comparisons were made using the 10 µM-N enrichments only or the averages of all N enrichments, the F_v/F_m values in July were comparable over the range of 25-33°C on July 27 and 28 and over the range of 25-30°C on July 21 ($p > 0.05$) (Figs. 4.3D-H, S4.1D-H). When values for all N enrichments were averaged, the F_v/F_m values measured at 15°C were significantly lower than values measured at warmer temperatures ($p < 0.05$) (Fig. S4.1D-H, Table S4.3). At two temperatures, 15°C and 30°C, differential responses on N forms were observed on July 28. At 15°C, values of F_v/F_m were lower in the urea-enriched cells compared to those of the NH_4^+- and NO_3^--treated cells ($p < 0.05$). On the other hand,

F_v/F_m values were significantly higher in urea-enriched cells compared to those of NH_4^+- and NO_3^--treated cells at 30°C ($p < 0.05$).

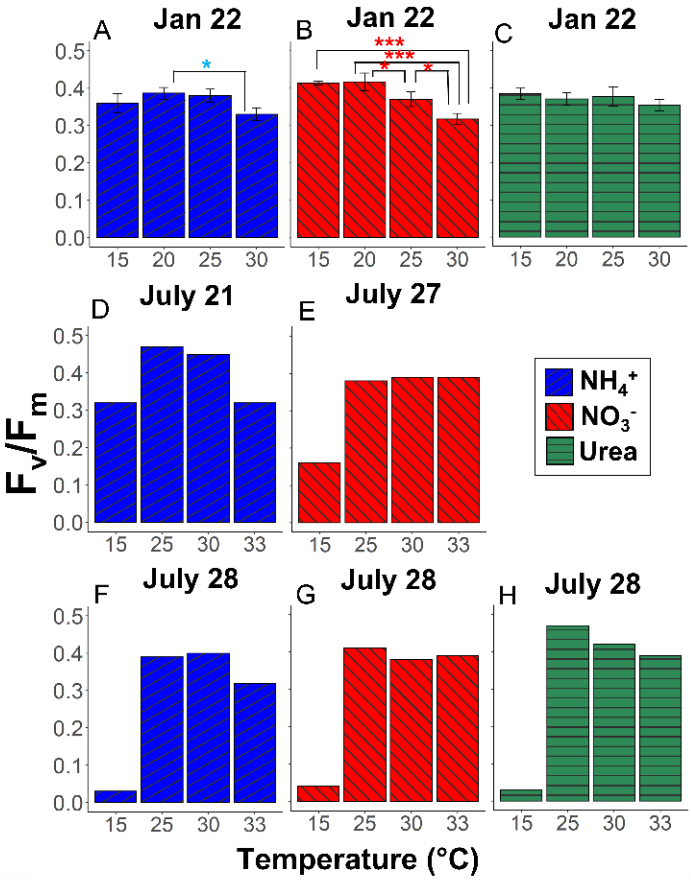

Figure 4.3. The maximum quantum efficiency of PSII photochemistry, F_v/F_m, of winter (January 22) and summer (July 21, 27, 28) *K. brevis* populations exposed to 4 different temperatures (15, 20, 25 30°C or 15, 25, 30, 33°C) and 3 different nitrogen forms (NH_4^+, NO_3^-, urea) at a level of 10 µM-N. The comparison of F_v/F_m between winter (3 coastal stations) and summer (New Pass) for the averaged N-enriched *K. brevis* populations is presented in Figure S4.1. Detailed values and related statistics are given in Table S4.3.

Photosynthesis-irradiance responses: $rETR_{max}$

Clear differences emerged between the different seasons in values of $rETR_{max}$ for samples exposed to different temperatures. In winter, a decline in $rETR_{max}$ was observed for the coastal populations at 30°C in the NH_4^+- and NO_3^--enriched cells, but not in the urea-enriched cells, although this trend was not statistically significant ($p > 0.05$) (Fig. 4.4A-C, Table S4.4). No differences between different N form treatments were observed for the winter populations at each temperature ($p > 0.05$).

For the summer populations, $rETR_{max}$ was depressed significantly at 15°C compared to values at 25-30°C ($p < 0.05$), regardless of how comparisons were made with respect to N enrichment (Figs. 4.4D-H, S2D-H, Table S4.4). However, unlike F_v/F_m, $rETR_{max}$ at 33°C was significantly lower than at 30°C except on July 21 (Fig. S4.2D). The effect of N form was only found at 25°C, revealing a higher value of $rETR_{max}$ of NO_3^--enriched cells compared to those of NH_4^+- and urea-enriched cells on July 28 ($p < 0.05$).

The averaged $rETR_{max}$ values of summer samples from all N treatments regardless of how calculated (10 µM-N samples: 17.3 ± 9.0 µmol electrons m^{-2} s^{-1}; all concentrations: 17.1 ± 8.2 µmol electrons m^{-2} s^{-1}) were lower than those of the winter samples (32.8 ± 10.2 µmol electrons m^{-2} s^{-1}) ($p < 0.01$). Even though $rETR_{max}$ values at 15°C were not included in summer values, averaged $rETR_{max}$ of summer populations (10 µM-N samples: 21.6 ± 4.6 µmol electrons m^{-2} s^{-1}; all concentrations: 21.1 ± 4.3 µmol electrons m^{-2} s^{-1}) were lower than averaged $rETR_{max}$ of winter samples ($p < 0.01$).

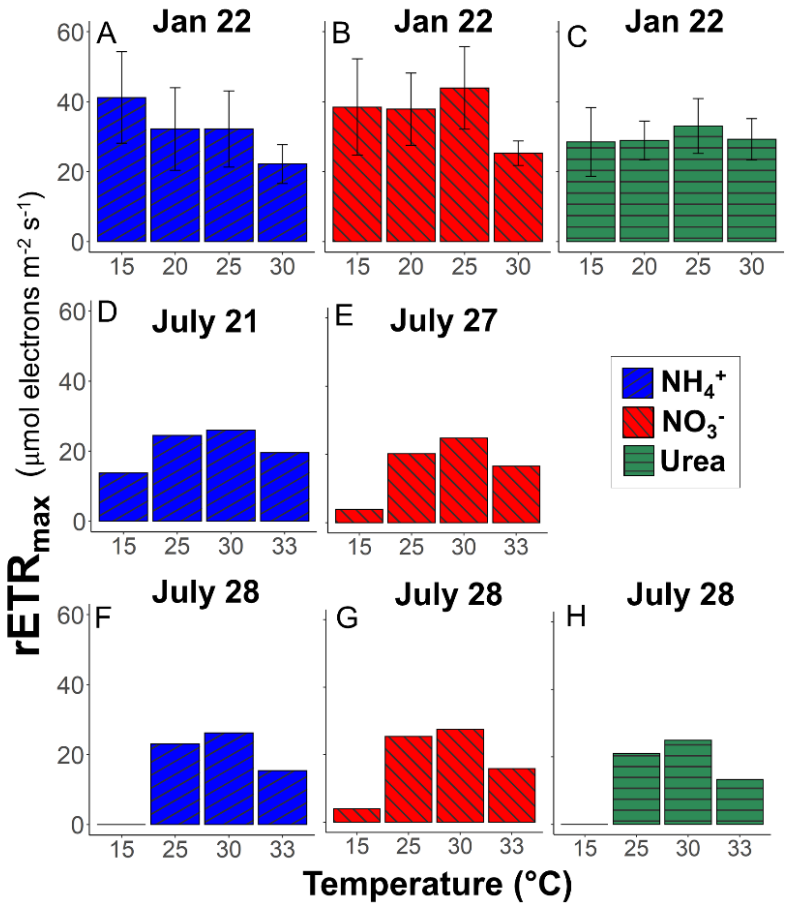

Figure 4.4. The maximum relative electron transfer rate, $rETR_{max}$, of winter (January 22) and summer (July 21, 27, 28) *K. brevis* populations exposed to 4 different temperatures (15, 20, 25 30°C or 15, 25, 30, 33°C) and 3 different nitrogen forms (NH_4^+, NO_3^-, urea) at a level of 10 µM-N. The comparison of $rETR_{max}$ between winter (3 coastal stations) and summer (New Pass) for the averaged N-enriched *K. brevis* populations is presented in Figure S4.2. Detailed values and related statistics are given in Table S4.4.

Quenching and heat dissipation

While values of F_v/F_m were maintained in both summer (except at 15°C) and winter within a relatively narrow range, seasonal differences were clear between summer and winter in the fractions of YNPQ and YNO.

Overall, in winter, YNO of the coastal stations averaged 0.63 (± 0.04) for all treatments enriched with 10 µM-N (Fig. 4.5A-C, Table S4.5). The YNO at 30°C was the highest regardless of N forms on January 22 ($p < 0.05$). YNPQ of the winter populations were not significantly different between temperatures (Fig. 4.6A-C and Table S4.6). At each temperature, no differences in YNO and YNPQ were found between different N substrate treatments ($p > 0.05$).

In contrast, for the summer populations, values of YNO were generally higher and values of YNPQ were generally lower than those of the winter populations, regardless of how the N enrichment treatments were compared (Figs. 4.5-6D-H, S4.3-4D-H). Thermal responses were also found within each N treatment. At the coolest temperature, 15°C, YNO was the highest, especially when cells were treated with urea ($p < 0.01$) (Table S4.5). Generally, when all N enrichment treatments were compared, YNO over the range of 25-33°C were comparable (Fig. S4.3D-H). No differences of YNPQ between temperatures were found on July 21 and July 27 (Fig. S4.6D-E, Table S4.6). On the other hand, on July 28, YNPQ was the lowest at 15°C ($p < 0.05$) while values at 25-33°C were comparable (Fig. S4.4F-H).

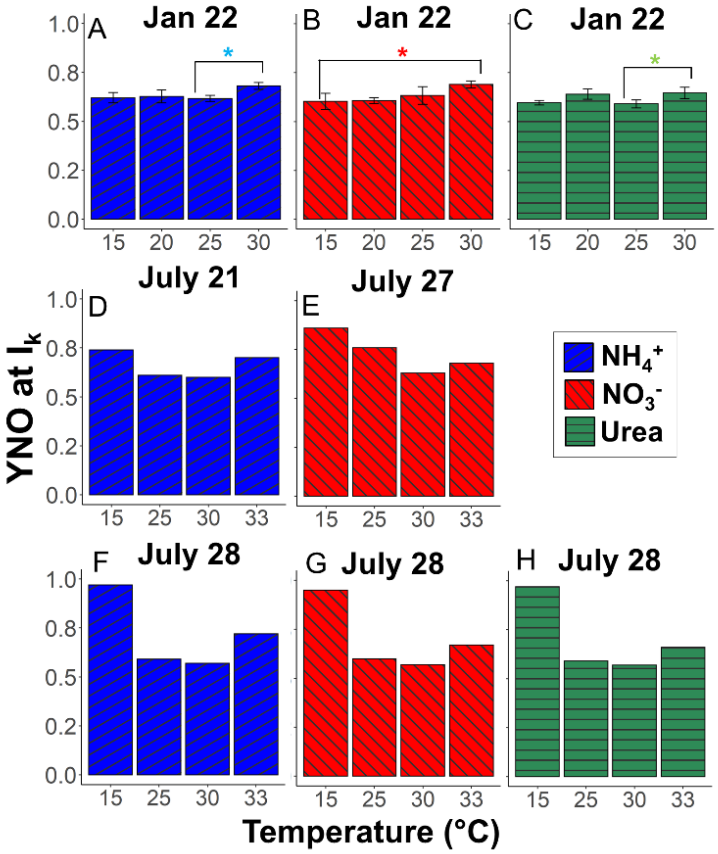

Figure 4.5. The quantum yield of non-regulated non-photochemical quenching, YNO, of winter (January 22) and summer (July 21, 27, 28) *K. brevis* populations exposed to 4 different temperatures (15, 20, 25 30°C or 15, 25, 30, 33°C) and 3 different nitrogen forms (NH_4^+, NO_3^-, urea) at a level of 10 µM-N. The comparison of YNO between (3 coastal stations) and summer (New Pass) for the averaged N-enriched *K. brevis* populations is presented in Figure S4.3. Detailed values and related statistics are given in Table S4.5.

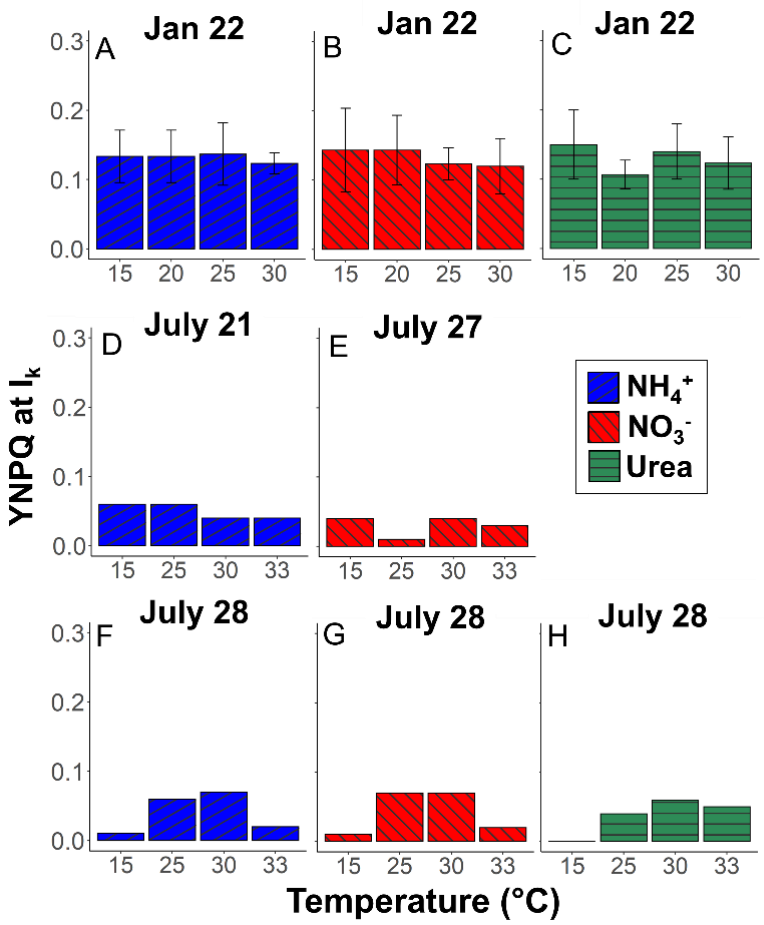

Figure 4.6. The quantum yield of regulated non-photochemical quenching, YNPQ, of winter (January 22) and summer (July 21, 27, 28) *K. brevis* populations exposed to 4 different temperatures (15, 20, 25 30°C or 15, 25, 30, 33°C) and 3 different nitrogen forms (NH_4^+, NO_3^-, urea) at a level of 10 µM-N. The comparison of YNPQ between winter (3 coastal stations) and summer (New Pass) for the averaged N-enriched *K. brevis* populations is presented in Figure S4.4. Detailed values and related statistics are given in Table S4.6.

Nitrogen uptake as a function of temperature: ρ_{max}

In both winter and summer, the maximum N uptake rates per cell, $\rho_{max,}$ of all N forms generally increased with increasing temperatures, but there were differences (Fig. 4.7, Table S4.7). In winter, with increasing temperature, ρ_{max} increased for NH_4^+ and for urea, but it did not increase for NO_3^- uptake (Fig. 4.7A-C). Of the N forms, ρ_{max} of NO_3^- was the highest at 25°C compared to other temperatures (Fig. 4.7B). From 15°C to 30°C, ρ_{max} was 2.0-fold higher for NH_4^+ uptake and 1.2-fold higher for urea uptake compared to ρ_{max} of NO_3^-. Overall, the winter Sanibel population had the highest value of ρ_{max} of NH_4^+ (0.00036 ± 0.00007 pmol-N $cell^{-1}$ h^{-1}) compared with the rates of NO_3^- (0.00019 ± 0.00005 pmol-N $cell^{-1}$ h^{-1}) or urea (0.00013 ± 0.00004 pmol-N $cell^{-1}$ h^{-1}) (Table S4.7).

Generally, in summer, ρ_{max} increased with increasing temperature, especially for the chemically reduced forms of N (Fig. 4.7D-H). From 15°C to 33°C, ρ_{max} of NH_4^+ and urea was 3.3- and 3.0-fold higher than that of NO_3^- on July 28. Overall, the averaged ρ_{max} values across temperatures was the highest for NH_4^+ (0.00013 ± 0.00008 pmol-N $cell^{-1}$ h^{-1}), followed by urea (0.00010 ± 0.00007 pmol-N $cell^{-1}$ h^{-1}) and NO_3^- (0.00006 ± 0.00004 pmol-N $cell^{-1}$ h^{-1}) (Table S4.7).

Mean ρ_{max} of NH_4^+ and NO_3^- at all measured temperatures of the summer populations was significantly lower than those of the winter populations ($p < 0.01$) while no significant differences were found for ρ_{max} urea ($p > 0.05$).

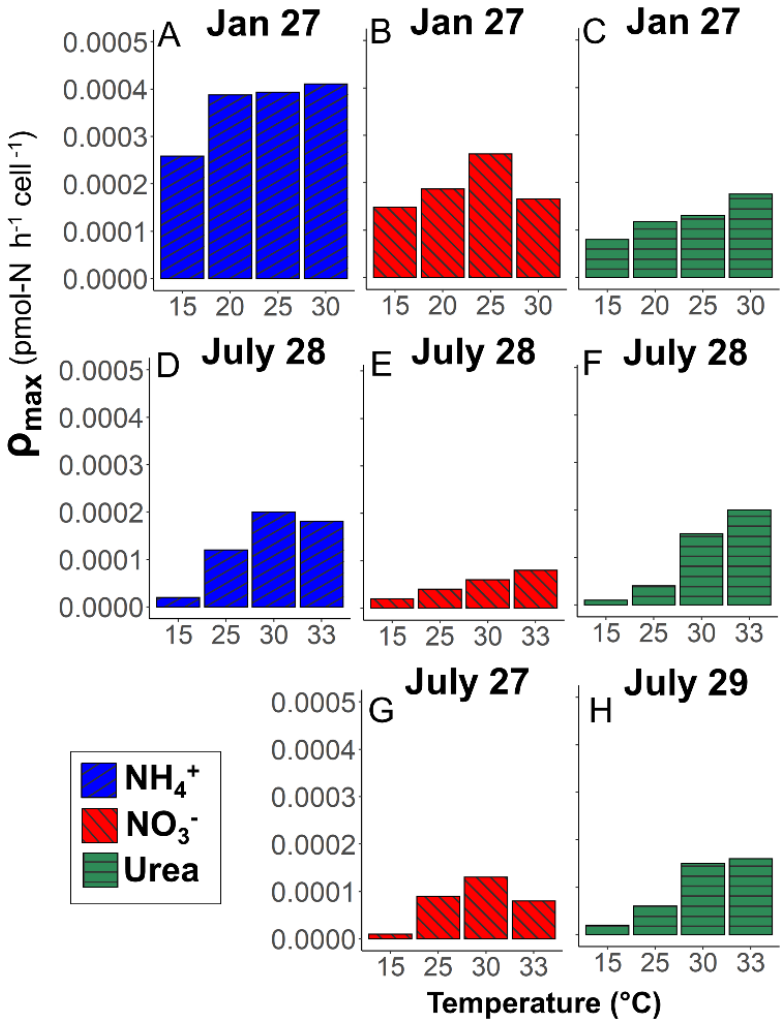

Figure 4.7. The maximum absolute uptake rate, ρ_{max}, of winter (January 27) and summer (July 27, 28, 29) *K. brevis* populations exposed to 4 different temperatures (15, 20, 25 30°C or 15, 25, 30, 33°C) and 3 different nitrogen forms (NH_4^+, NO_3^-, urea). Detailed values are given in Table S4.7.

Carbon and nitrogen cell content

When samples from all treatments are compared by season, it was apparent that smaller cells were present in summer than in winter, and these cells had a lower N content, leading to a higher C:N ratio in summer compared to winter.

In the winter Sanibel Island population, no significant differences in total C and N (pmol cell^{-1}) were found across temperature and N treatments ($p > 0.05$) (Figs. 4.8-9A-C, Table S4.8). Thus, molar C:N ratios were also comparable across the temperature range, from 8.7 to 9.0 ($p > 0.05$).

In summer, total C content (pmol cell^{-1}) was comparable across the temperature gradient for the NO_3^-- and NH_4^+-enriched cells ($p > 0.05$), but not in the cells treated with urea ($p < 0.05$) (Figs. 4.8D-H, Table S4.8). The total C content of urea-enriched cells was lower at 15°C compared to that at 30-33°C ($p < 0.05$) (Fig. 4.8F, H). In the case of cellular N (pmol cell^{-1}), there were no consistent trends between temperature or N substrate treatments (Fig. 4.9D-H, Table S4.8). Overall, total cellular N was highest in the cells enriched with urea compared with NO_3^-- and NH_4^+-enriched cells, although only that for NO_3^- was significantly different ($p < 0.01$). Thus, the molar C:N ratio increased from July 21 (10.8 ± 0.7) and July 27 (12.0 ± 1.5) to July 28 (15.4 ± 1.5) and July 29 (15.5 ± 1.7).

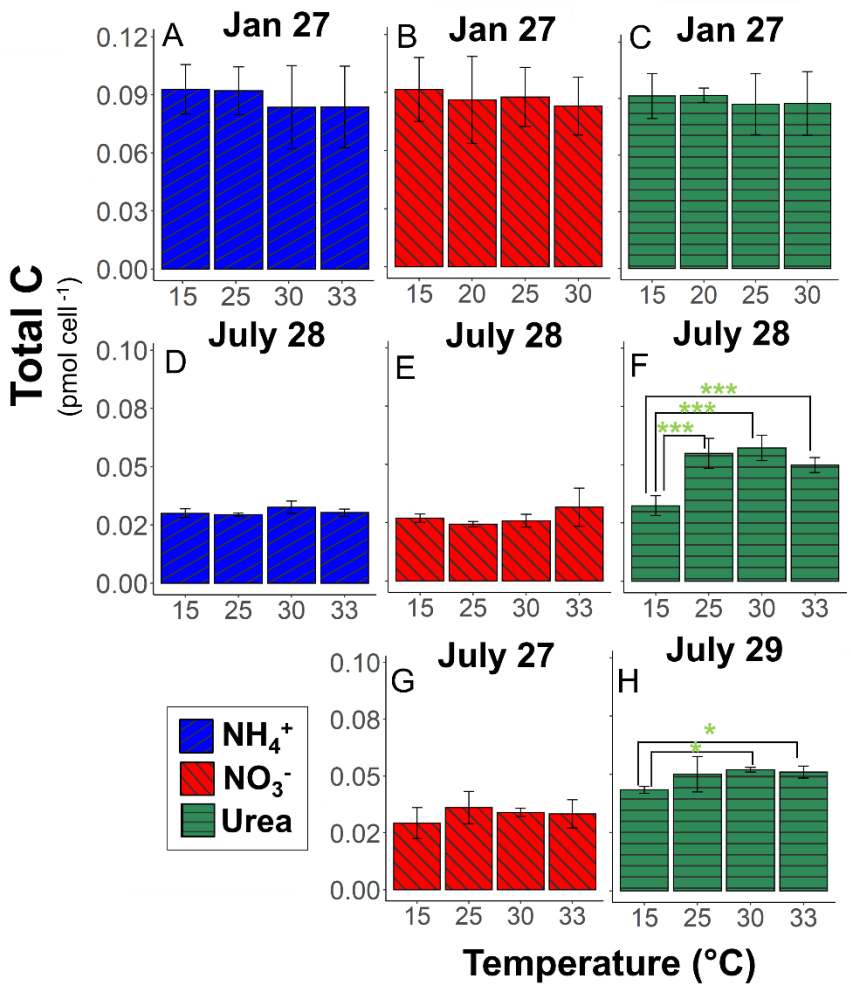

Figure 4.8. Total carbon (C) cell^{-1} of winter (January 27) and summer (July 27, 28, 29) *K. brevis* populations exposed to 4 different temperatures (15, 20, 25 30°C or 15, 25, 30, 33°C) and 3 different nitrogen forms (NH_4^+, NO_3^-, urea). Note that the scale of X axis is different depending on season. Detailed values and related statistics are given in Table S4.8.

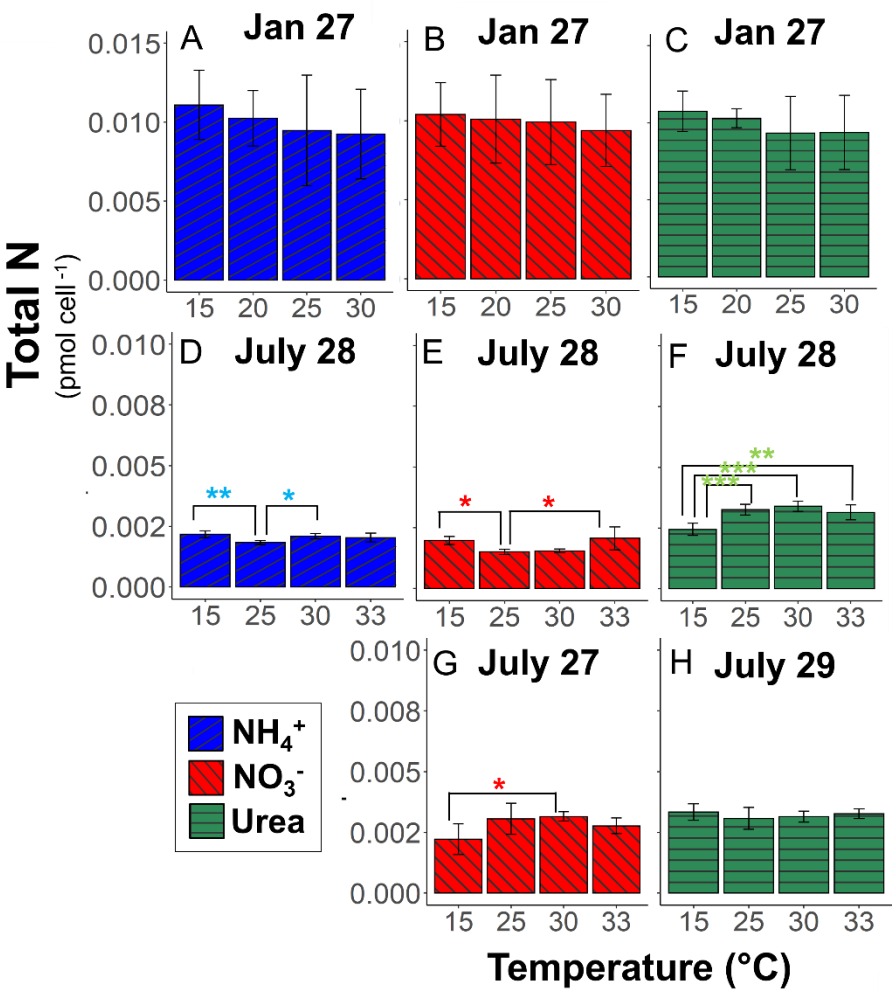

Figure 4.9. Total nitrogen (N) cell^{-1} of winter (January 27) and summer (July 27, 28, 29) *K. brevis* populations exposed to 4 different temperatures (15, 20, 25 30°C or 15, 25, 30, 33°C) and 3 different nitrogen forms (NH_4^+, NO_3^-, urea). Note that the scale of X axis is different depending on season. Detailed values and related statistics are given in Table S4.8.

Discussion

During July 2021, a massive *K. brevis* bloom with cell abundances > 1.0 x 10^6 cells L^{-1} was sustained along the Gulf Coast of Florida. It has historically been thought that the supra-optimal temperature of the hot summer months is one of the barriers that prevents *K. brevis* from flourishing during this time (Vargo, 2009). Although the summer *K. brevis* populations were able to form massive blooms during the summer of 2021, these cells were photosynthetically and nutritionally stressed compared to late winter populations. Although this aspect of the original hypothesis was supported, differences in the effects of N enrichment and N form were not as large as had been hypothesized.

Importance of thermal history

Although *Karenia brevis* has a relatively narrow optimal thermal range, 22-28°C, the data presented herein supports their capacity for short-term acclimation to a wide range of temperatures (Figs. 4.3-6, S4.1-4). Wilson (1955) found that if temperature change is gradual, e.g., 1°C h^{-1}, thermal tolerance of *K. brevis* can be extended to the lower end of temperature range (e.g., 8°C). Aldrich (1960) suggested that the thermal history of *K. brevis* influences the growth and survival tolerance: cultures acclimated to 19°C survived longer at 12°C than cultures acclimated to 25°C. The January *K. brevis* coastal station populations possibly were acclimated to ~20°C. Therefore, the cool water adapted coastal populations did not show any stress responses at 15°C, but showed moderate heat stress at 30°C. On the other hand, the warm-water adapted (~27°C) summer New Pass populations showed significant stress responses at 15°C, but not at 30-33°C.

The optimal temperature for photosynthesis (as well as growth) can increase with growth temperature (Hikosaka et al., 2006). However, only a few laboratory experiments have reported the survival of this species at > 30°C and even then, viability declined sharply over this thermal barrier with no growth observed even though cells were surviving (e.g., Kusek et al., 1999). In this study, comparable F_v/F_m, but relatively lower $rETR_{max}$ at 33°C compared to 25-30°C, suggests that summer *K. brevis* populations could tolerate 33°C, at least for a short time (several hours) and, once PSII of the cells are relaxed (e.g., dark-adapted, oxidized), they could process absorbed light energy as efficiently as those at 25-30°C.

On the other hand, a sharp decrease of both F_v/F_m and $rETR_{max}$ at 15°C of the summer populations suggests that these populations were experiencing low-temperature induced photoinhibition. Reduced C assimilation (as well as N assimilation) at low temperatures can lead to excess light energy in the photosynthetic apparatus, causing high dissipation of absorbed light energy as heat and fluorescence emission. Dissipating excess energy through non-regulated mechanisms, YNO, mainly occurs due to closed PSII reaction centers or damaged PSII, while YNPQ is a photoprotective pathway that operates mainly through converting a proportion of PSII antennae complex (via trans-thylakoid pH gradient and xanthophyll cycling) (Hendrickson et al., 2004; Klughammer and Schreiber, 2008). Therefore, significantly higher YNO at 15°C, especially the high YNO at the expense of YNPQ (e.g., July 28), reflects a suboptimal capacity of photoprotective mechanism at the PSII antenna level, possibly representing damaged PSII.

Clear differences were found between the January and July population fluorescence parameters (Figs. 4.3-6, S4.1-4). Even though the size of summer *K. brevis* bloom was much larger, the rates of photosynthesis, as $rETR_{max}$, were lower, and more of the absorbed energy was dissipated as heat. In particular, a higher portion of energy was dissipated through YNO that can be associated with photodamage of the summer cells, indicating photosynthetically stressed summer *K. brevis* populations.

Nitrogen form effects

As consistent with previous studies, the maximum uptake rate of N per cell, ρ_{max}, was higher when the populations were treated with chemically reduced forms of N, NH_4^+ or urea, compared with the oxidized form of N, NO_3^- (Sinclair et al., 2009; Bronk et al., 2014; Heil et al., 2014a), especially at the warmer temperatures (Fig. 4.7). The increases in ρ_{max} of NH_4^+ and urea as a function of warming temperatures were also generally higher than the increase in ρ_{max} of NO_3^- across the same temperature range. Such differences are consistent with the sensitivities of different N metabolic processes with temperature. The enzyme involved in NH_4^+ assimilation, GS-GOGAT typically has a positive relationship to temperature (generally between 12°C and 25°C) (Glibert et al., 2016 and references therein). Urease, the enzyme involved in urea metabolism, also has a positive relationship with temperature and has been shown to have a higher thermostability at > 20-30°C in some dinoflagellates (Fan et al., 2003). On the other hand, the enzyme involved in NO_3^- reduction, NO_3^- reductase (NR) which converts NO_3^- to NO_2^-, has a negative relationship with temperature (generally between 12°C and 25°C) (Glibert et al., 2016 and references

therein) or shows a unimodal thermal response with a sharper decline in supra-optimal temperature (e.g., 30-35°C) compared to suboptimal temperatures (e.g., 0-5°C). That is, NR is less tolerant to heat than cold (Kristiansen, 1983; Witt et al., 1999). Therefore, the metabolism of reduced forms of N, NH_4^+ and urea, would be expected to be higher at warmer temperatures while the metabolism of NO_3^- would be higher at cooler temperatures.

Although the rates of ρ_{max} of NH_4^+ were the highest of the N substrates compared (except 33°C), total C and N $cell^{-1}$ were higher in summer *K. brevis* populations treated with urea (Fig. 4.8-9), possibly indicating the high assimilation efficiency of urea. Sinclair et al. (2009) examined the rates of N uptake and N assimilation into protein of three strains of *K. brevis* grown on NO_3^-, NH_4^+ and urea. Although that experiment was conducted only at 22°C, it showed 31% higher assimilation efficiency of urea than that of NH_4^+ and 64% higher efficiency than that of NO_3^-. Overall, the metabolism of reduced forms of N (taken up and assimilated) were two times higher than that of the oxidized form (Sinclair et al. 2009). Although direct assimilation efficiency of urea was not measured in the present study, the relatively high content of total C and N $cell^{-1}$ in urea-enriched cells may be associated with higher level of urea assimilation. High assimilation efficiency of urea might be due to the presence of the urea cycle in this dinoflagellate (Dagenais-Bellefeuille and Morse, 2013) and several candidate enzymes involved in the urea cycle have been identified in *K. mikimotoi* (Shi et al., 2021) and *K. brevis* (Morey et al., 2011). In diatoms, a full urea cycle has been described and appears to play a role in C and N redistribution via the tricarboxylic acid cycle and GS-GOGAT (Allen et al., 2011;

Glibert et al. 2016). If the urea cycle in *K. brevis* has the same function, the internal reallocation of C and N may promote synthesis of biomass (C and N) more with urea than with other N substrates, especially at warmer waters. Ambient urea concentrations are typically very low, but recycling from decaying biomass and dead fish that are associated with *K. brevis* blooms may provide these cells with such a source (e.g., Heil et al. 2014a).

Unlike the findings from Ahn and Glibert (2022), differential responses depending on N forms were less obvious in photosynthetic parameters. Although the values of F_v/F_m in urea-enriched cells were the highest at 30°C compared to those of NO_3^-- and NH_4 -enriched cells in summer samples, at the highest temperature, 33°C, no differences were found in any fluorescence parameters. However, the *K. mikimotoi* cultures from Ahn and Glibert (2022) study were non-nutrient limited, exponential phase cells, while *K. brevis* populations tested here were derived from nutrient limited conditions and given only short exposure periods to N enrichment.

Nutritionally stressed summer populations

Total C and N $cell^{-1}$ values were significantly lower in the summer populations compared to the winter Sanibel Island population. It is of note that the cell size of the summer populations was smaller than that of the winter population. Heil et al. (2004) reported *Karenia* can change their cell size by a factor of two depending on environmental factors and they described some of these small cells as ‘gamete-like’. However, vegetative cells, gametes, and planozygotes of *K. brevis* are morphologically very similar and hard to differentiate in the field (Cuadrado et al., 2019). In addition, their photo-physiology also could be similar. Persson et al. (2021)

reported that F_v/F_m of vegetative cells and gametes in dinoflagellate *Scrippsiella lachrymosa* were not different. Indeed, some paired cells were found under light microscopy on July 28 and 29 samples. Limitation by N is one of the important stimuli for gamete formation (Brawley and Johnson, 1992). In this study, the C:N ratio was significantly higher in the summer populations than in the winter population, implying N limitation of the summer populations. Another possible explanation is that the winter Sanibel Island population was mixed more (~11%) with other planktonic protists such as unidentified microflagellates and their physiological responses can differ from those of *K. brevis* although the contribution of such cells to the total protist community remained low.

Karenia brevis has also been shown to be mixotrophic with the capability of grazing *Synechococcus* spp. (e.g., Jeong et al. 2005, Glibert et al. 2009). *Synechococcus* spp. generally grows well in warm waters, and it is well documented to thrive on the West Florida Shelf (Wawrik et al., 2009). An inverse relationship between the abundance of *K. brevis* and that of *Synechococcus* was previously shown on the West Florida Shelf in late spring through signature pigment distributions (Heil et al. 2007). While no data are available to assess use of mixotrophic nutrition by *K. brevis* during the 2020-2021 bloom, experiments are underway to explore the temperature dependence of this process.

Conclusions

The summer of 2021 was unusual in the prolonged summer *K. brevis* bloom that was able to be sustained in temperatures higher than its thermal niche. Although the biomass of summer *K. brevis* populations was significantly higher, $rETR_{max}$ and

ρ_{max} were substantially reduced relative to the winter populations, implying photosynthetically and nutritionally stressed summer cells. The data herein provide evidence that photosynthetic performance can be affected by thermal history, shifting the window of optimal range for photosynthesis. However, differences in photosynthetic parameters as a function of N forms were less clear. Both the winter and summer populations of *K. brevis* showed higher ρ_{max} of NH_4^+ or/and urea compared to NO_3^-. The higher increasing rates in ρ_{max} with rising temperature (from 15°C to 30-33°C) with chemically reduced forms of N may be a function of the different optimal temperature for the different enzymes related to each N form. The C and N cell^{-1} were also remarkably lower in summer populations but, when populations were treated with urea, relatively higher C and N cell^{-1} were observed. Recent modeling efforts (Chen et al. 2023) suggest that nutrients from the Piney Point effluent spill may have been remineralized over the summer, following an initial but short-lived bloom of diatoms, thus providing a large source of NH_4^+ to sustain *K. brevis* in the Tampa Bay region for many months. The extent to which this was a source of N that also helped to sustain *K. brevis* in the offshore waters is at yet unknown, but tidal and other exchange at the mouth of Tampa Bay would imply that this was at least a potential source of N that may have contributed to *K. brevis* during the summer (Morrison et al. 2023).

Appendix II: Supplementary Material

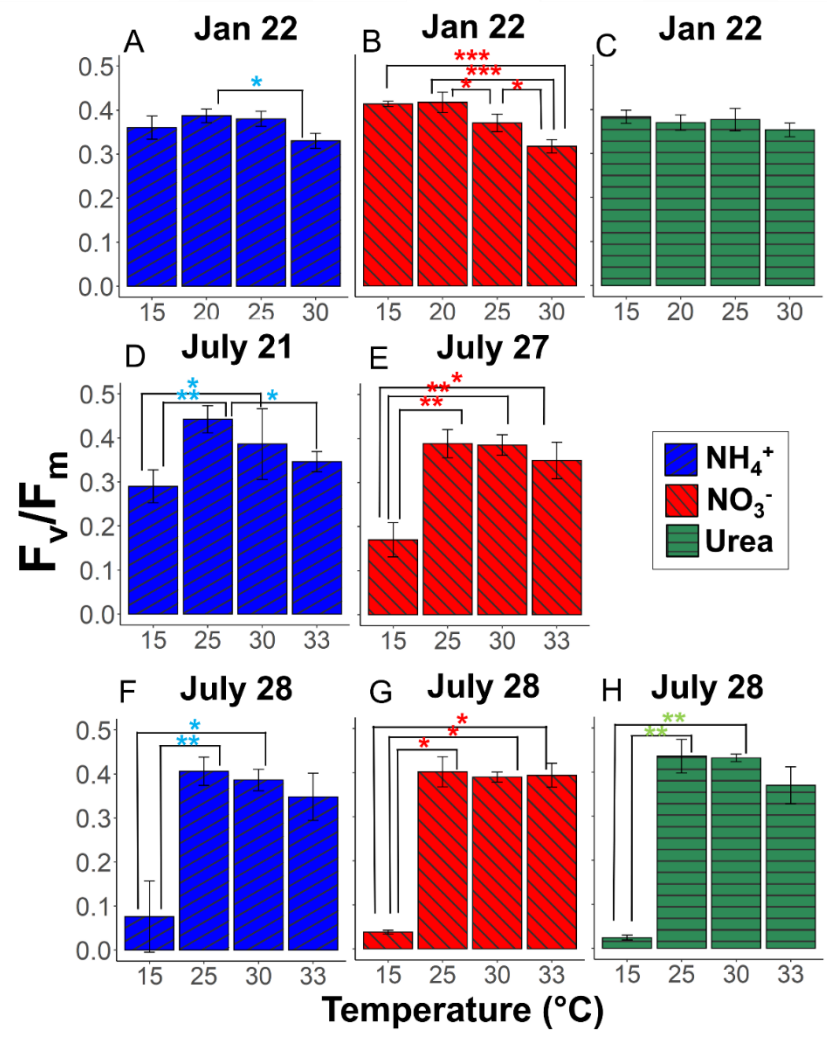

Figure S4.1. The maximum quantum efficiency of PSII photochemistry, F_v/F_m, of winter (January 22) and summer (July 21, 27, 28) *K. brevis* populations exposed to 4 different temperatures (15, 20, 25 30°C or 15, 25, 30, 33°C) and 3 different nitrogen forms (NH_4^+, NO_3^-, urea). Note that, at each temperature, January 22 values were averaged from 3 different coastal stations that were pulsed with 10µM, while July samples were averaged from 5 - 6 concentrations at each temperature.

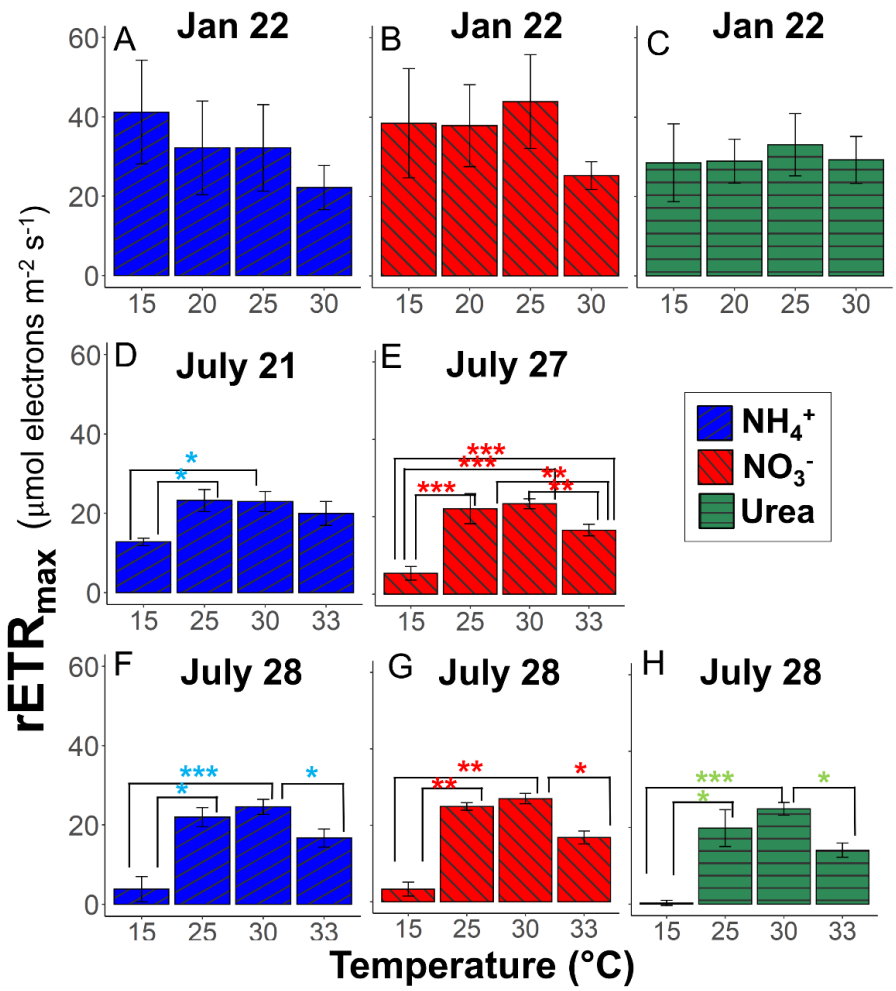

Figure S4.2. The maximum relative electron transfer rate, $rETR_{max}$, of winter (January 22) and summer (July 21, 27, 28) *K. brevis* populations exposed to 4 different temperatures (15, 20, 25 30°C or 15, 25, 30, 33°C) and 3 different nitrogen forms (NH_4^+, NO_3^-, urea). Note that, at each temperature, January 22 values were averaged from 3 different coastal stations that were pulsed with 10µM, while July samples were averaged from 5 - 6 concentrations at each temperature.

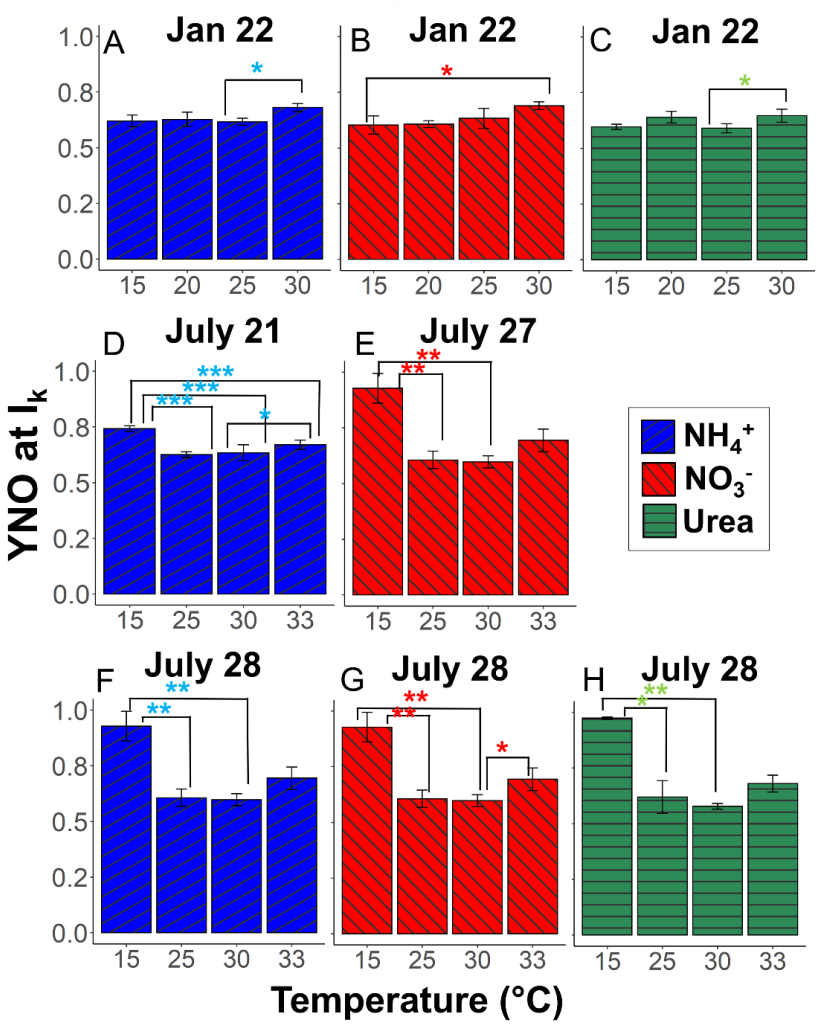

Figure S4.3. The quantum yield of non-regulated non-photochemical quenching, YNO, of winter (January 22) and summer (July 21, 27, 28) *K. brevis* populations exposed to 4 different temperatures (15, 20, 25 30°C or 15, 25, 30, 33°C) and 3 different nitrogen forms (NH_4^+, NO_3^-, urea). Note that, at each temperature, January 22 values were averaged from 3 different coastal stations that were pulsed with 10µM, while July samples were averaged from 5 - 6 concentrations at each temperature.

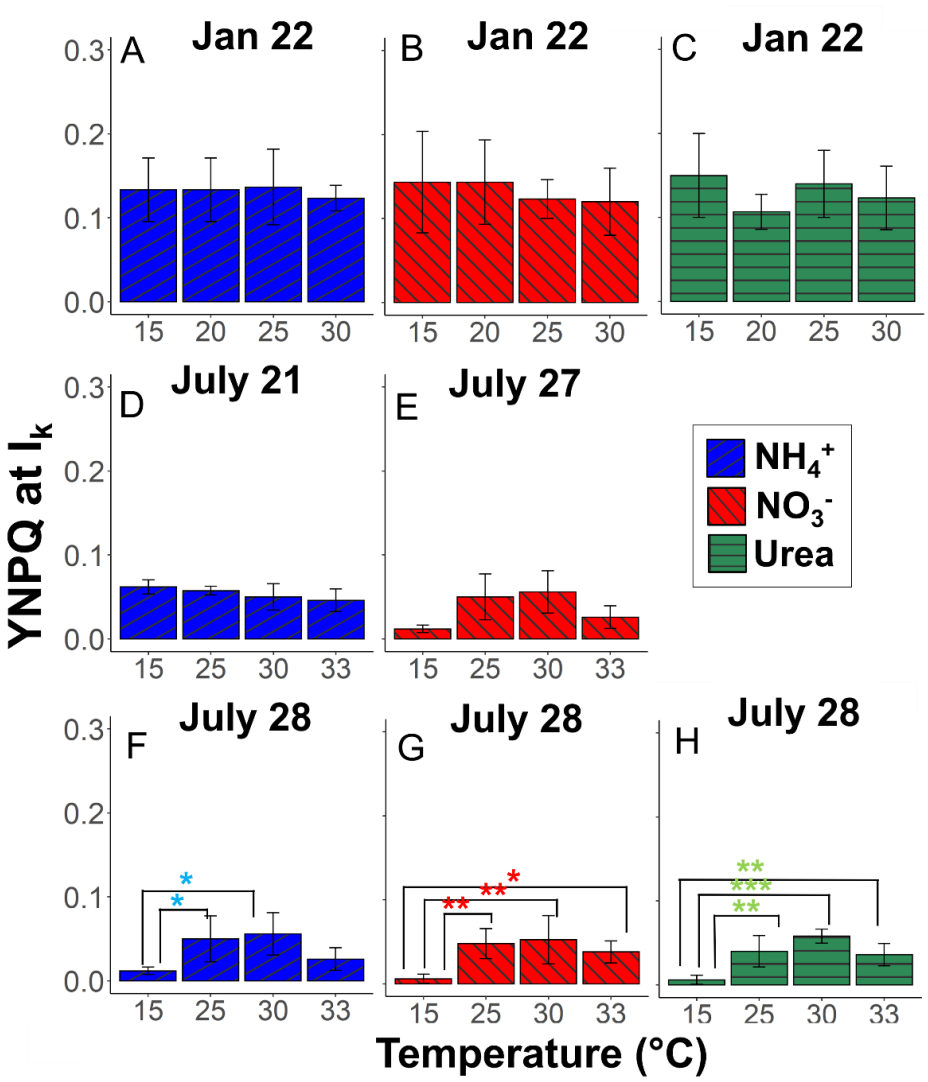

Figure S4.4. The quantum yield of regulated non-photochemical quenching, YNPQ, of winter (January 22) and summer (July 21, 27, 28) *K. brevis* populations exposed to 4 different temperatures (15, 20, 25 30°C or 15, 25, 30, 33°C) and 3 different nitrogen forms (NH_4^+, NO_3^-, urea). Note that, at each temperature, January 22 values were averaged from 3 different coastal stations that were pulsed with 10µM, while July samples were averaged from 5 - 6 concentrations at each temperature.

Table S4.1. Sampling and experimental manipulation information. N, NO_3^-, NH_4^+ and PAM stand for nitrogen, nitrate, ammonium and pulse-amplitude-modulation, respectively.

Date	Location	Temperature (°C)	Treatment	N concentration (µM) for ^{15}N uptake	N concentration (µM) for PAM fluorometry
22-Jan	*Coastal stations	15,20,25,30	^{15}N-NO_3^-, NH_4^+, Urea		10
27-Jan	Sanibel Island	15,20,25,30	^{15}N-NO_3^-, NH_4^+, Urea	1, 5, 10, 20	
21-Jul	New Pass	15,25,30,33	^{15}N-NH_4^+	0, 1, 5, 10, 20, 50	1, 5, 10, 20, 50
27-Jul	New Pass	15,25,30,33	^{15}N-NO_3^-	0, 1, 5, 10, 20, 50	0, 1, 5, 10, 20, 50
28-Jul	New Pass	15,25,30,33	^{15}N-NO_3^-, NH_4^+, Urea	1, 5, 10, 20, 50	1, 5, 10, 20, 50
29-Jul	New Pass	15,25,30,33	^{15}N-Urea	1, 5, 10, 20, 50	

*Coastal stations: 13S:26.33900°N -82.11900° W; 15S: 26.3896N, -81.9800W; 19S: 26.28625N, -82.34284W

Table S4.2. List and abundance of protist plankton taxa identified with light microscopy. Unit is cells L^{-1}.

	January coastal stations			January Sanibel Island	New Pass		
	CS 13S	CS 15S	CS 19S		27-Jul	28-Jul	29-Jul
Dinoflagellate							
Karenia brevis	88,000	206,667	30,000	520,000	3,253,333	15,000,000	7,300,000
Karenia mikimotoi					6,667		
Karenia spp.					33,333		
Prorocentrum micans		6,667			6,667		
Gymnodinum sp.				10,000	6,667		
Gyrodinium sp.				5,000			
Unkown dinoflagellate		6,667					
Diatom							
Coscinodiscus sp.					13,333		
Guinardia flacida	4,000						
Asterionelopsis glacialis				10,000			
Cylindrotheca clostridium				5,000	13,333		
Pleurosigma sp.					13,333		
Pseudo-nitzschia	4,000	20,000		25,000		20,000	40,000
Leptocylindrum minimus						160,000	
Rhizosolenia sp.			10,000		13,333	60,000	
Skeletonema costatum					93,333	360,000	400,000
Chaetoceros sp.					6,667	180,000	420,000
Unidentified pennate diatom				30,000			20,000
Others							
Dictyocha				5,000			
Flagellate	8,000	93,333	10,000	70,000	6,667		20,000
Ciliate	4,000				6,667		
Radiolarian	4,000						

*CS=Costal Station: 13S:26.33900°N -82.11900° W; 15S: 26.3896N, -81.9800W; 19S: 26.28625N, -82.34284W

Table S4.3. The averaged maximum photochemical efficiency of PSII, F_v/F_m at each temperature. The significance between different temperature was tested using one-way analysis of variance (ANOVA). If data did not satisfy the normality assumption, a non-parametric Kruskal-Wallis's analysis of variance was applied. Significant results are shown in bold.

	January coastal stations			**New Pass**				
	22-Jan			**21-Jul**	**27-Jul**	**28-Jul**		
	NH_4^+	**NO_3^-**	**Urea**	**NH_4^+**	**NO_3^-**	**NH_4^+**	**NO_3^-**	**Urea**
15°C	0.36 ± 0.03	0.41 ± 0.01	0.38 ± 0.02	0.29 ± 0.04	0.17 ± 0.04	0.08 ± 0.08	0.04 ± 0.00	0.02 ± 0.01
20°C	0.39 ± 0.02	0.42 ± 0.02	0.37 ± 0.02					
25°C	0.38 ± 0.02	0.37 ± 0.02	0.38 ± 0.03	0.44 ± 0.03	0.39 ± 0.03	0.41 ± 0.03	0.40 ± 0.03	0.44 ± 0.04
30°C	0.33 ± 0.02	0.32 ± 0.02	0.35 ± 0.02	0.39 ± 0.08	0.39 ± 0.02	0.39 ± 0.02	0.39 ± 0.01	0.43 ± 0.01
33°C				0.35 ± 0.02	0.35 ± 0.02	0.35 ± 0.05	0.39 ± 0.03	0.37 ± 0.04
	ANOVA or Kruskal-Wallis test							
F or $\chi 2$ (df=3)	5.07	21.88	1.42	7.71	14.18	12.69	11.18	14.86
p -value	**0.030**	**0.000**	0.307	**0.002**	**0.003**	**0.005**	**0.011**	**0.002**

Table S4.4. The averaged relative electron transfer rate, rETRmax at each temperature. The significance between different temperature was tested using one-way analysis of variance (ANOVA). If data did not satisfy the normality assumption, a non-parametric Kruskal-Wallis's analysis of variance was applied. Significant results are shown in bold. Unit is μmol electrons m^{-2} s^{-1}.

	January coastal stations			**New Pass**				
	22-Jan			**21-Jul**	**27-Jul**	**28-Jul**		
	NH_4^+	**NO_3^-**	**Urea**	**NH_4^+**	**NO_3^-**	**NH_4^+**	**NO_3^-**	**Urea**
15°C	41.2 ± 13.1	38.5 ± 13.8	28.5 ± 9.8	12.9 ± 0.9	5.4 ± 1.7	3.8 ± 3.2	3.3 ± 1.8	0.3 ± 0.7
20°C	32.2 ± 11.8	37.9 ± 10.3	28.9 ± 5.5					
25°C	32.2 ± 10.9	43.9 ± 11.8	33.1 ± 7.8	23.2 ± 2.8	22.1 ± 3.9	22.0 ± 2.4	24.9 ± 1.0	19.9 ± 4.8
30°C	22.2 ± 5.6	25.3 ± 3.5	29.2 ± 5.9	23.0 ± 2.5	23.4 ± 1.3	24.6 ± 1.9	27.0 ± 1.4	24.9 ± 1.7
33°C				20.0 ± 3.0	16.6 ± 1.5	16.7 ± 2.3	16.8 ± 1.7	14.1 ± 1.9
	ANOVA or Kruskal-Wallis test							
F or $\chi 2$ (df=3)	1.58	1.66	0.24	12.18	19.54	16.58	16.20	16.84
p -value	0.269	0.251	0.866	**0.007**	**0.000**	**0.001**	**0.001**	**0.001**

Table S4.5. The averaged quantum yield of non-regulated non-photochemical quenching, YNO, at each temperature. The significance between different temperature was tested using one-way analysis of variance (ANOVA). If data did not satisfy the normality assumption, a non-parametric Kruskal-Wallis's analysis of variance was applied. Significant results are shown in bold.

	January coastal stations			**New Pass**				
	22-Jan			**21-Jul**	**27-Jul**	**28-Jul**		
	NH_4^+	**NO_3^-**	**Urea**	**NH_4^+**	**NO_3^-**	**NH_4^+**	**NO_3^-**	**Urea**
15°C	0.62 ± 0.03	0.60 ± 0.04	0.60 ± 0.01	0.74 ± 0.01	0.85 ± 0.03	0.93 ± 0.07	0.95 ± 0.01	0.97 ± 0.01
20°C	0.63 ± 0.03	0.61 ± 0.02	0.64 ± 0.03					
25°C	0.62 ± 0.02	0.63 ± 0.05	0.59 ± 0.02	0.63 ± 0.01	0.65 ± 0.06	0.61 ± 0.04	0.62 ± 0.02	0.62 ± 0.07
30°C	0.68 ± 0.02	0.69 ± 0.02	0.65 ± 0.03	0.63 ± 0.04	0.63 ± 0.01	0.60 ± 0.03	0.60 ± 0.02	0.58 ± 0.01
33°C				0.67 ± 0.02	0.70 ± 0.03	0.69 ± 0.05	0.66 ± 0.01	0.68 ± 0.04
	ANOVA or Kruskal-Wallis test							
F or $\chi 2$ (df=3)	4.68	4.59	4.93	25.00	17.39	14.93	16.11	15.28
p -value	**0.036**	**0.038**	**0.032**	**0.000**	**0.001**	**0.002**	**0.001**	**0.002**

Table S4.6. The averaged quantum yield of regulated non-photochemical quenching, YNPQ, at each temperature. The significance between different temperature was tested using one-way analysis of variance (ANOVA). If data did not satisfy the normality assumption, a non-parametric Kruskal-Wallis's analysis of variance was applied. Significant results are shown in bold.

	January coastal stations			**New Pass**				
	22-Jan			**21-Jul**	**27-Jul**	**28-Jul**		
	NH_4^+	**NO_3^-**	**Urea**	**NH_4^+**	**NO_3^-**	**NH_4^+**	**NO_3^-**	**Urea**
15°C	0.13 ± 0.04	0.14 ± 0.06	0.15 ± 0.05	0.06 ± 0.01	0.03 ± 0.02	0.01 ± 0.00	0.01 ± 0.01	0.01 ± 0.01
20°C	0.13 ± 0.04	014 ± 0.05	0.11 ± 0.02					
25°C	0.14 ± 0.05	0.12 ± 0.02	0.14 ± 0.04	0.06 ± 0.01	0.03 ± 0.02	0.05 ± 0.03	0.05 ± 0.02	0.04 ± 0.02
30°C	0.12 ± 0.02	0.12 ± 0.04	0.12 ± 0.04	0.05 ± 0.02	0.05 ± 0.01	0.06 ± 0.03	0.05 ± 0.03	0.06 ± 0.01
33°C				0.05 ± 0.01	0.03 ± 0.01	0.03 ± 0.01	0.04 ± 0.01	0.04 ± 0.01
	ANOVA or Kruskal-Wallis test							
F or $\chi 2$ (df=3)	0.08	0.23	0.73	4.41	5.06	11.39	6.94	13.60
p -value	0.970	0.874	0.562	0.221	0.168	**0.010**	**0.004**	**0.004**

Table S4.7. The maximum absolute uptake rate, ρ_{max}, calculated from Michalis-Menten formula, at each temperature. Unit is pmol-N h^{-1} $cell^{-1}$.

	Sanibel Island			**New Pass**				
	27-Jan			**27-Jul**		**28-Jul**		**29-Jul**
	NH_4^+	**NO_3^-**	**Urea**	**NO_3^-**	**NH_4^+**	**NO_3^-**	**Urea**	**Urea**
15°C	0.00026	0.00015	0.00008	0.00001	0.00002	0.00002	0.00001	0.00002
20°C	0.00039	0.00019	0.00012					
25°C	0.00039	0.00026	0.00013	0.00009	0.00012	0.00004	0.00004	0.00006
30°C	0.00041	0.00017	0.00018	0.00013	0.00020	0.00006	0.00015	0.00015
33°C				0.00008	0.00018	0.00008	0.00020	0.00016

Table S4.8. The total carbon (C) and nitrogen (N) at each temperature. The significance between different temperature was tested using one-way analysis of variance (ANOVA). If data did not satisfy the normality assumption, a non-parametric Kruskal-Wallis's analysis of variance was applied. Significant results are shown in bold. Unit is pmol cell-1.

	Sanibel Island						**New Pass**									
	27-Jan						**27-Jul**		**28-Jul**						**29-Jul**	
	NH_4^+		**NO_3^-**		**Urea**		**NO_3^-**		**NH_4^+**		**NO_3^-**		**Urea**		**Urea**	
	Total C	**Total N**	**Total C**	**Total N**	**Total C**	**Total N**	**Total C**	**Total N**	**Total C**	**Total N**	**Total C**	**Total N**	**Total C**	**Total N**	**Total C**	**Total N**
15°C	0.091 ± 0.014	0.0109 ± 0.0020	0.092 ± 0.017	0.0104 ± 0.0020	0.091 ± 0.012	0.0108 ± 0.0013	0.029 ± 0.007	0.0022 ± 0.0006	0.030 ± 0.002	0.0022 ± 0.0001	0.027 ± 0.002	0.0020 ± 0.0002	0.032 ± 0.004	0.0024 ± 0.0003	0.043 ± 0.002	0.0033 ± 0.0003
20°C	0.091 ± 0.013	0.0103 ± 0.0018	0.086 ± 0.022	0.0101 ± 0.0028	0.092 ± 0.004	0.0103 ± 0.0006										
25°C	0.084 ± 0.022	0.0097 ± 0.0038	0.088 ± 0.015	0.0099 ± 0.0027	0.087 ± 0.016	0.0093 ± 0.0024	0.036 ± 0.007	0.0031 ± 0.0006	0.029 ± 0.001	0.0018 ± 0.0001	0.024 ± 0.001	0.0015 ± 0.0001	0.055 ± 0.006	0.0033 ± 0.0002	0.050 ± 0.008	0.0031 ± 0.0004
30°C	0.082 ± 0.023	0.0092 ± 0.0032	0.082 ± 0.015	0.0094 ± 0.0023	0.087 ± 0.017	0.0094 ± 0.0024	0.034 ± 0.002	0.0032 ± 0.0002	0.033 ± 0.003	0.0021 ± 0.0001	0.026 ± 0.003	0.0015 ± 0.0001	0.057 ± 0.006	0.0034 ± 0.0002	0.052 ± 0.001	0.0031 ± 0.0002
33°C							0.033 ±	0.0028 ±	0.030 ±	0.0020 ±	0.032 ±	0.0021 ±	0.050 ±	0.0031 ±	0.051 ±	0.0033 ±
	ANOVA or Kruskal-Wallis test															
F or $\chi 2$ (df=3)	0.42	0.49	0.21	0.15	0.18	0.73	1.41	4.46	2.87	5.81	5.33	11.32	25.20	14.36	4.56	0.691
p -value	0.742	0.693	0.890	0.930	0.908	0.552	0.269	**0.015**	0.069	**0.007**	0.149	**0.010**	**0.000**	**0.000**	**0.017**	0.57

Chapter 5: *Karenia brevis* grazing on *Synechococcus* and *Rhodomonas*: Effects of food quantity and quality and photophysiological responses of predator and prey

Abstract

In 2005, it was reported that *Karenia brevis*, which forms red tide almost annually in Florida's Gulf coasts, exhibited mixotrophic behavior by grazing on picocyanobacteria *Synechococcus*. However, since then, only limited research has been conducted on mixotrophy of this species. In this study, the nutritional quality and quantity of prey impacts on rates of grazing by *K. brevis* and how grazing affects the photophysiological responses of both predator and prey were investigated. Prey quality was manipulated by growing *Synechococcus* under different nitrogen (N) : phosphate (P) conditions, and by providing an alternate prey (*Rhodomonas*, a photosynthetic eukaryote). Prey cultures, N:P balanced, N-limited, P-limited *Synechococcus,* and *Rhodomonas salina* were inoculated into *K. brevis* in varying ratios. No consistent patterns were observed in ingestion rates based on the different quality of *Synechococcus*, but ingestion rates were a function of prey-to-grazer ratios (R^2=0.76) and prey amounts (R^2=0.71) across all treatments (24.4 – 92.0 *Synechococcus K. brevis*$^{-1}$ d^{-1}). Although ingestion rates were remarkably lower than those of *Synechococcus*, *K. brevis* could feed on *R. salina* (5.2 – 7.4 *R. salina K. brevis*$^{-1}$ d^{-1}). Cellular incorporation of *Synechococcus* N into *K. brevis* biomass through grazing was confirmed by ^{15}N labeling following by NanoSIMS analysis of

single *K. brevis* cells. There were no significant changes in growth, densities, and photosynthetic performance, measured by the maximum relative electron transport rate, $rETR_{max}$, of *K. brevis* under mixotrophic conditions, but prey photosynthesis was negatively affected.

Introduction

The toxigenic dinoflagellate, *Karenia brevis*, which forms red tides almost annually in Florida's southwest Gulf coasts, is a mixotroph, exhibiting both photo-autotrophy and phago-heterotrophy (Jeong et al., 2005; Glibert et al., 2009). Jeong et al. (2005) first discovered that *K. brevis* in culture could ingest the picocyanobacterium *Synechococcus* sp. at a rate of 5 *Synechococcus K. brevis*$^{-1}$ h^{-1}. Glibert et al. (2009) measured grazing rates of *K. brevis* on *Synechococcus* at varying prey:grazer ratios and showed that grazing rates were higher when prey were more abundant, with rates ranging from ~1 to 84 *Synechococcus K. brevis*$^{-1}$ h^{-1}. These studies have clearly shown that *K. brevis* can graze this picoplankter, but many questions remain unanswered, including how grazing rates change with prey nutritional quality, with prey availability, whether *K. brevis* can graze larger cells, and how quickly prey biomass is incorporated into *K. brevis* cells. Experiments were conducted herein to begin to answer these questions.

Mixoplankton may utilize phagotrophy to supplement their dissolved inorganic nutrient and/or carbon (C) budgets during periods of nutrient and/or C limitation (Stoecker et al., 2017). Some species do not even graze when inorganic nutrients are plentiful (examples in Stoecker et al., 2017). Depending on the nutritional history of the grazer, mixotrophs might selectively graze on prey with

different nutritional histories, thus acquiring nutrients that they lack (e.g., Lundgren et al., 2016, Lin et al., 2017). Indeed, many mixotrophic harmful algae are found in eutrophic waters that deviate from classic stoichiometric nutrient proportions, such as high nitrogen (N): phosphate (P) or low N:P waters (Burkholder et al., 2008; Heisler et al., 2008).

Florida's Gulf coasts are typically considered N-limited environments due to a long history of P-mining and its influence on nearby waters (Heil et al., 2007; Duan et al., 2021). Heil et al. (2007) reported *K. brevis* was the dominant planktonic protist in West Florida Shelf waters with N:P ratios < 8 (Tampa Bay to Sanibel Island) in the late spring of 2003. The Heil et al. (2007) study also revealed an inverse pattern of the spatial extent of picocyanobacteria (e.g., *Synechococcus*) and *K. brevis*, based on signature pigment analysis (Heil et al., 2007). Additionally, Sipler et al. (2013) reported an inverse relationship between densities of *Synechococcus*-like species and *K. brevis* collected near Sanibel Island, Florida. Collectively, these patterns suggest the potential for mixotrophy to play an important role in either the growth of, or maintenance of, *K. brevis* blooms in the coastal waters of Florida.

This laboratory study, involving batch and chemostat cultures of *K. brevis*, aimed to investigate the ability of *K. brevis* to graze on *Synechococcus* when it was grown under variable nutrient conditions, and to test whether this dinoflagellate could graze larger cells, namely *Rhodomonas salina*. We hypothesized that *K. brevis* could indeed graze on larger cells than picoplankton and that N-limited *K. brevis* would feed more on N-rich prey and have photosynthetic advantages with N-rich prey compared to P-rich prey.

Materials and methods

Stock cultures

A culture of non-axenic *K. brevis* (estimated spherical diameter [ESD] = 18-25 µm), originally isolated from New Pass, Sarasota, Florida, was obtained from Mote Marine Laboratory, Sarasota, Florida, U.S. Prey cultures, *Synechococcus* sp. (CCMP836, [ESD] = ca. 1 µm) and *Rhodomonas salina* ([ESD] = 6-9 µm) were obtained from the National Center for Marine Algae and Microbiota at the Bigelow Laboratory for Ocean Sciences, West Boothbay Harbor, Maine, U.S. and from the Oyster Hatchery of Horn Point Laboratory, Cambridge, Maryland, U.S., respectively.

All media were prepared using nutrient-poor offshore Gulf of Mexico seawater that had been previously collected and stored at < 4 °C in the dark before use. The seawater was filtered through GF/F filters (nominal pore size: ~ 0.7 µm; Whatman, Maidstone, Germany), and salinity was adjusted to 30 by diluting this seawater (salinity of ~34) with deionized water. Then, salinity-adjusted seawater was autoclaved, and 0.2 µm-filtered nutrient stocks were added based on the L1 (-Silicate) media recipe (~880 µM nitrate (NO_3^-), ~36 µM phosphate (PO_4^{3-}); Guillard and Hargraves, 1993). All cultures were maintained at 20°C in walk-in temperature-controlled rooms with a light intensity of 100 µmol photons m^{-2} s^{-1} in a 12h light: 12h dark cycle. Light intensities were measured with ULM-500 Light Meter & Logger with a micro quantum sensor (Heinz Walz GmbH, Effeltrich, Germany).

Experimental design

Four experiments were conducted. Each experiment varied the growth conditions of the mixotroph, the prey quantity or the prey quality. In Experiment 1, N-limited *K. brevis* was grown in batch culture and grazing manipulations were undertaken during exponential growth. In Experiments 2-4, *K. brevis* was grown in N-limited chemostats with growth rates at 60% of maximum growth rate. Different experiments were designed to provide the mixotroph with different amounts of picoplankton prey, with picoplankton prey of different nutritional quality (as N:P balanced, N- or P-limited), and to provide an alternate prey (Fig. 5.1). In Experiments 1-4, the prey provided was *Synechococcus*, and in Experiments 3 and 4, treatments compared *Synechococcus* and *R. salina* as prey.

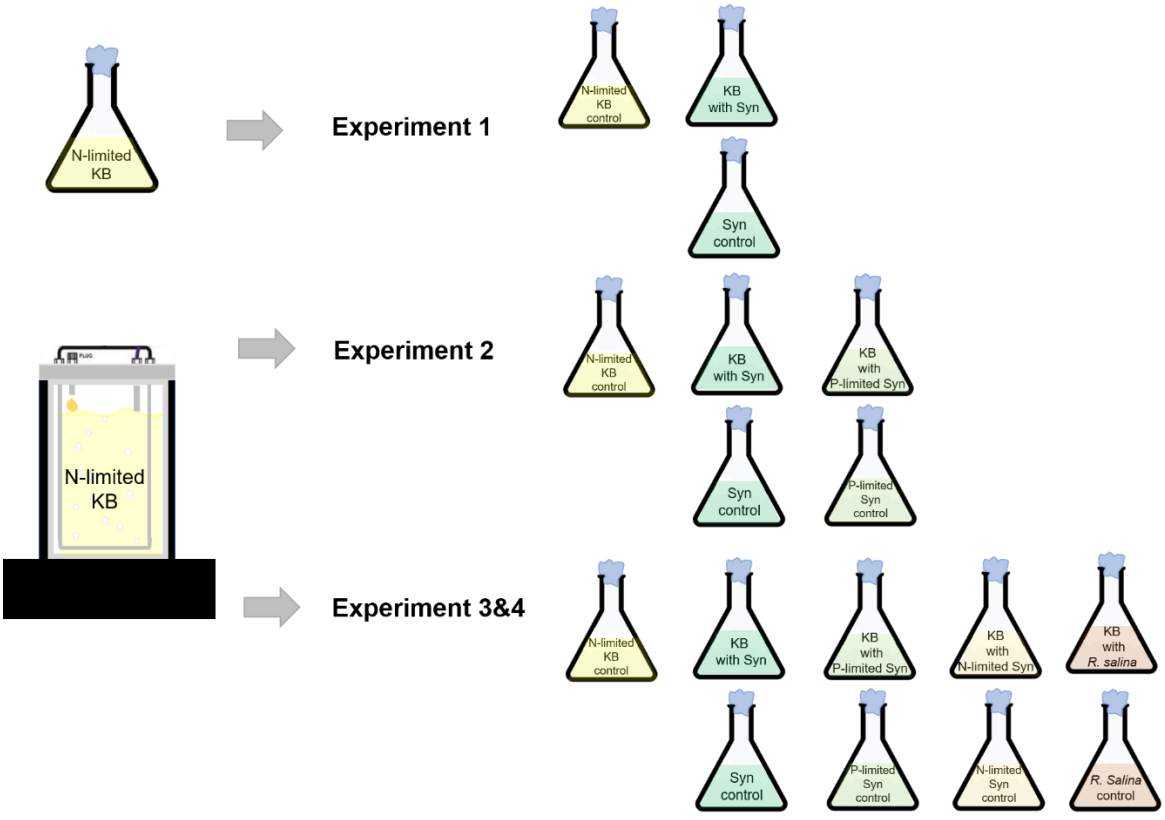

Figure 5.1. Schematic of experimental design. KB and Syn represent *Karenia brevis* and *Synechococcus,* respectively. Different quality of Syn are symbolized as different colors.

Experiment 1: Batch culture

A subculture of the stock *K. brevis,* initially grown in L1 media, was transferred into media with the NO_3^- concentration reduced so that it was only 20% of the initial recipe. All other substrates were maintained consistent with L1. Grazers were grown in new media for more than 3 generations. The *Synechococcus* culture were grown in N:P balanced, 50% enriched L1 media prepared with ^{15}N-NO_3^- (Cambridge Isotope Laboratories, Inc., Massachusetts, U.S.) in order to isotopically label the prey. The final isotope composition of *Synechococcus* culture was 6.4 (± 1.7) ^{15}N atom% measured during Nanoscale secondary ion mass spectrometry (NanoSIMS) analyses.

Once exponential growth was established for the mixotroph, *K. brevis* cultures were transferred into 4 flasks and the filtrates of *K. brevis* culture were transferred into 2 flasks, totaling 6 flasks. The former included *K. brevis* controls and *K. brevis* provided with *Synechococcus* and the latter included *Synechococcus* controls (Fig. 5.1). All treatments were duplicated. Exponentially-growing ^{15}N pre-labelled *Synechococcus* cultures were centrifuged at 6000 rpm (1000 x g) (Eppendorf, Hamburg, Germany) for 5 min to remove culture media, and then pellets at the bottom were resuspended into treatment flasks. The concentrations of ^{15}N pre-labelled *Synechococcus* were measured before inoculation and calculated amounts were resuspended into each flask.

All experiments were conducted at the same temperature and light conditions for the stock cultures, except that LED light lamps were used. Samples for cell counting and fluorescence measurements were collected over time at 0, 3, 7, 24, 28, 72 h. Cell counts were used to establish the extent of grazing (disappearance) of the prey, and fluorescence was used to track the photosynthetic performance of both predator and prey (see detail below). Samples for NanoSIMS were collected at 72 h. The subcultures from *K. brevis* controls, and mixed treatments were fixed with glutaraldehyde (final concentration 2%). The ^{15}N pre-labeled *Synechococcus* was inoculated into fixed *K. brevis* controls (killed *K. brevis* control). All fixed samples were stored in the fridge (4 °C) for at least 1-2 h. Thereafter, samples were filtered onto 0.2 µm pore-size, 25 mm Isopore polycarbonate membrane filters (Millipore, Massachusetts, U.S.) and rinsed with 0.2 µm-filtered MilliQ water. Samples were stored at -20 °C until further analysis.

Experiments 2-4: Chemostat culture

Once *K. brevis,* grown in batch culture conditions in L1 media with NO_3^- reduced to L/5 proportions, reached the exponential phase, ~200mL of cultures were transferred into FMT-150 Photobioreactors (Photon Systems Instruments, Drasov, Czech Republic), and ~200mL of fresh media were added to each photobioreactor. Before each inoculation, calibrations for optical density (OD) measurements were done with the media (blank), and for pH was done with buffer pH 4, 7, and 10 (Mettler-Toledo, Ohio, U.S.). The culturing system received 0.2 µm-filtered (Thermo Fisher Scientific, Massachusetts, U.S.) air pumped into the photobioreactor through the closed top (Fig. S5.1A). Cultures were gently mixed by bubbles emitted from

apertures across the bottom of stainless-steel tubes. Cultures were maintained at 20°C (± 0.01°C) and illuminated with LED lights at an intensity of 100 µmol photons m^{-2} s^{-1} on a 12 h light: 12 h dark cycle. These *K. brevis* cultures were grown in batch mode without dilution in the exponential phase (~ 6-7 days) in photobioreactors (Fig. S5.1B-D). Measurements of OD were done at wavelengths of 680 nm (OD680) to measure the biomass proxy. A water sample (3 mL) was collected each day during exponential phase to count the cell density, in order to calculate cell-specific growth rates. Then, Rabbit plus peristaltic pumps (Rainin, California, U.S.) were turned on to deliver fresh media (Fig. S5.1A). Dilution rates were set at 60 % of cell-specific maximum growth rates (0.6 μ_{max}) obtained during the exponential phase from each run. Temperature and pH were monitored with InPRo 3253/SG/120/PT1000 sensors (Mettler-Toledo, Ohio, U.S.) immersed in the cultures. The steady state of culture was defined by less than 10 % biomass change over > 5 days, and changes in OD680 were less than 6 % in all chemostat culture systems (Fig. S5.1B-D).

The *Synechococcus* stock cultures were manipulated in batch culture to yield varying cellular nutrient conditions: subcultures that were growing on L1, subcultures on L1 media with NO_3^- reduced to L/5 proportions, and subcultures on L1 media with PO_4^{3-} at L/5 proportions, thus yielding cells that were presumably in balanced N:P, N-limited, and P-limited growth conditions. All cultures were acclimated to the new media for more than 3 generations. *Synechococcus* cultures were harvested at stationary phase to ensure different nutritional conditions (Fig. S5.2). Cultures of *R. salina* maintained in batch at balanced N:P were also provided as prey.

In Experiment 2, chemostat cultures were distributed into 8 flasks, including 2 flasks containing filtrates of chemostat cultures. This included *K. brevis* control (duplicated), balanced N:P and P-limited *Synechococcus* controls, and *K. brevis* with balanced N:P and P-limited *Synechococcus* (duplicated). Cell counts and fluorescence parameters were sampled at 0, 4, 24, 48, 72 h.

In Experiments 3-4, chemostat cultures were transferred into 5-6 flasks, and filtrates of culture were transferred into 4 flasks, yielding a total 9 and 10 flasks for Experiments 3 and 4, respectively. Experiments 3-4 included all treatments in Experiment 2, and controls of N-limited *Synechococcus* and *R. salina*, and *K. brevis* inoculated with N-limited *Synechococcus* and with *R. salina*. Samplings were conducted at 0, 24, 48, 72, 96, 120 h for Experiment 3 and 0, 24, 48, 72, 96 h for Experiment 4. *R. salina* treatments were monitored until 72 h. Sampling within the first 24 h was not conducted in Experiments 3-4.

Cell counts and rates calculations

Samples of *K. brevis* were enumerated at 100× magnification using a Sedgewick-Rafter chamber, and *R. salina* were counted at 400× magnification using a hemocytometer (Hausser Scientific, Pennsylvania, U.S.) under light microscopy after Lugol's fixation (2% final concentration). *Synechococcus* samples were fixed with paraformaldehyde (0.5% final concentration) and stored at 4 °C for at least 1 h. Then, samples were filtered onto 0.2 µm pore-size, 25 mm black polycarbonate membrane filters (GVS, Bologna, Italy). Each black filter was mounted on a glass slide, and a drop of mounting solution (Thermo Fisher Scientific, Massachusetts, U. S.) was added to the top of the filter and covered with a coverslip. *Synechococcus* cells on

slides were counted using an Axiophot epifluorescent microscope (Zeiss, Oberkochen, Germany) using a light excitation filter set (excitation 550 nm and emission 605 nm) at 1000× magnification. *Synechococcus* cells were autofluorescent in red because they were phycocyanin-type. At least 400 red cells from 20 random fields were counted per sample.

The specific growth rates (μ; h^{-1} or d^{-1}) were calculated as $\mu = (\ln N_2\text{-}N_1) \times (t_2\text{-}t_1)^{-1}$ where N_2 and N_1 are concentrations of prey or grazer cells at respective times, t_2 and t_1. Grazing coefficients (g; h^{-1} or d^{-1}) were determined as the differences between specific growth rates of prey in controls and those with grazers. Clearance rates (μl *K. brevis*$^{-1}$ h^{-1} or μl *K. brevis*$^{-1}$ d^{-1}) were calculated by dividing grazing coefficient, g, with mean predator density, $P = (P_0 \times (e^{\mu t}\text{-}1)) \times (\mu t)^{-1}$ where P_o is the initial grazer concentration (Heinbokel, 1978). Ingestion rates by grazer on prey (prey *K. brevis*$^{-1}$ h^{-1} or prey *K. brevis*$^{-1}$ d^{-1}) were calculated by multiplying clearance rate with prey abundance, $C = (C_o \times (e^{\mu t}\text{-}1)) \times (\mu t)^{-1}$ where C_o is the initial abundance of prey cells (Frost, 1972). Daily ingestion rates were calculated after the first 24 h while hourly grazing rates were calculated within the initial 24 h.

Chlorophyll *a*

Chlorophyll *a* (Chl *a*) samples were collected for *K. brevis* at the start of experiments (0 h) except in Experiment 2. Cultures were filtered onto 25 mm GF/F filters in duplicate to triplicate (Whatmam, Maidstone, United Kingdom) and stored at -20°C. The samples were extracted in 90% acetone (v/v) overnight in darkness at -

20°C and subsequently measured using a 10-AU Fluorometer (Turner Designs, California, U.S.) according to Arar and Collins (1997).

Pulse-amplitude-modulated (PAM) fluorometry analysis

Photosynthetic parameters of predator and prey were measured using a Phyto-PAM-II fluorometer (Heinz Walz GmbH, Effeltrich, Germany). After dark-adapting subsamples from each flask for 20 min, measurements of rapid light curves consisting of 10 light steps (20s for each step, from 0 to ~600 µmol photons m^{-2} s^{-1}) were made. The relative electron transport rate (rETR) was obtained for each light step, and a modified nonlinear function of Platt et al. (1980) was fitted to calculate $rETR_{max}$, the maximum rETR, using R package 'phytools'. Based on the excitation of five measuring light wavelengths (440, 480, 540, 590, and 625nm), the Phyto-PAM-II fluorometer can differentiate 4 functional algae groups–green algae, blue-green algae (cyanobacteria), phycoerythrin-containing algae, and brown algae (diatom or dinoflagellate)–with single measurements. Reference calibrations for *K. brevis* for brown algae and for *Synechococcus* for blue-green algae were used. Due to possible slight changes in pigment fluorescence spectra due to nutrient conditions (Fig. S5.2), separate references were made for (N:P balanced) *Synechococcus*, P-limited *Synechococcus*, and N-limited *Synechococcus*.

NanoSIMS analysis and calculation

Filters for NanoSIMS were dried overnight at 50°C prior to excising a portion to mount onto a carbon conductive tab (Ted Pella, Redding, CA) adhered to an aluminum stub. Mounted samples were sputter coated with ~5 nm of gold for

conductivity and analyzed at Lawrence Livermore National Laboratory. Filters were first imaged using a scanning electron microscope (FEI Quanta model 450) with the secondary electron detector (5 Kv) to identify the location of *K. brevis* cells, and then subsequently with a nanoSIMS 50 using a primary Cs^+ beam of 150 mm diameter. Areas were sputtered with ~60 pA Cs^+ for 5 cycles (327 s) over 33 x 33 µm rasters to prior to collecting 20 cycles over a 33 x 33 µm acquisition area with ~2 pA Cs^+. After tuning the secondary ion beam to ~9500 mass resolving power (MRP), automatic secondary ion beam centering was performed every 20 cycles based on $^{12}C^{14}N^-$. Secondary electron (SE) and secondary ion images were collected simultaneously for masses, $^{12}C^{14}N^-$, $^{12}C^{15}N^-$, and $^{31}P^-$ on individual electron multipliers (e.g., Xavier et al., 2023). From each sample, 10 fields were selected and inspected with the secondary electron detector of the NanoSIMS. Regions of interest (ROI) were manually drawn inside the *K. brevis* cell outlines recorded by the $^{12}C^{14}N^-$ signal, and the signals from *Synechococcus* were excluded by avoiding high $^{12}C^{15}N^-/^{12}C^{14}N^-$ regions through software L'Image (Carnegie Institution of Washington, Washington, D.C., U.S.). ROIs for *Synechococcus* were separately drawn, and these values were used for N_{net} calculations. The levels of ^{15}N enrichments of each ROI were expressed using the delta (δ) in units of per mil of stable N isotope ratios calculated as: $\delta^{15}N$ (‰) = $[^{15}N/^{14}N_{sample}/^{15}N/^{14}N_{standard}-1]\times1000$ where $^{15}N/^{14}N_{standard}$ was 0.00367. The newly synthesized N from *Synechococcus* relative to the final N was calculated as: N_{net} (%) = $[F_s/(F_s+F_i)] \times100$, where F_s was a fraction of N from the isotopically labeled *Synechococcus*, and F_i is the fraction of N from original *K. brevis* (Dekas et al., 2019). Approximately 10 cells were imaged for each filter (one killed *K. brevis*

control and duplicated mixed treatments) and averaged values of $\delta^{15}N$ and N_{net} are presented.

Statistical analysis

Differences in Chl *a*, cell densities, growth rates, and $rETR_{max}$, $\delta^{15}N$ of prey and grazer across different treatments were analyzed using a t-test or a one-way analysis of variance (ANOVA) with the data passing normality (Shapiro-Wilk test) and equal variance tests (Levene's test). If data did not satisfy the normality assumption, the non-parametric Wilcoxon rank sum test or Kruskal-Wallis's analysis were applied. Linear regression was used to explore the relationship between ingestion rates by *K. brevis* on *Synechococcus* and ratios of *Synechococcus* to *K. brevis*.

Results

Chl *a* concentration of *Karenia brevis*

Total Chl *a* per cell of *K. brevis* at 0 h differed significantly between cultures from batch (Experiment 1) and chemostat (Experiments 3-4) ($p < 0.01$). The average Chl *a* concentration of *K. brevis* from Experiment 1 was 23.3 (± 1.1) pg Chl *a* $cell^{-1}$, while concentrations from Experiments 3 and 4 were 4.7 (± 0.3) and 4.4 (± 0.1) pg Chl *a* $cell^{-1}$, respectively.

Cell densities of *Karenia brevis* and prey

In all experiments, after 24-48 h, the densities of N:P balanced *Synechococcus* were lower in mixed culture treatments compared to those of controls (Fig. 5.2),

demonstrating that they were being removed by *K. brevis*. In Experiment 1, *Synechococcus* with and without *K. brevis* both increased significantly over time, but the rate of increase in cell numbers from 0 h to 72 h was lower in the presence of the grazer (3.4-fold) than without (4-fold) (Fig. 5.2A). From time 0 to time final, controls of *Synechococcus* density increased from 2.1 to 4.1-fold, while the density of *Synechococcus* mixed with *K. brevis* increased from 0.9 to 1.5-fold in Experiments 2-4 (Fig. 5.2B-D). The differences in *Synechococcus* density between controls and mixed cultures were statistically compared when the initial cell abundances were similar: Experiment 1, Experiment 3 except for N-limited treatments, and Experiment 4. No differences were found in Experiment 1 ($p > 0.05$), while *Synechococcus* densities in the presence of *K. brevis* were significantly lower than those of controls in Experiments 3 and 4 ($p < 0.01$).

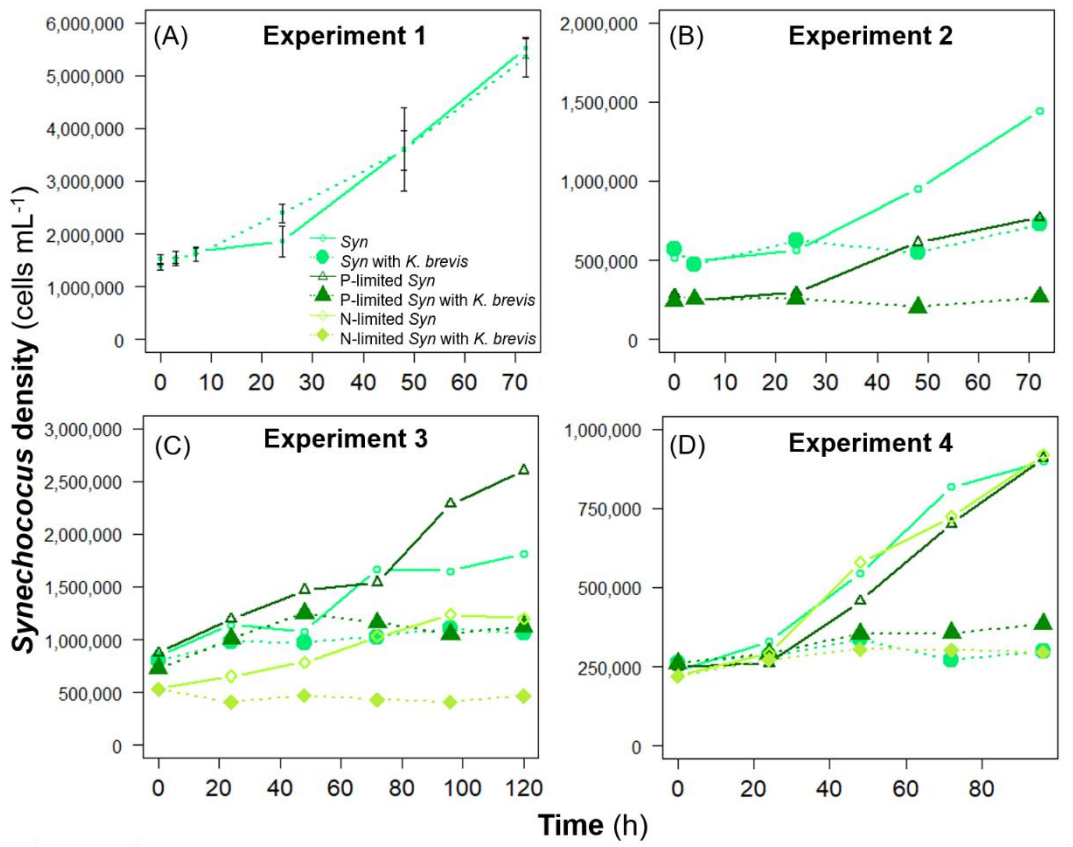

Figure 5.2. The density of *Synechococcus* with or without grazer, *K. brevis*, over time in Experiment 1 (A), Experiment 2 (B), Experiment 3 (C), and Experiment 4 (D). Dotted lines with filled symbols represent *Synechococcus* mixed with *K. brevis*, while straight lines with empty symbols represent controls of *Synechococcus*: Circle (○, ●) for (N:P balanced) *Synechococcus*, triangle (△, ▲) for P-limited *Synechococcus*, (♦, ◊) for N-limited *Synechococcus*. Note that symbol size is reduced in Experiment 1 to show standard deviation.

In contrast with the changes in *Synechococcus* cell densities, the densities of *K. brevis* did not change considerably between treatments ($p > 0.05$) and with time except for Experiment 1 (Fig. 5.3). In Experiment 1, the densities of *K. brevis* both

with and without prey increased from 0 h to 72 h, but they increased more when prey were available (82% increase) compared to the controls (30% increase) (Fig. 5.3A). When comparing only the densities of *K. brevis* at 72 h, the densities of *K. brevis* in the control treatments were significantly lower than those of *K. brevis* inoculated with *Synechococcus* in Experiment 1 ($p < 0.05$). On the other hand, in Experiments 2-4, the *K. brevis* densities of the control treatments consistently decreased in a range of -12% to -2% from time 0 to the final time (Fig. 5.3B-D). Changes in *K. brevis* densities were variable when prey were added, ranging from -12% to +10% in Experiments 2-4.

Growth rates of *K. brevis* for each treatment were calculated over the whole experimental period for each experiment. In Experiment 1, from 0 h to 72 h, growth rates were 0.09 (± 0.01) d^{-1} and 0.20 (± 0.02) d^{-1} for *K. brevis* control and *K. brevis* inoculated with *Synechococcus*, respectively. Growth rates of *K. brevis* controls were all -0.03 d^{-1} from time 0 to the final time, while they varied between -0.03 d^{-1} to +0.02 d^{-1} in mixed cultures in Experiments 2-4. However, differences in density changes or growth rates between controls and mixed cultures were insignificant in Experiments 2-4 ($p > 0.05$).

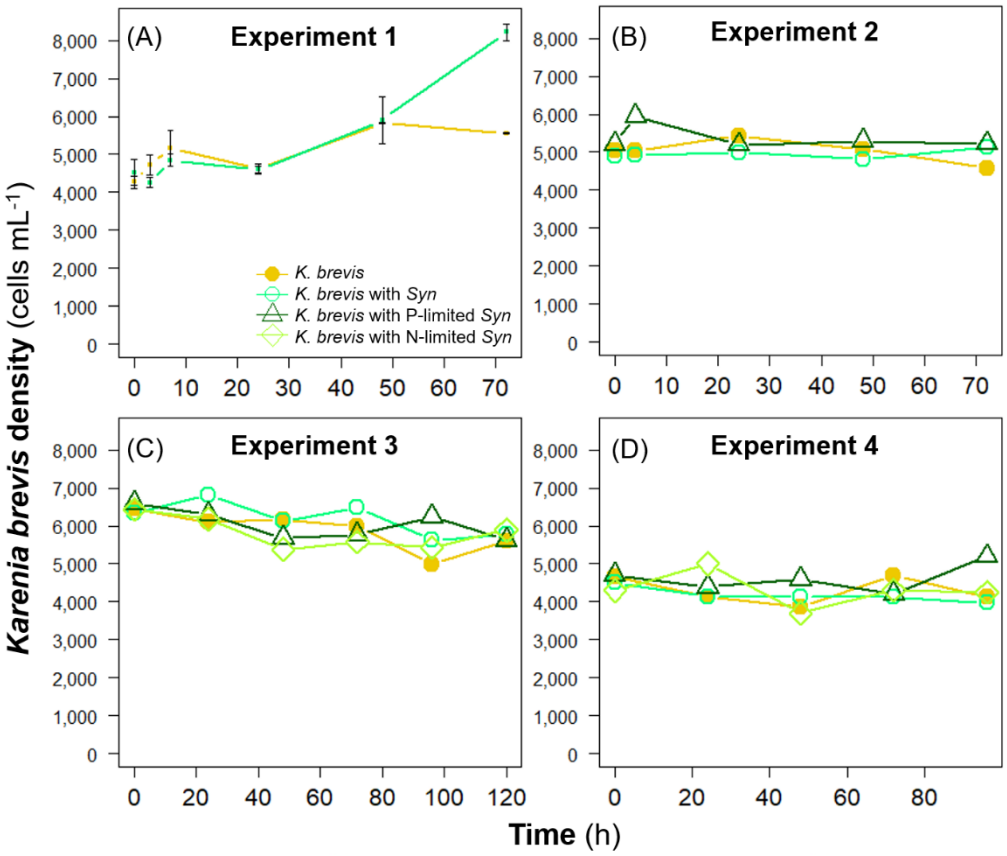

Figure 5.3. The density of *K. brevis* with or without *Synechococcus*, over time in Experiment 1 (A), Experiment 2 (B), Experiment 3 (C), and Experiment 4 (D). Note that the symbol size is reduced in Experiment 1 to show standard deviation.

For the experiment involving *R. salina* as prey, the densities of *R. salina*, both with or without grazers, increased with time (Fig. 5.4A), while the abundance of *K. brevis*, with or without prey, did not show any consistent patterns (Fig. 5.4B). In Experiments 3 and 4, the densities of *R. salina* were significantly higher without predators than those mixed with *K. brevis* ($p < 0.05$). The growth rates of controls of *K. brevis* over 72 h were -0.03 and 0.00 d^{-1}, while the growth rates of *K. brevis* mixed with *R. salina* were -0.01 and 0.00 d^{-1} in Experiment 3 and Experiment 4, respectively.

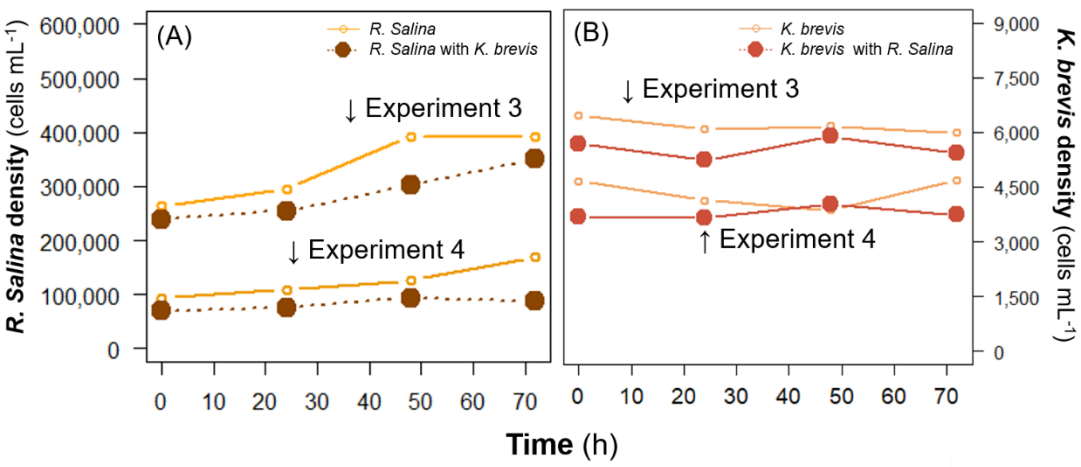

Figure 5.4. The density of *R. saline* with or without *K. brevis* (A) and *K. brevis* with or without *R. salina* (B) from 0 h to 72 h in Experiments 3 and 4.

Ingestion rates of *K. brevis* on prey

The daily grazing rates on *Synechococcus*, calculated after the first 24 h during each treatment, ranged from 24.4 to 92.0 (± 29.9) *Synechococcus K. brevis*$^{-1}$ d^{-1} (Table 5.1). No consistent patterns were observed in ingestion rates on the different quality of *Synechococcus*—N:P balanced, P-limited, and N-limited *Synechococcus*. Ingestion rates did vary as a function of prey to grazer ratios ($R^2 = 0.76$, Fig. 5.5A) as

well as prey amounts ($R^2 = 0.71$, Fig. 5.5B) across all treatments. If more prey were available, grazing rates by *K. brevis* on *Synechococcus* were higher. The hourly ingestion rates on *Synechococcus*, calculated from Experiment 1 and Experiment 2, were 41.2 (± 8.6) and 22.1 *Synechococcus K. brevis*$^{-1}$ h^{-1}, respectively (Table 5.1).

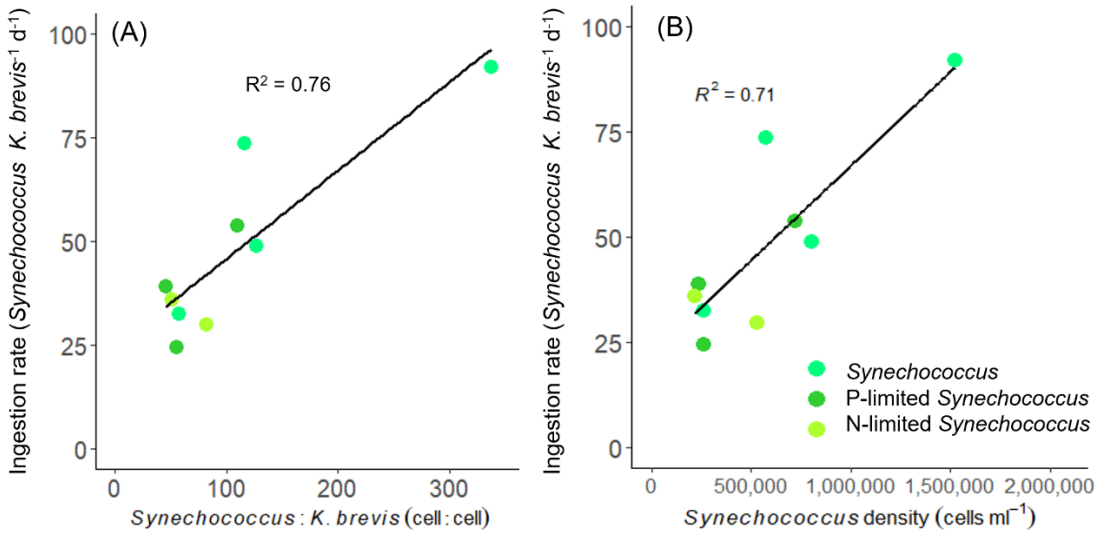

Figure 5.5. The relationship between daily ingestion rates by *K. brevis* on *Synechococcus* and the ratios of *Synechococcus* to *K. brevis* (A) and *Synechococcus* density (B) across all experiments. The linear regression line and R^2 are shown.

The daily grazing rates on *R. salina* from Experiment 3 and 4 were 5.2 and 7.4 *R. salina K. brevis*$^{-1}$ d^{-1}, respectively (Table 5.1), substantially lower than the daily grazing rates on *Synechococcus*.

Table 5.1. Initial conditions of predator and prey densities and prey:predater ratios, calculated (maximum) hourly and daily ingestion rates.

	Prey type	Initial *K. brevis* density ($\times 10^3$ cells ml^{-1})	Initial prey density ($\times 10^5$ cells ml^{-1})	prey:*K. brevis* (cell:cell)	Ingestion rate (prey *K. brevis*$^{-1}$ h^{-1})	Ingestion rate (prey *K. brevis*$^{-1}$ d^{-1})
Experiment 1	*Syn*	4.5 (± 0.3)	15.53 (± 0.84)	337 (± 6):1	41.2 (± 8.6)	92.0 (± 29.9)
Experiment 2	*Syn*	4.9	5.72	117:1	22.1	73.6
	P-limited *Syn*	5.2	2.38	46:1	-	39.0
Experiment 3	*Syn*	6.3	8.04	127:1	-	48.8
	P-limited *Syn*	6.6	7.23	110:1	-	49.2
	N-limited *Syn*	6.4	5.29	82:1	-	27.9
	R. salina	5.6	2.39	43:1	-	5.2
Experiment 4	*Syn*	4.5	2.62	58:1	-	32.5
	P-limited *Syn*	4.7	2.60	55:1	-	24.4
	N-limited *Syn*	4.3	2.20	51:1	-	35.9
	R. salina	3.6	0.69	19:1	-	7.4

NanoSIMS confirmation of N incorporation from *Synechococcus*

Significant differences in cell-specific $\delta^{15}N$ were found between killed *K. brevis* controls and *K. brevis* grazed on ^{15}N pre-labeled *Synechococcus* at 72 h (Fig. 6). However, at both the single cell level, as well as between cells in the same treatments, differences were apparent (Fig. 5.6, Table S5.1): the $\delta^{15}N$ of killed *K. brevis* controls (61 ± 15 ‰) were significantly lower than those grazed on *Synechococcus* (221 ± 78 ‰) ($p < 0.01$) (Fig. 5.6F). The N_{net} of *K. brevis*, the fraction of N came from isotopically labeled prey, was 1.1 (± 0.5) % at 72 h.

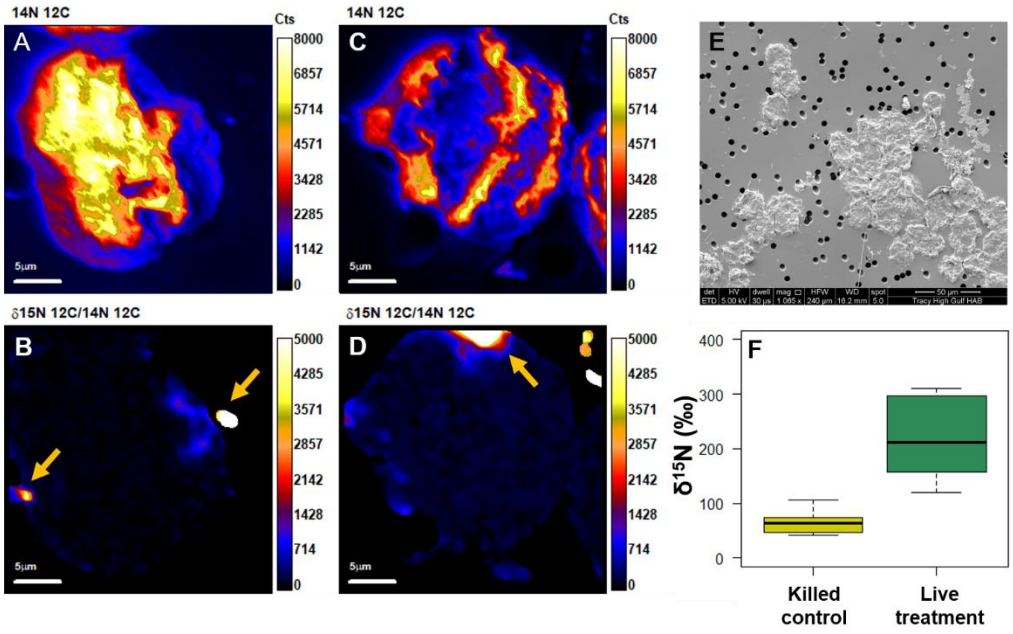

Figure 5.6. NanoSIMS images of killed *K. brevis* control (A, B) and *K. brevis* grazed on *Synechococcus* (C, D) and SEM image of *K. brevis* cells (E). The averaged cell-specific $\delta^{15}N$ of killed *K. brevis* control and *K. brevis* grazed on *Synechococcus* were calculated from each ROIs (F). Values for individual cells are presented in Table S5.1. The images of $^{12}C^{14}N^-$ were used as an indicator of *K. brevis* cell to draw ROIs and calculate cell-specific $\delta^{15}N$. High $\delta^{15}N$ values (orange arrows), the isotopically

enriched *Synechococcus*, were excluded when manually drawing ROIs of *K. brevis* (Fig. S5.3)

Chlorophyll Fluorescence: $rETR_{max}$

Photosynthetic performance, as measured by $rETR_{max}$, of *Synechococcus* and *K. brevis* were monitored at each sampling time until 72 h (Fig. 5.7). In all *Synechococcus* controls, after inoculation into filtrate of N-limited *K. brevis* culture (from the batch culture in Experiment 1 and from chemostat cultures in Experiments 2-4), $rETR_{max}$ decreased slightly and then generally increased until 72 h (Fig. 5.7A, C, E, G, I, K, M, O, Q). No differences in $rETR_{max}$ were observed among *Synechococcus* controls of different N:P at each experiment ($p > 0.05$). Thus, $rETR_{max}$ of *Synechococcus* controls across all treatments were averaged at each experiment and were 16.0 (± 1.4), 20.8 (± 4.4), 19.1 (± 3.3), and 18.0 (± 2.4) µmol electrons m^{-2} s^{-1} for Experiments 1, 2, 3 and 4, respectively.

In mixed cultures, $rETR_{max}$ of *Synechococcus* of all nutritional states increased more with time than the control *Synechococcus* until 72 h (Fig. 5.7B, H, J) or until $rETR_{max}$ dropped significantly (Fig. 5.7D, N, P, R). However, when P-limited *Synechococcus* in Experiment 2 (Fig. 5.7F) and N-limited *Synechococcus* in Experiment 3 (Fig. 5.7L) were inoculated into *K. brevis* culture, $rETR_{max}$ rose immediately and then decreased. When prey:grazer ratios were < ~100:1, $rETR_{max}$ rates of all types of *Synechococcus* dropped significantly or were less than the detection limit after 24-48 h, with the exception of the N:P balanced *Synechococcus* mixed with *K. brevis* in Experiment 2 (Fig. 5.7D, Table 5.1). In each experiment, no significant differences in $rETR_{max}$ were observed among various treatments ($p >$

0.05), and the average $rETR_{max}$ values were 17.6 (± 2.4), 28.3 (± 5.3), 20.4 (± 10.2) and 26.2 (± 13.6) µmol electrons m^{-2} s^{-1} for Experiment 1, 2, 3 and 4, respectively. Only in Experiments 1 and 2 did values differ significantly from the controls ($p < 0.05$). However, when the values that dropped substantially were excluded (e.g., 72 h values in mixed culture in Experiment 4), mean $rETR_{max}$ values were 24.1 (± 6.0) and 31.3 (± 8.4) µmol electrons m^{-2} s^{-1} for Experiment 3 and 4, respectively. These were significantly higher than those of controls ($p < 0.05$).

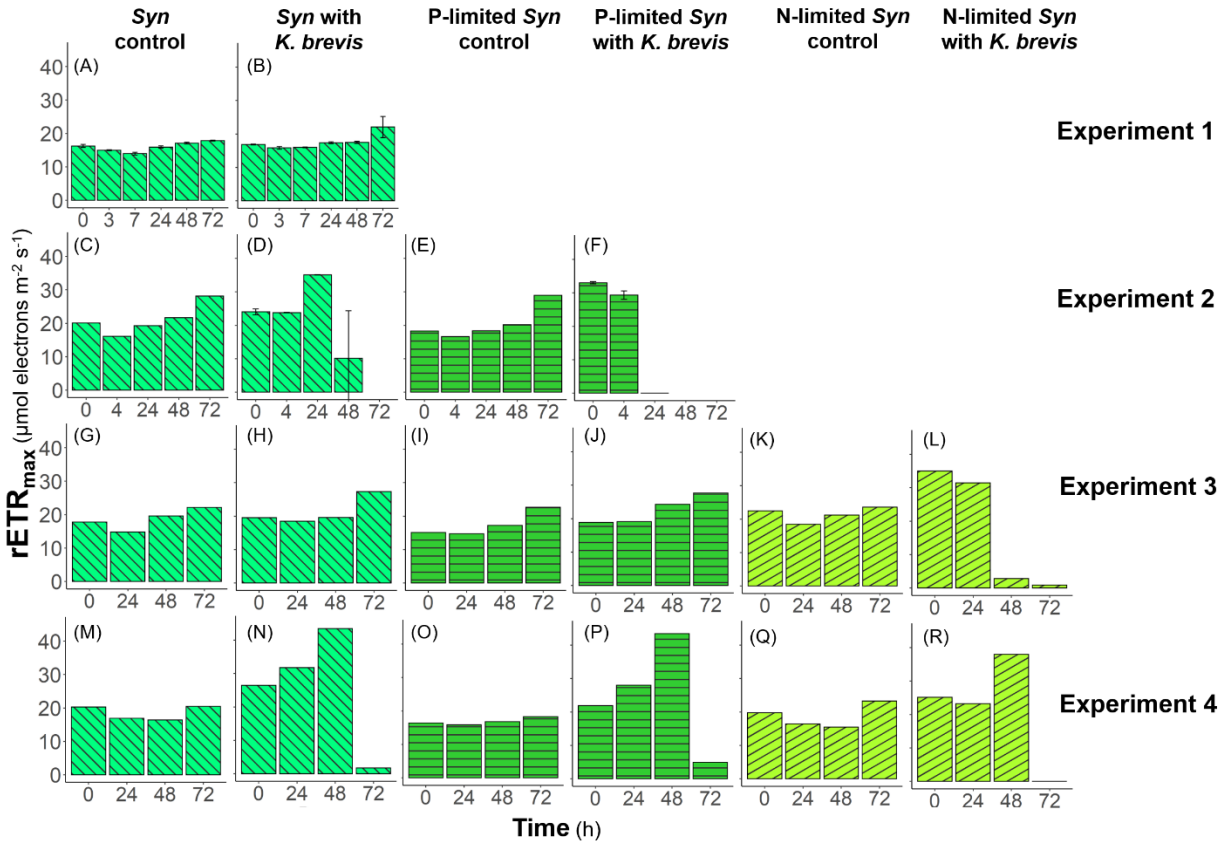

Figure 5.7. The maximum relative electron transport rate, $rETR_{max}$, of *Synechococcus* with or without grazer, *K. brevis* in Experiment 1 (A-B), Experiment 2 (C-F), Experiment 3 (G-L) and Experiment 4 (M-R) over 72 h. Different colors and patterns

represented prey with different qualities. Note the different time scales of the different experiments.

The $rETR_{max}$ rates of *K. brevis* with or without *Synechococcus* did not show consistent trends (Fig. S5.4). All changes in $rETR_{max}$ with time were marginal, and no differences were found between treatments in each experiment ($p > 0.05$). The mean $rETR_{max}$ values of Experiment 1 (20.3 ± 1.5 µmol electrons m^{-2} s^{-1}) was significantly higher than those of Experiment 2 (14.1 ± 1.7 µmol electrons m^{-2} s^{-1}), Experiment 3 (12.3 ± 1.1 µmol electrons m^{-2} s^{-1}), and Experiment 4 (14.1 ± 1.0 µmol electrons m^{-2} s^{-1}) ($p < 0.001$). This was due to their reduced growth rates and Chl *a* content in chemostat growth.

Discussion

This study examined the grazing ability of *K. brevis* on larger cells than its previously known prey, *Synechococcus*, and compared the effects of nutritional history of prey on ingestion rates and photosynthetic performance by *K. brevis* on *Synechococcus*. This study documented that *K. brevis* could graze on *R. salina*, but the impacts of different prey qualities (N:P balanced, P- and N-limited *Synechococcus*) on N-limited *K. brevis* were not prominently reflected in terms of ingestion rates and photosynthetic rates, as measured by $rETR_{max}$. This study also confirmed, although the contribution level was low, the incorporation of the prey-N by *K. brevis* using NanoSIMS techniques.

Mixotrophy in *Karenia brevis*

As consistent with previous studies (Jeong et al., 2005; Glibert et al., 2009), *K. brevis* could graze on *Synechococcus* (Fig. 5.2), and the ingestion rates were a function of prey to predator ratios ($R^2 = 0.76$, Fig. 5.5A) as well as prey amounts ($R^2 = 0.71$, Fig. 5.5B). Therefore, the ingestion rates herein were compared with the rates at similar prey:grazer ratios from Glibert et al. (2009). If the daily ingestion rates are converted to hourly ingestion rates, they ranged from 1 to 3.8 *Synechococcus K. brevis*$^{-1}$ h^{-1}. These rates were significantly lower than Glibert et al. (2009) in similar prey to grazer ratios. When the ratios were ~ 40:1, ingestion rates ranged from 24 to 47 *Synechococcus K. brevis*$^{-1}$ h^{-1}, depending on strains of *K. brevis* culture (Glibert et al., 2009). Jeong et al. (2005) did not report the prey to grazer ratio.

However, the hourly ingestion rates of *Synechococcus* measured within the first 24 h in Experiments 1 and 2 were comparable to those reported by Glibert et al. (2009), who also measured their rates within the first 24 h. Although rates reported here were lower than the ingestion rates in similar prey:grazer ratios from Glibert et al. (2009), considering other differences, such as strains of a grazer, light intensities, growth rates, and nutrient concentrations, the estimates herein did not substantially deviate from the previous study. There was a significant discrepancy between hourly and daily ingestion rates in this study (Table 5.1), probably due to equilibrium of digestion and grazing. Li et al. (1999) reported relatively longer digestion time by *Karlodinium veneficum* (=*K. micrum* =*Gyrodinium galatheanum*), which belongs to the family *Kareniaceae* like *Karenia* species, on prey *Storeatula major*, ranging from 6 h of the half-life for food vacuole turnover at 30°C to 139 h at 10°C.

The ability to graze on larger cells than its known prey, *Synechococcus*, was shown here with *R. salina* (Fig. 5.4). Although ingestion rates on *R. salina* were notably lower than those on *Synechococcus*, rates fell within a similar range to the findings of Zhang et al. (2013). They reported that ingestion rates by *K. mikimotoi* on *I. galbana* ([ESD] = ~5 µm) and on *H. virescens* ([ESD] = ~ 6 µm) were 2.1-16.7 and 1.8-16.7 prey *K. brevis*$^{-1}$ d^{-1}, respectively, depending on nutrient conditions. It is likely that the cell size of prey plays a crucial role in determining the ingestion rates by *Karenia*. Kamiyama and Arima (2001) reported the strong inverse relationships between the ingestion rates of two ciliate species and the cell volume of their 10 prey species, which spanned a wide size spectrum. Martín-Cereceda et al. (2008) also reported negative correlation between ingestion rates by dinoflagellate *Oxyrrhis marina* on diverse biovolume of the prey. However, the size range of prey as well as optimal prey size for *K. brevis* has not been investigated yet and thus more types of prey should be tested.

Synergistic effects of mixotrophy as a nutrient source

Unlike previous studies, neither growth rates nor final densities of *K. brevis* were considerably enhanced, except in Experiment 1 (Fig. 5.3). Depending on *Synechococcus* concentrations, the growth rates of *K. brevis* increased substantially (when maintained at 43 µmol photons m^{-2} s^{-1}; 0.14 to 0.58 d^{-1}), although this pattern was not observed when light intensity was higher (300 µmol photons m^{-2} s^{-1}; 0.26 to 0.35 d^{-1}) (Glibert et al., 2009). Zhang et al. (2013) also reported enhanced growth of *K. mikimotoi* (maintained at 30 µmol photons m^{-2} s^{-1}) when prey were provided. However, the magnitude of the increase differed depending on the prey organism and

ambient inorganic nutrient conditions, and even zero growth was observed when prey organisms were inoculated into the grazer in N, P-limited medium (Zhang et al., 2013).

In this study, increased growth rates and densities of grazers in Experiment 1, but not in Experiments 2-4, may have been due to differing inorganic nutrient concentrations in the media. The experimental setup in Experiment 1 was almost identical to Glibert et al. (2009) and Zhang et al. (2013). Both studies used *K. brevis* in the (late) exponential phase from batch culture, as was done here in Experiment 1. Although N-limited L/5 media was used in our study, intense N limitation would be less likely during the exponential phase. On the other hand, in Experiments 2-4, *K. brevis* culture from the chemostat system was used, and grazers may have been experiencing a more substantial degree of N limitation. Indeed, Chl *a* cell^{-1}, closely related to cellular N content, was about 5-fold higher in Experiment 1 than in Experiments 3-4 ($p < 0.01$). These estimates from chemostat culture were comparable with Chl *a* cell^{-1} of chemostat-grown *K. brevis* under N-limited conditions (Corcoran et al., 2014; 4.1-5.7 pg cell^{-1}). Therefore, the nutrients that grazers obtained from the prey, especially N, in Experiments 2-4 would not be enough to promote the growth or density but could be used in other processes. In addition, a decrease in incorporation efficiencies of nutrients from prey has been observed in other species in nutrient-stressed cultures (Caron et al., 1990; Johnson, 2015). Johnson (2015) suggested the importance of the degree of nutrient stress for growth efficiency, as measured by the ratio of growth in grazers to their intake of prey of grazers.

These results also demonstrate that phagotrophic mixotrophy is not a simply additive process of phototrophy but has synergistic effects on the growth (and possibly other processes) of *K. brevis.* Especially under conditions of greater availability of inorganic nutrients, feeding on prey could promote the growth of *K. brevis*. This finding aligns with the observations from Zhang et al. (2013), who also reported the enhanced growth of *K. mikimotoi* in the presence of prey organisms, especially under nutrient-replete conditions. The single-cell approach of prey-driven ^{15}N assimilation into *K. brevis* was low; however, note that assimilation rates were from the surface of the grazer cells. Therefore, higher incorporation rates might be observed if ^{15}N assimilation rates of food vacuole in grazers can be estimated. In addition, our culture was non-axenic, thus bacteria-N could contribute to density and growth increase in grazer cells, especially under higher inorganic nutrient availability conditions.

Prey quality effects

The importance of the nutritional history of the predator or prey on mixotrophy has been observed in various dinoflagellates, including *K. veneficum* (e.g., Lin et al., 2017), *Prorocentrum minimum* (e.g., Johnson, 2015), and *Ceratium furca* (e.g., Smalley et al., 2003). Although direct comparisons are complicated due to differences in experimental designs across studies, this study, in contrast to previous research, did not observe selective feeding by N-limited *K. brevis* on *Synechococcus* with differing qualities (Fig. 5.2 and Table 5.1). No discernible differences were found in $rETR_{max}$ values of *Synechococcus* controls with varying qualities and those mixed with grazers (Fig. 5.7). Additionally, there were no evident patterns in growth

rates and $rETR_{max}$ values of *K. brevis* grazed on *Synechococcus* with different nutritional histories (Figs. 5.3 and S5.4).

Several factors could potentially account for the non-selective grazing on *Synechococcus* and little to no influence on the photosynthetic performance of both prey and predator in this study. First, although a gradient of nutritional states of *Synechococcus* was achieved (Fig. S5.2), it is possible that N or P limitation of prey may not necessarily have been attained. Indeed, Garcia et al. (2016) observed relatively invariable elemental quotas of N between N- and P-limited *Synechococcus*, although cellular P quota varied strongly depending on growth rates and nutrient conditions. Second, while no differences in cell-specific ingestion rates were observed, differences in N- or P-specific grazing rates on *Synechococcus* by *K. brevis* were attained. However, the cellular N and P contents of prey were not measured in this study (mainly due to the limitation of the culture volume). Lastly, ingestion rates per biovolume may vary. In *Synechococcus*, N-limited cells were larger than P-limited cells (especially at higher growth rates), as cellular C quota varies strongly with P limitation but not with N limitation (Garcia et al., 2016). Alternatively, *K. brevis* might not selectively graze on small *Synechococcus* with different nutritional histories. However, further testing with larger prey with varying qualities is needed to comprehend the mechanisms underlying the grazing behavior and nutritional history interactions between prey and predator of this species.

Implications for natural *K. brevis* blooms on the West Florida Shelf

Synechococcus spp. are ubiquitous picocyanobacterial that thrive well in the Gulf of Mexico (Paul et al., 2000; Wawrik et al., 2009), and an inverse relationship

between picocyanobacteria, including *Synechococcus* spp., and *K. brevis* was found in earlier studies (Heil et al., 2007; Sipler et al., 2013). As expected, this study showed that *K. brevis* could graze on *Synechococcus*. When inorganic nutrient concentrations were low, densities of *Synechococcus* were maintained at background levels (i.e., initial concentrations) with the presence of *K. brevis*. Furthermore, even though cell densities of *Synechococcus* remained similar to the initial densities when mixed with *K. brevis*, the photosynthetic ability of the prey decreased or became undetectable with our instrument within 24-48 h after exposure to the grazer. This demonstrates that the presence of *K. brevis* can not only directly affect *Synechococcus* through grazing but can also indirectly affect *Synechococcus*, partly due to nutrient competition and potentially due to allelopathy. Although *Synechococcus* grew well in the filtrate of *K. brevis* culture, potential negative effects of the allelopathic compounds released by *K. brevis* could not be excluded (Kubanek et al., 2005; Poulson-Ellestad et al., 2014; Poulin et al., 2018). Indeed, Kubanek et al. (2005) reported weaker inhibitory effects of filtrates on other co-occurring protist plankton than those exposed to live *K. brevis*.

On the West Florida Shelf, multiple (> 12) nutrient sources contributing to *K. brevis* blooms have been identified, including grazing on *Synechococcus* (Heil et al., 2014a and references therein). Although dissolved inorganic N and P concentrations are typically low on the West Florida Shelf, N and P fluxes from complex nutrient sources, such as benthic flux, estuarine flux, and nitrification, could meet the requirements to form large *K. brevi*s blooms (1×10^6 cells L^{-1}) in estuarine and coastal sites. If the nutrient source from grazing on *Synechococcus* were accounted

for solely, the N and P flux would be sufficient to supply a small *K. brevis* bloom (1×10^5 cells L^{-1}) in both sites (Heil et al., 2014a). However, this study demonstrated that *K. brevis* could graze on larger cells, namely *R. salina*, and other studies have also reported the grazing ability of *K. mikimotoi*—often co-blooming on the West Florida Shelf—on *I. galbana*, *H. virescens*, and *T. amphioxeia* (Zhang et al., 2013; Ok et al., 2023). Therefore, it is likely that the spectrum of *K. brevis*' prey could be broader than previously thought, and thus the contribution of mixotrophy to bloom maintenance might be more significant. However, caution is required to avoid overestimation when incorporating nutrient flux through grazing. Over a longer term, ingestion rates and, consequently, N and P flux through grazing may not be as high as the rates based on short term studies, as demonstrated in this study using hourly and daily ingestion rates from the same samples.

Summary and Conclusions

This study has shed light on several key aspects of mixotrophy in *K. brevis*. *K. brevis* grazed on *Synechococcus* as a function of prey quantity, but no substantial evidence of selective feeding by N-limited *K. brevis* on *Synechococcus* with varying nutritional qualities—N:P balanced, N-limited, P-limited—was found. Incorporation of the *Synechococcus* was confirmed by NanoSIMS analysis. Furthermore, *K. brevis* could graze on a larger cell than its recognized prey, *Synechococcus*, as demonstrated by the ingestion of *R. salina*. The ingestion rates of the latter were substantially lower, possibly due to differences in biovolume between the two prey.

Notably, the synergistic effects of phago-mixotrophy as a nutrient source were evident, with results indicating growth and density-promoting effects by feeding on prey under higher inorganic nutrient availability conditions. On the other hand, prey quality and quantity effects on growth, densities, and photosynthetic performance, measured by $rETR_{max}$, on grazers were not clearly observed when inorganic nutrients were insufficient.

These insights have implications for our understanding of *K. brevis* bloom dynamics in the West Florida shelf. Grazing on *Synechococcus* could directly regulate the density of picocyanobacteria but also indirectly might reduce the photosynthetic performance of *Synechococcus*. The demonstrated ability of *K. brevis* to feed on a broader range of prey species expands the potential spectrum of nutrient flux through grazing, although caution is needed in interpreting the contribution through grazing, as the rates can vary considerably over different timescales. Consequently, mixotrophy by *K. brevis* may be more significant in bloom formation and maintenance than previously anticipated.

Appendix III: Supplementary Material

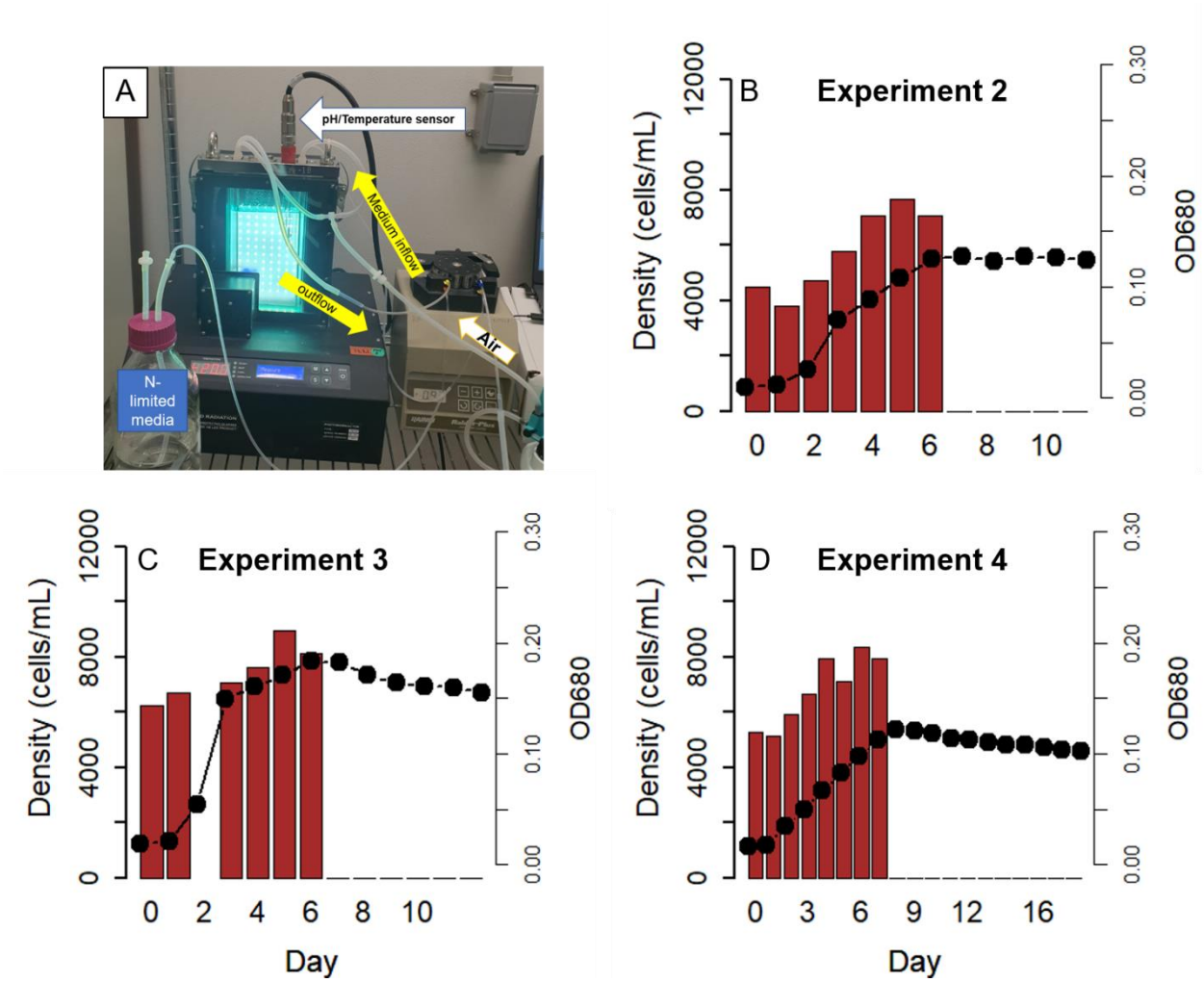

Figure S5.1. Chemostat setup growing *K. brevis* in N-limited L1 media (A) and optical density at 680nm (OD680) and *K. brevis* density measurements in Experiment 2 (B), Experiment 3 (D) and Experiment 4 (D). Black dots and brown bars represent OD680 and *K. brevis* density, respectively.

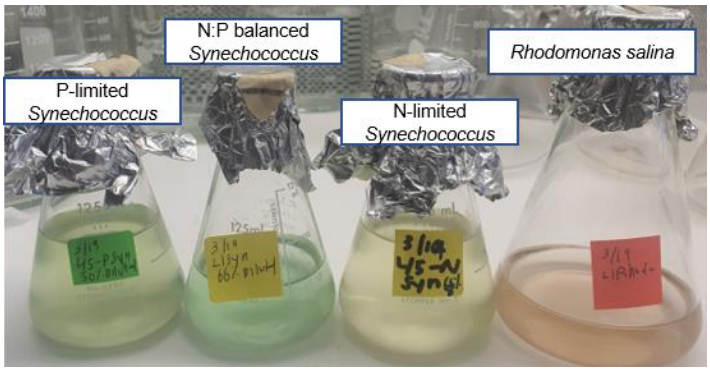

Figure S5.2. Prey cultures, N:P balanced, P-limited and N-limited *Synechococcus* and N:P balanced *Rhodomonas salina*.

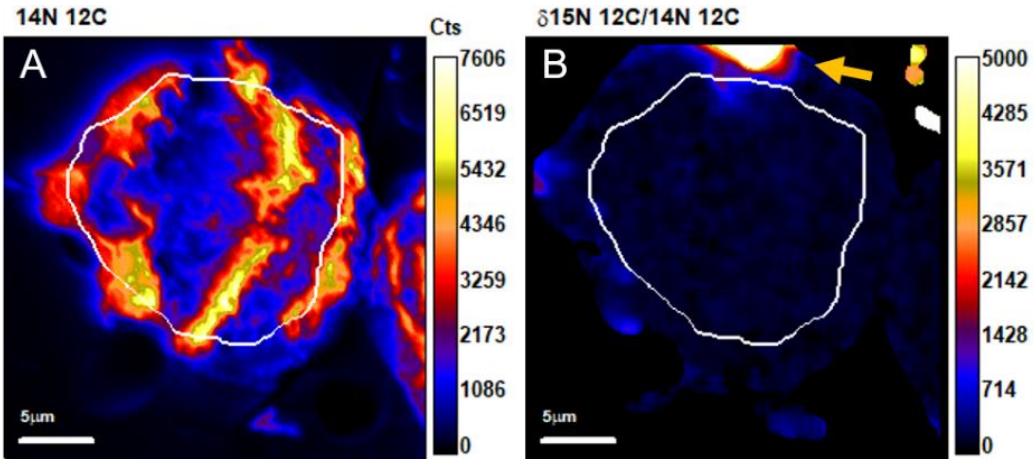

Figure S5.3. NanoSIMS images of $^{12}C^{14}N^-$ (A) and $\delta^{15}N$ (B) of *K. brevis* grazed on *Synechococcus*. The images of $^{12}C^{14}N^-$ were used as an indicator of *K. brevis* biomass to draw ROIs (white lines) and calculate cell-specific $\delta^{15}N$. High $\delta^{15}N$ values (orange arrows), the isotopically enriched *Synechococcus*, were excluded when manually drawing ROIs of *K. brevis*.

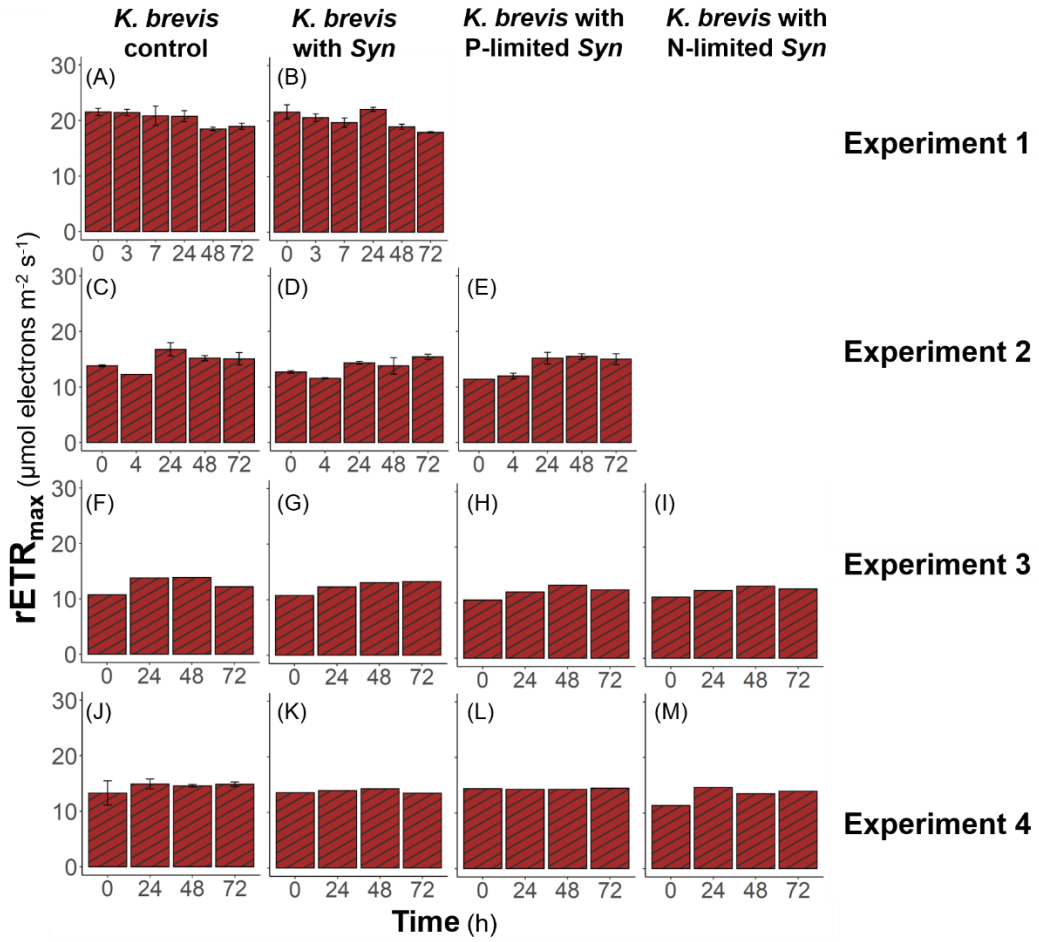

Figure S5.4. The maximum relative electron transport rate, $rETR_{max}$, of *K. brevis* with or without *Synechococcus* in Experiment 1 (A-B), Experiment 2 (C-E), Experiment 3 (F-I), and Experiment 4 (J-M) over 72 h.

Table S5.1. The single-cell $^{15}N/^{14}N$ ratios, ^{15}N isotopic abundance (atom%), and $\delta^{15}N$ (‰) of ROIs at 72 h in Experiment 1.

ROI Name	$^{15}N/^{14}N$	^{15}N isotopic enrichment	$\delta^{15}N$
K. brevis killed control	0.0039	0.391	69
K. brevis killed control	0.0039	0.389	65
K. brevis killed control	0.0038	0.382	45
K. brevis killed control	0.0040	0.394	79
K. brevis killed control	0.0039	0.390	66
K. brevis killed control	0.0038	0.383	47
K. brevis killed control	0.0038	0.381	42
K. brevis killed control	0.0040	0.398	88
K. brevis killed control	0.0039	0.385	52
K. brevis killed control	0.0039	0.388	61
K. brevis grazed on prey	0.0043	0.433	184
K. brevis grazed on prey	0.0043	0.424	159
K. brevis grazed on prey	0.0042	0.414	133
K. brevis grazed on prey	0.0043	0.427	169
K. brevis grazed on prey	0.0043	0.425	163
K. brevis grazed on prey	0.0039	0.390	66
K. brevis grazed on prey	0.0043	0.431	180
K. brevis grazed on prey	0.0042	0.417	140
K. brevis grazed on prey	0.0044	0.437	195
K. brevis grazed on prey	0.0043	0.423	158
K. brevis grazed on prey	0.0048	0.473	296
K. brevis grazed on prey	0.0048	0.474	297
K. brevis grazed on prey	0.0051	0.504	379
K. brevis grazed on prey	0.0047	0.463	268
K. brevis grazed on prey	0.0048	0.482	321
K. brevis grazed on prey	0.0046	0.463	266
K. brevis grazed on prey	0.0046	0.457	252
K. brevis grazed on prey	0.0046	0.454	244
K. brevis grazed on prey	0.0048	0.479	311
K. brevis grazed on prey	0.0045	0.452	238

Chapter 6: Temperature-dependent mixotrophy in natural populations of the toxic dinoflagellate *Karenia brevis*

Abstract

Previous studies have revealed that mixotrophs could become more heterotrophic as temperature rise, but these studies have mostly been conducted in the laboratory under temperature-acclimated conditions of grazers. This study investigated the short-term thermal regulation of grazing and photosynthetic performance by natural *Karenia brevis* populations on cultured *Synechococcus*. Bloom waters (> 5,000 cells mL^{-1}) were collected at and near Mote Marine Laboratory in Sarasota, Florida, every morning for three days during the fall of 2022. The cultured *Synechococcus* were inoculated into *K. brevis* bloom waters in varying ratios and incubated at ambient (24°C) and ambient temperature ± 5°C (19, 29°C). The densities and photosynthetic performance, measured by PAM fluorometry, of both predator and prey were monitored on various time scales. At each treatment, generally, the grazing coefficients (g), clearance rates, and ingestion rates were higher in warmer waters. However, ingestion rates were significantly regulated by the prey-to-grazer ratios and by temperatures to a lesser degree and ranged from 8 to 204 *K. brevis Synechococcus*$^{-1}$ d^{-1}. Photosynthetic performance of grazer and prey, measured as maximum relative electron transport rate ($rETR_{max}$), exhibited different responses depending on time, temperature, and the presence of grazer or prey. In general, $rETR_{max}$ of *K. brevis* in the control groups and mixed treatments decreased with time, while $rETR_{max}$ of *Synechococcus* controls increased over time with a more substantial increase at

warmer temperatures. However, in the presence of grazers, $rETR_{max}$ of *Synechococcus* did not increase or remarkably decreased. These results suggest that grazing on *Synechococcus* could directly regulate the density of *Synechococcus* populations but also indirectly reduce the photosynthetic performance of prey. Furthermore, this study demonstrates that thermal regulations of grazing and photosynthetic performance can occur on a short-term basis.

Introduction

The metabolic theory of ecology predicts that metabolic rates increase with rising temperatures, with heterotrophic metabolism being more temperature-sensitive than autotrophic metabolism (Brown et al., 2004; Allen et al., 2005). Several studies have demonstrated that mixotrophs became more phago-heterotrophic as temperatures increase (e.g., Wilken et al., 2013; Liu et al., 2021) or exhibit increased temperature tolerance when provided with a food source (e.g., You et al., 2020). These findings suggest potential alterations in the role of mixotrophs in global food webs and carbon cycling in response to climate change. However, most studies were conducted in controlled laboratories with grazers acclimated to specific temperatures. Therefore, we conducted short-term grazing experiments using natural *Karenia* populations to subject them to sudden temperature changes, mimicking the conditions that cells are likely to experience in the field.

Karenia brevis is a toxic mixotrophic dinoflagellate responsible for the nearly annual Florida Red Tide (e.g., Brand et al., 2012; Heli et al. 2022). This species can be found throughout the year in the waters of the Gulf of Mexico, especially in the West Florida Shelf, but typically initiates blooms from later summer to early fall

(Brand and Compton, 2007; Heil et al., 2022). On a daily basis, *K. brevis* experiences thermal fluctuations. These cells disperse to deeper depths at night but migrate into surface waters during the daytime due to phototactic and negative geotactic responses (Heil et al., 2014b). Sharp vertical thermal gradients may be encountered in the surface water during the day (e.g., Weisberg et al., 2014), or cells might experience stronger temperature gradients while undergoing vertical migration. Therefore, grazing and photosynthetic responses to ambient temperature and ± 5°C variations were herein investigated.

Previous studies of the mixotrophic behavior by *K. brevis* were conducted in controlled laboratory environments with grazers acclimated to 20°C (Jeong et al., 2005; Glibert et al., 2009). Grazing responses of *K. mikimotoi*—a close relative to *K. brevis*— have also been investigated at a single temperature, 20°C (Zhang et al., 2011, 2013; Ok et al., 2023). Additionally, to our knowledge, ingestion rates and photosynthetic rates of *K. brevis*, especially natural populations, have not yet been investigated simultaneously. Therefore, in the present study, we examined the feeding behavior and photosynthetic responses of natural *K. brevis* populations and prey to short-term temperature variations. We hypothesized that *K. brevis* will become more heterotrophic when exposed to warmer temperatures.

Materials and methods

Field Sampling

Bloom waters were collected over three days from 11/28/2022 to 11/30/2022. Surface waters at the South Dock (SD; dock near Sarasota Sailing Squadron) and Bay

Dock (BD; Mote Marine Laboratory dock) were collected daily between 9 am and 10 am using a bucket. Samples were transported within 30 min under shade to the location where experiments were conducted. Surface temperatures were measured with a YSI hand-held instrument (YSI Inc., Ohio, USA). Samples for determining dissolved inorganic nutrients (nitrate + nitrite, ammonium, and phosphate) were filtered through Whatman GF/F filters (Whatman, Maidstone, United Kingdom) and filtrates were frozen for subsequent analysis. The filtrates were later analyzed at the Bigelow Laboratory for Ocean Sciences, West Boothbay Harbor, Maine, United States.

Prey culture

A culture of non-axenic *Synechococcus* sp. (CCMP836) was maintained at 20°C with a salinity of 30 and a light intensity of 100 µmol photons m^{-2} s^{-1} in a 12h light:12h dark cycle. The media for the original stock culture were prepared using previously-collected, nutrient-poor offshore Gulf of Mexico seawater. The seawater was filtered through GF/F filters (nominal pore size: ~ 0.7 µm; Whatman, Maidstone, Germany) and autoclaved. Then, 0.2 µm-filtered nutrient stocks were added based on the L1-silicate media recipe (Guillard and Hargraves, 1993).

Before starting the grazing experiments, exponentially growing *Synechococcus* cultures were centrifuged at 1000 x g for 5 min to isolate them from nutrient-rich culture media. Subsequently, *Synechococcus* pellets at the bottom of the tubes were resuspended into nutrient-poor offshore Gulf of Mexico seawater with a salinity of 33 - 34. Resuspended *Synechococcus* cultures were maintained at 22 -

24°C with a light intensity of 50-100 µmol photons m^{-2} s^{-1} in a 12h light:12h dark cycle.

Short-term ingestion experiments

Bloom waters collected from SD (11/28-11/30/2023) and BD (11/30/2323) were divided into 50 mL polypropylene tubes for separate treatments: grazer control, prey control, and grazers mixed with prey at one or two different ratios (R_1 and R_2). The prey-to-grazer water ratios (volume:volume) were determined using a Phyto-PAM-II fluorometer (Heinz Walz GmbH, Effeltrich, Germany) to obtain fluorescence signals of both *Karenia* and *Synechococcus.* These treatments were exposed to two (Experiments 1, 2) to three (Experiment 3) different temperatures, including ambient (24^{o}C) and ambient temperature ± 5°C (19, 29°C) (Fig. 6.1). All incubations were conducted in custom-made temperature-controlled water baths (Bay Instruments LLC, Maryland, USA), illuminated by LED lights with 100-150 µmol photons m^{-2} s^{-1}.

Bloom waters collected from SD were used as grazer controls and also as grazers mixed with resuspended *Synechococcus* cultures in Experiments 1 and 2. In Experiment 1, the prey-to-predator water ratios (R_1 and R_2) were 3:1 and 5:4, respectively, and samplings were conducted at T_0 ($Time_0$), T_3, T_{24} T_{72}. In Experiment 2, R_1 and R_2 for the mixed treatments were 2:3 and 5:8, respectively, and prey controls were diluted using filtrates of bloom waters in the same ratios as the mixed treatments (prey control R_1 and R_2). Samplings were carried out at T_0, T_5, T_{24}, T_{48} in Experiment 2. All incubations were conducted at 24°C and 29°C in Experiments 1 and 2. Samples for cell counting and PAM analysis were obtained at all sampling points except at T_{24} for prey control R_2 of Experiment 2.

In Experiment 3, SD and BD waters were used as grazer controls and were mixed with prey cultures in ratios of 1:4 (R_1) for SD and 1:1 (R_1) for BD. Prey controls were diluted in the same ratios as the mixed treatments (Prey control R_1). Incubations took place under the same temperatures as described above and samplings were conducted at T_0, T_4, T_{24} for SD treatments and at T_0, T_4, T_{24}, T_{48} for BD treatments. Additional PAM analysis of mixed treatments was performed at T_2 and T_1 for SD and BD treatments, respectively. The actual ratios of prey-to-grazer (cell:cell) were determined after subsequent counting of the cell densities (Table 6.2).

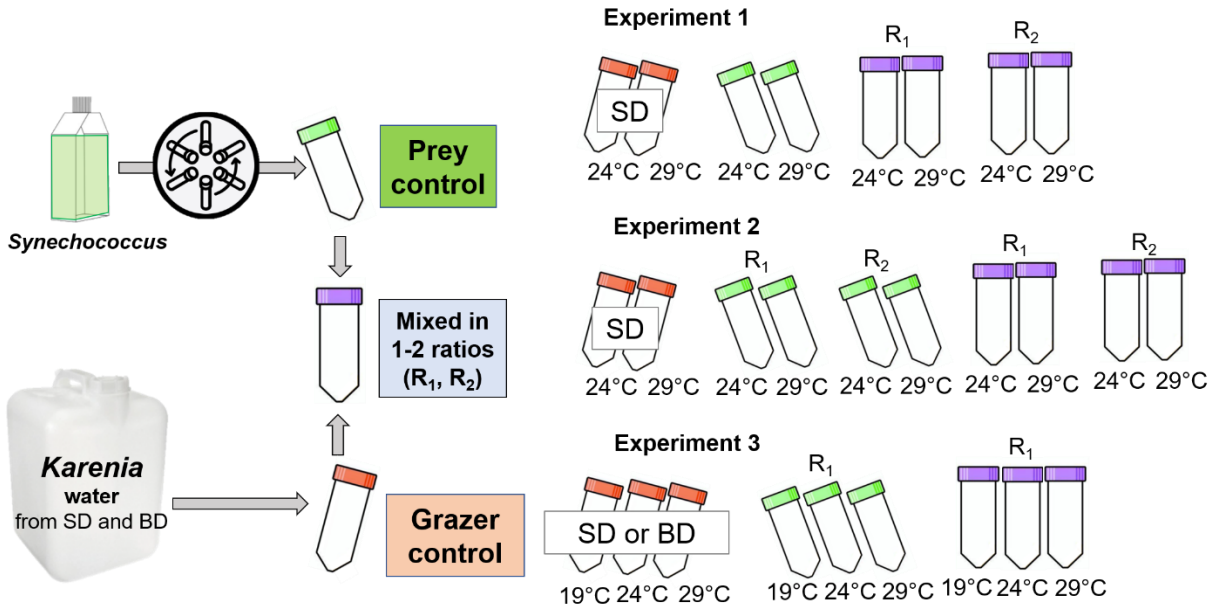

Figure 6.1. Experimental design examining temperature effects on grazing rates by *K. brevis* on *Synechococcus*. SD, BD, R_1, and R_2 represent South Dock, Bay Dock, and ratios 1 and 2, respectively.

Enumeration of grazer and prey and rate calculations

Samples for determining the cell abundance of grazers were fixed in Lugol's solution (2% final concentration), while those for prey were fixed with glutaraldehyde (0.5% final concentration). Grazers were enumerated at 100× magnification using a Sedgewick-Rafter chamber under light microscopy. Samples for prey were filtered onto 0.2 µm pore-size, 25 mm black polycarbonate membrane filters (GVS, Bologna, Italy) and then mounted onto glass slides with mounting solution (Thermo Fisher Scientific, Massachusetts, United States) under a cover slip.

Specific growth rates were calculated as $\mu = (\ln N_2 - \ln N_1) \times (t_2 - t_1)^{-1}$ where N_2 and N_1 denote the concentrations of prey or grazer cells at respective times, t_2 and t_1, respectively. The grazing coefficient was calculated as $g = \mu_{\text{prey control}} - \mu_{\text{prey mixed with grazer}}$. Clearance rates were calculated by dividing grazing coefficient, g, with mean predator density, $P = (P_0 \times (e^{\mu t} - 1)) \times (\mu t)^{-1}$ where P_o is the initial grazer concentration (Heinbokel, 1978). Using the equation of Frost (1972), ingestion rates were calculated by multiplying clearance rates with mean prey abundance, $C = (C_o \times (e^{\mu t} - 1)) \times (\mu t)^{-1}$ where C_o is the initial abundance of prey cells.

Pulse-amplitude-modulated (PAM) fluorometry

The photosynthetic characteristics of grazer and prey were examined using a Phyto-PAM-II fluorometer (Heinz Walz GmbH, Effeltrich, Germany). Rapid light curves consisting of 10 light steps increasing at intervals of 20s (0 to ~600 µmol photons m^{-2} s^{-1}) were performed after the dark adaptation of the samples. A modified nonlinear function of Platt et al. (1980) was fitted to each curve to obtain the

maximum relative electron transport rate ($rETR_{max}$). Fluorescence signals of both grazer and prey were obtained by single measurement because the Phyto-PAM-II fluorometer can differentiate blue-green algae, green algae, brown algae, and phycoerythrin-containing algae.

Statistical analysis

Differences in cell densities, grazing coefficients, clearance rates, ingestion rates, and $rETR_{max}$ of prey and grazer across different treatments (control or mixed, 2-3 different temperatures) were analyzed using a t-test or a one-way analysis of variance (ANOVA) with the data passing normality (Shapiro-Wilk test) and equal variance tests (Levene's test). If data did not satisfy the normality assumption, the non-parametric Wilcoxon rank sum test or Kruskal-Wallis's analysis was applied. Multiple linear regression was used to explore the relationship between ingestion rates by *K. brevis* on *Synechococcus* and prey-to-predator ratios and temperatures.

Results

Environmental conditions

The surface water temperatures varied marginally over three sampling days (Table 6.1). Therefore, incubation temperatures, ambient and ambient + 5°C, followed the setting of Experiment 1 (24°C, 29°C) although ambient temperature was slightly lower in Experiment 2. The concentrations of major inorganic nutrients, nitrate + nitrite, ammonium, and phosphate, were low (< 0.6 µM) during sampling dates, but concentrations of ammonium were somewhat higher (> 2 µM) on 11/28 and 11/30 at site SD (Table 6.1).

All samples were dominated by *K. brevis*, ranging from 4,300 to 15,800 cells mL^{-1} at T_0 samples (Table 6.2). Few other protists (e.g., *Prorocentrum* sp., *Chaetoceros* sp.) were also found, but they did not exceed 1% of the total community in Experiments 1 SD and 3 BD. In Experiments 2 SD and 3 SD, the percentages of *K. brevis* to total communities were 93% and 96%, respectively. Undefined flagellates in two size ranges, 2-3 µm and 5-6 µm, were also found in samples over the three days of sampling. In Experiments 1 SD and 3 BD, undefined flagellates contributed < 0.5% at T_0 samples but increased somewhat at T_{final} when incubated at 29°C (1 - 5%). In Experiment 2, the percentages of flagellates were 4% at T_0 samples increased up to ~15% at 24°C and ~34% at 29°C by the final sampling points.

Table 6.1. Ambient temperature and nutrients concentrations during three days of sampling from South Dock (Experiment 1-3) and Bay Dock (Experiment 3).

	South Dock			Bay Dock
	Experiment 1	Experiment 2	Experiment 3	Experiment 3
Temperature (°C)	24.0	22.5	23.5	23.9
Nitrate + Nitrite (µM)	0.53	0.25	< 0.05	0.19
Ammonium (µM)	3.77	0.59	2.41	0.53
Phosphate (µM)	0.21	0.12	0.10	0.25

Table 6.2. Initial conditions of predator (P_0) and prey (C_0) densities and prey:predater ratios (volume:volume, cell:cell), calculated daily grazing coefficient (g) , clearance rate, and ingestion rates.

	Prey:grazer (vol:vol)	Tempe rature	P_0 ($\times 10^3$ cells ml^{-1})	C_0 ($\times 10^6$ cells ml^{-1})	C_0: P_0 (cell:cell)	g (d^{-1})	Clearance rate (mL *K. brevis*$^{-1}$ d^{-1})	Ingestion rate (cells *K. brevis*$^{-1}$ d^{-1})
Experiment 1	3:1	24°C	13.2	1.2	90 :1	0.40	0.00003	31
		29°C	13.0	1.4	106:1	1.26	0.00012	65
	5:4	24°C	15.8	0.9	63:1	0.57	0.00004	26
		29°C	19.1	0.9	48:1	2.51	0.00014	26
Experiment 2	2:3	24°C	5.3	1.3	243:1	0.93	0.00018	176
		29°C	5.9	1.2	209:1	1.43	0.00025	166
	5:8	24°C	4.8	1.0	216:1	0.45	0.00009	79
		29°C	4.3	1.0	242:1	2.43	0.00074	204
Experiment 3	1:4	19°C	5.4	1.1	208:1	0.23	0.00003	32
		24°C	5.4	1.1	208:1	0.84	0.00017	152
		29°C	5.4	1.1	208:1	0.51	0.00010	100
	1:1	19°C	10.9	1.5	141:1	0.04	0.000004	8
		24°C	10.9	1.5	141:1	0.29	0.00003	48
		29°C	10.9	1.5	141:1	1.37	0.00013	63

Synechococcus density changes

The densities of *Synechococcus* controls were higher than those in the presence of *K. brevis* although only Experiments 1 and 2 exhibited significant differences ($p < 0.05$) (Fig. 6.2). In most of the prey controls, concentrations of *Synechococcus* increased or remained similar from T_0 to T_{Final} (solid lines in Fig. 6.2), but the concentration of prey in the control at 29°C was reduced by 37% of initial concentration at T_{Final} in Experiment 3 BD (Fig. 6.2D). When *Synechococcus* were mixed with grazers, prey concentrations generally decreased with time except in BD treatments in Experiment 3. At 19°C and 24°C, prey densities in mixed treatments increased by 39% and 13% from T_0 to T_{Final}, respectively. In addition, at T_4, the density of *Synechococcus* mixed with grazers at 29°C increased remarkably, although they eventually were reduced to 6% of the initial concentration at T_{Final}. In other experiments, generally, densities of *Synechococcus* in the presence of grazers decreased with time, with more substantial reduction at 29°C (e.g., 10% and 1% of initial concentrations at T_{Final} in Experiment 1 R_1 at 24°C and 29°C, respectively).

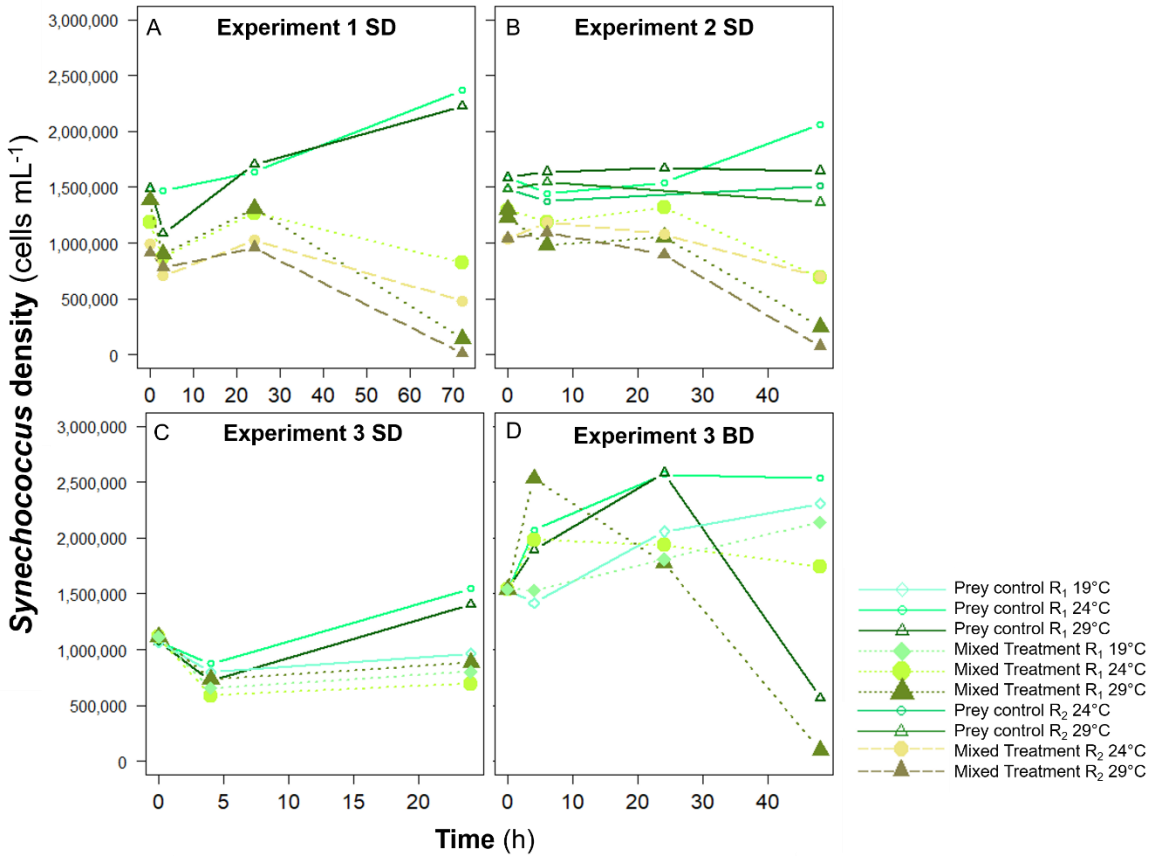

Figure 6.2. The changes of *Synechococcus* densities with or without grazers at different temperatures and ratios in (A) Experiment 1 SD, (B) Experiment 2 SD, (C) Experiment 3 SD, and (D) Experiment 3 BD treatments. Solid lines with empty symbols represent controls of *Synechococcus*. In contrast, dotted lines with filled symbols represent *Synechococcus* mixed with *K. brevis* bloom waters from South Dock (SD) and Bay Dock (BD): Diamonds (♦, ◊) for the treatments at 19°C, circle (○, ●) for the treatments at 24°C and triangle (△, ▲) for the treatments at 29°C.

Karenia brevis density changes

The densities of *K. brevis* primarily decreased with time in all treatments except in Experiment 1 SD R_2 and in Experiment 3 SD treatments at 19°C (Fig. 6.3).

In Experiment 1, the density of *K. brevis* increased in both R_1 and R_2 treatments with a significant increase in the later treatments at T_3 (Fig. 6.3A). On the other hand, in all other treatments except Experiment 3 SD 19°C, densities of the grazers decreased at T_4-T_5 and generally maintained these densities until T_{Final} (Fig. 6.3B-D). In Experiments 1 and 2, density changes were higher at 29°C. In R_1 treatments, biomass of grazer decreased to 66% and 51% at 29°C while, at 24°C, they decreased to 84% and 83% of those at T_0 in Experiments 1 and 2, respectively. In Experiment 1 R_2 treatments, when *K. brevis* was exposed to 29°C, the density increased 7% compared to density at T_0, while it increased 43% to 24°C.

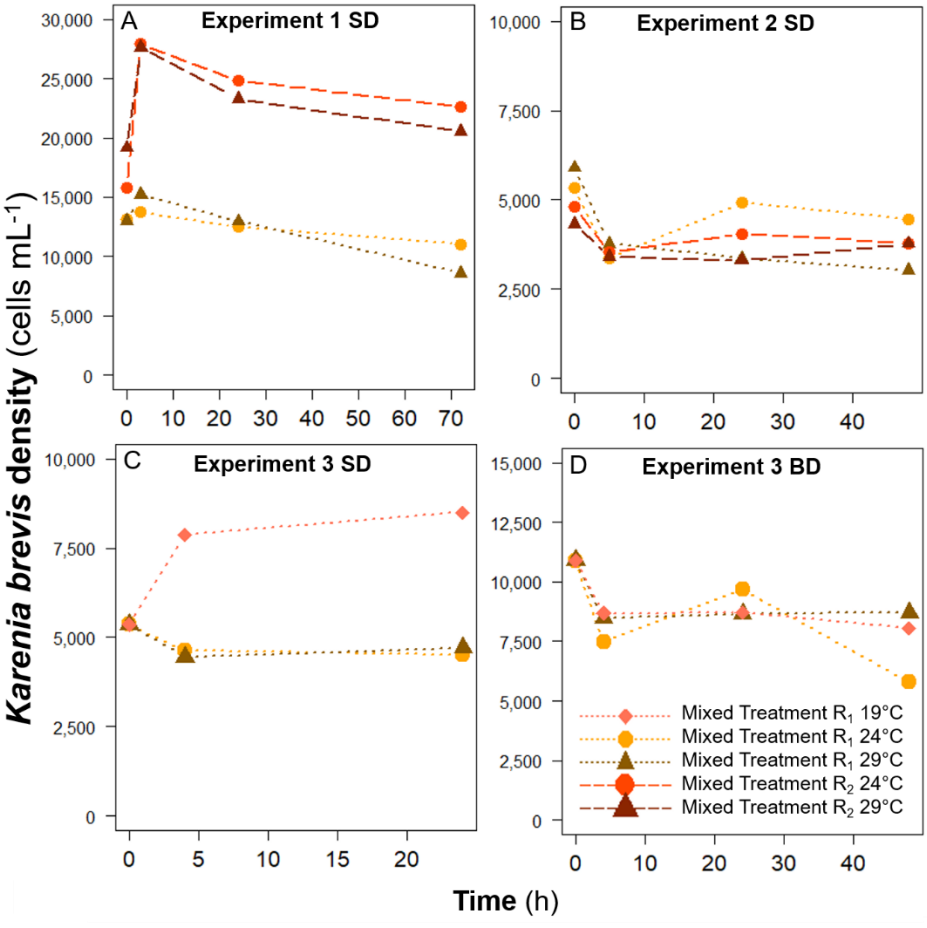

Figure 6.3. The changes in *Karenia brevis* densities at different temperatures and ratios in (A) Experiment 1 SD, (B) Experiment 2 SD, (C) Experiment 3 SD, and (D) Experiment 3 BD treatments. R_1, R_2, SD, and BD represent ratio 1, ratio 2, South Dock, and Bay Dock, respectively.

Temperature effects on grazing of *Karenia brevis* on *Synechococcus*

The daily maximum grazing coefficient (*g*), volume-specific clearance rate, and cell-specific ingestion rates of *K. brevis* on *Synechococcus* were generally higher at warmer temperatures (Fig. 6.4). In Experiments 1-2, the daily rate of *g* at 29°C were 1.5 to 5.4-fold higher than those at 24°C across different prey-to-grazer ratios (Fig. 6.4A, Table 6.2). In Experiment 3 SD and BD, the rates of *g* at 19°C were the lowest and gradually increased with rising temperature in BD treatments (from 0.04 to 1.37 d^{-1}), but not in SD treatments. Value of *g* was the highest at 24°C compared with other temperatures (Fig. 6.4A). The daily clearance rates exhibited a consistent pattern with *g*, exhibiting higher rates at warmer temperatures except in Experiment 3 SD treatments (Fig. 6.4B). Ingestion rates by *K. brevis* on *Synechococcus* generally showed similar patterns with other two parameters. Nevertheless, there were some differences (Fig. 6.4C). Daily ingestion rates by *K. brevis* on prey at 24°C were similar and higher than those at 29°C in Experiment 1 SD R_2 and Experiment 2 SD R_1 treatments, possibly due to slightly different prey-to-grazer ratios. Although daily ingestion rates did not dependent on prey amounts (R^2= 0.16), the ingestion rates were strongly dependent on prey-to-predator ratios ($p < 0.01$) than on temperature ($P < 0.05$), according to the relationship (R^2= 0.75):

$$\text{Ingestion rates} = 0.79\times\text{prey-to-predator ratios} + 8.16\times\text{Temperature} - 250.80 \quad \text{Eq(1)}$$

The lowest ingestion rate was observed at 19°C in Experiment 3 BD R_1 treatment (8 *Synechococcus K. brevis*$^{-1}$ d^{-1}), and the highest rate was found at 29°C in Experiment 2 R_2 treatment (204 *Synechococcus K. brevis*$^{-1}$ d^{-1}) when the prey-to-grazer ratio was the second highest (Table 6.2).

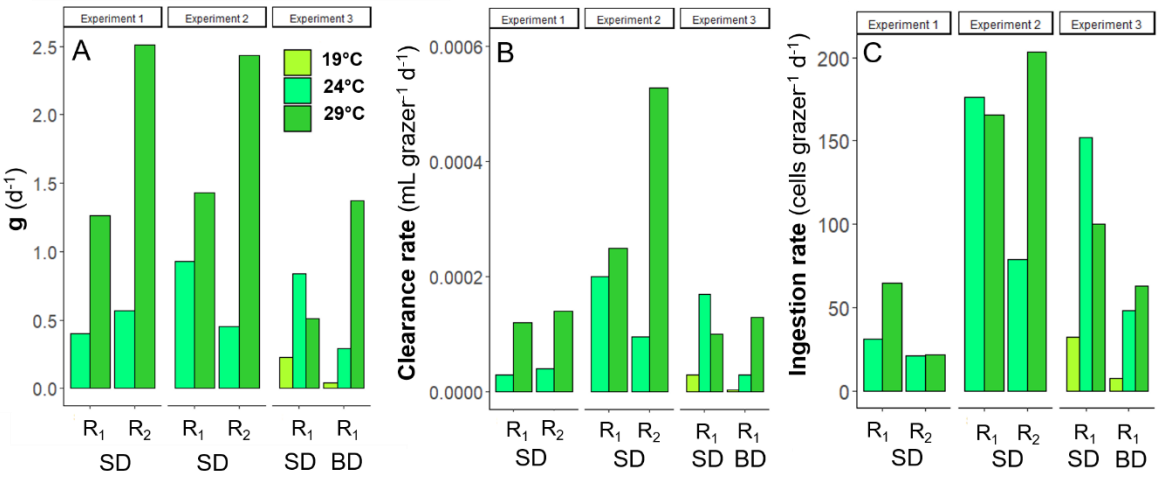

Figure 6.4. The maximum (A) grazing coefficient (*g*), (B) clearance rate, and (C) Ingestion rate of *K. brevis* on *Synechococcus* at 19, 24, 29°C. R_1, R_2, SD, and BD represent ratio 1, ratio 2, South Dock, and Bay Dock, respectively.

In contrast, the hourly ingestion rates that were calculated ≤ T_5 after mixing prey and grazers did not correlate with either prey-to-predator ratios or temperatures. Grazing activities were not observed in some treatments (Table 6.3). The hourly ingestion rates were mostly the highest at 24°C except for Experiment 2. Overall, ingestion rates ranged from 0 to 18 *Synechococcus K. brevis*$^{-1}$ h^{-1}.

Table 6.3. Initial conditions of predator (P_0) to prey (C_0) ratios (cell:cell) and calculated hourly grazing coefficient (g) , clearance rate, and ingestion rates.

	Temperature	C_0: P_0 (cell:cell)	g (h^{-1})	Clearance rate (mL *K. brevis*$^{-1}$ h^{-1})	Ingestion rate (cells *K. brevis*$^{-1}$ h^{-1})
Experiment 1	24°C	90 :1	0.10	0.000007	7
	29°C	106:1	0.04	0.000003	3
	24°C	63:1	0.11	0.000010	4
	29°C	48:1	0	0	0
Experiment 2	24°C	243:1	0	0	0
	29°C	209:1	0.05	0.000010	12
	24°C	216:1	0	0	0
	29°C	242:1	0	0	0
Experiment 3	19°C	208:1	0.06	0.000010	8
	24°C	208:1	0.11	0.000020	18
	29°C	208:1	0.01	0.000001	1
	19°C	141:1	0	0	0
	24°C	141:1	0.01	0.000001	2
	29°C	141:1	0	0	0

Temperature effects on photosynthetic performance

The effects of grazer presence and temperature on the photosynthetic rate of *Synechococcus*, measured by $rETR_{max}$, were significant ($p < 0.05$) in Experiments 1 and 2 (Fig 6.5). In Experiments 1-2, $rETR_{max}$ of *Synechococcus* controls increased with time, especially at 29°C in Experiment 2 (Fig. 6.5A, B, G, H, K, L). The values

of $rETR_{max}$ of *Synechococcus* increased 2.1- and 1.8-fold at 24°C in R_1 and R_2 control treatments while, at 29°C, they were enhanced 2.4- and 2.2-fold from T_0 to T_{final}. When prey were mixed with grazers, $rETR_{max}$ values of prey decreased (Fig. 6.5E, M, N) and even became undetectable (Figs. 6.5D, F) or remained similar (Figs. 6.5C, I, J) to values of T_0 at T_{final}. When mixed treatments were exposed to a warmer temperature, the values of $rETR_{max}$ of *Synechococcus* decreased more. For example, in Experiment 1 R_2 treatments, $rETR_{max}$ values of prey at 24°C were reduced to 6% of $rETR_{max}$ at T_0 after 72h, but values at 29°C were reduced to 5% of initial values of $rETR_{max}$ after 24 h (Fig. 6.5E, F). In Experiment 3, the values of $rETR_{max}$ of *Synechococcus* controls were the highest at 29°C and the lowest at 19°C at T_{Final} (Fig 6.6A-C, G-I). At 29°C, $rETR_{max}$ of *Synechococcus* controls were higher than those mixed with grazers at T_{Final} (Fig. 6.6C, F, I, L). However, these differences were not significant ($p > 0.05$). In addition, $rETR_{max}$ of *Synechococcus* controls at 19°C and 24°C decreased slightly until T_{24} (Fig. 6.6A-B, G-H).

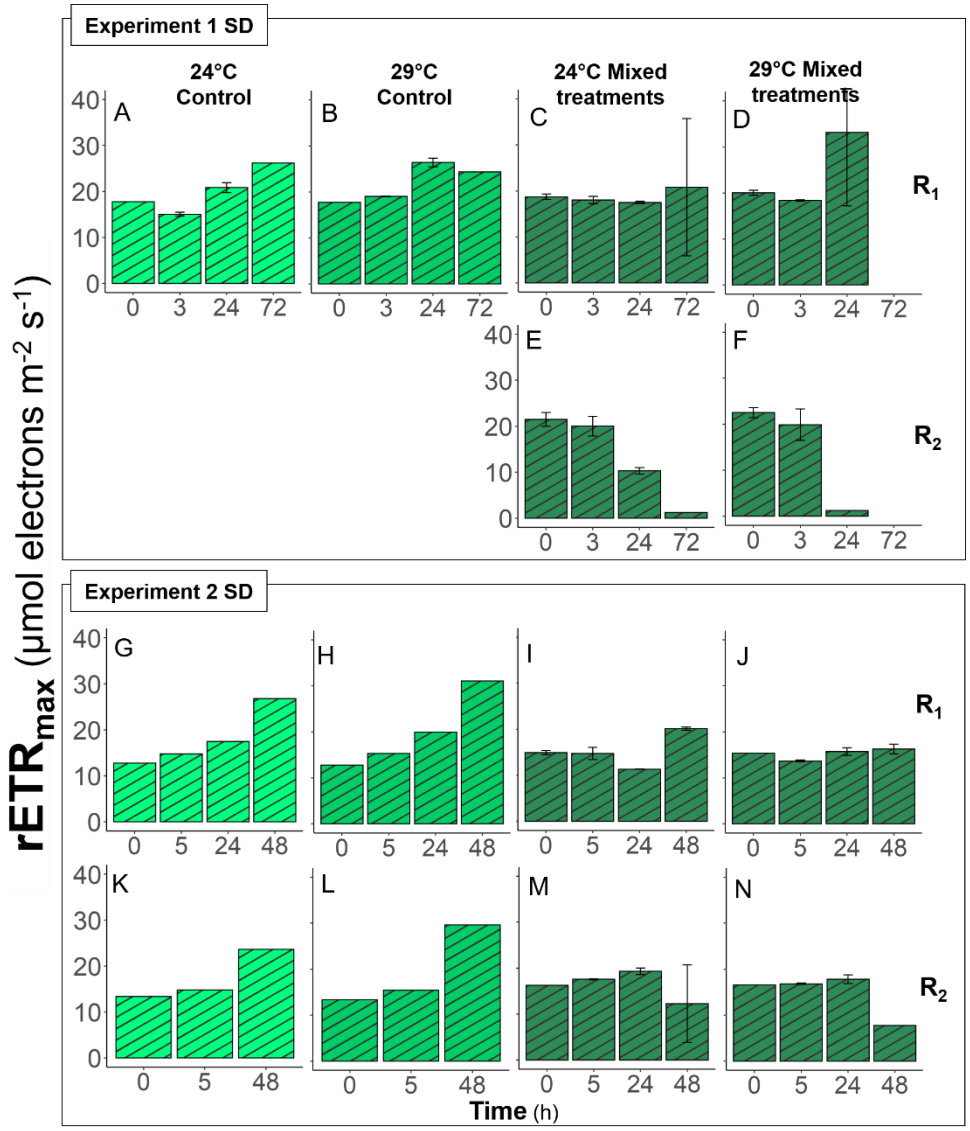

Figure 6.5. The maximum relative electron transfer rate, $rETR_{max}$, of *Synechococcus* over time in Experiments 1 (A-F) and 2 (G-N). R_1, R_2, SD, and BD represent ratio 1, ratio 2, South Dock, and Bay Dock, respectively.

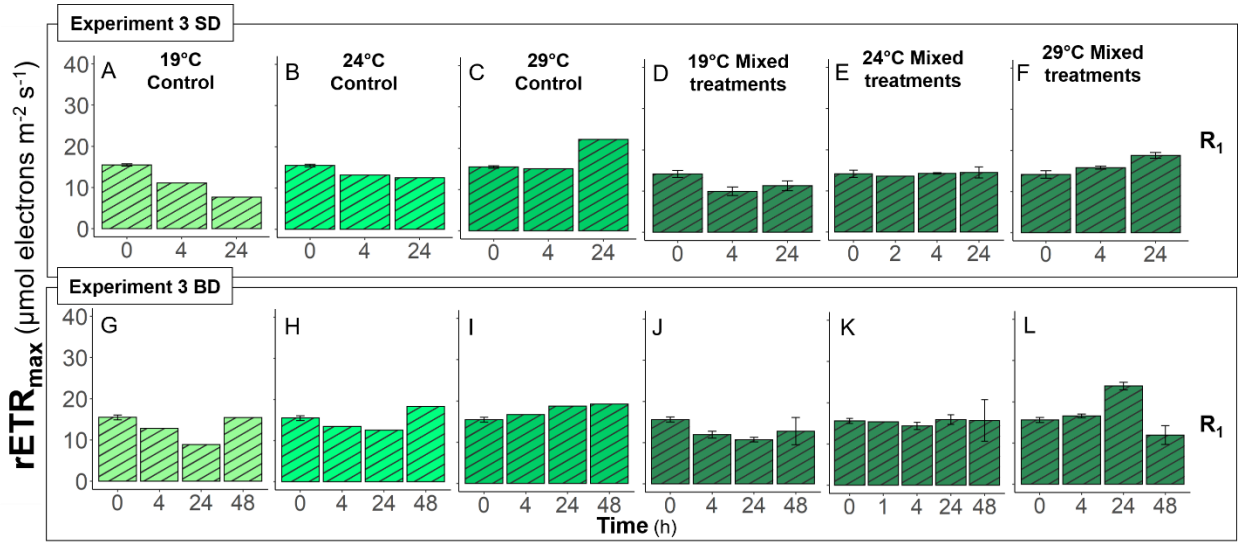

Figure 6.6. The maximum relative electron transfer rate, $rETR_{max}$, of *Synechococcus* over time in Experiments 3 SD (A-F) and BD (G-L). R_1, R_2, SD, and BD represent ratio 1, ratio 2, South Dock, and Bay Dock, respectively.

In all experiments and all treatments, $rETR_{max}$ values of *K. brevis* decreased over time (Fig. 6.7 and 6.8). No differences were found between grazer controls and those feeding on prey. Also, temperature effects on the photosynthetic rates of *K .brevis* with or without prey were not observed. The only differences were found in Experiment 1 at T_{final} (72 h). When *K. brevis* was fed with S*ynechococcus*, the values $rETR_{max}$ of grazers decreased to 73-82% of the initial values in R_1 and R_2 treatments. However, in grazer controls at 24 and 29°C, the $rETR_{max}$ values were reduced to 54% and 38% of those at T_0 (Fig. 6.7A-F).

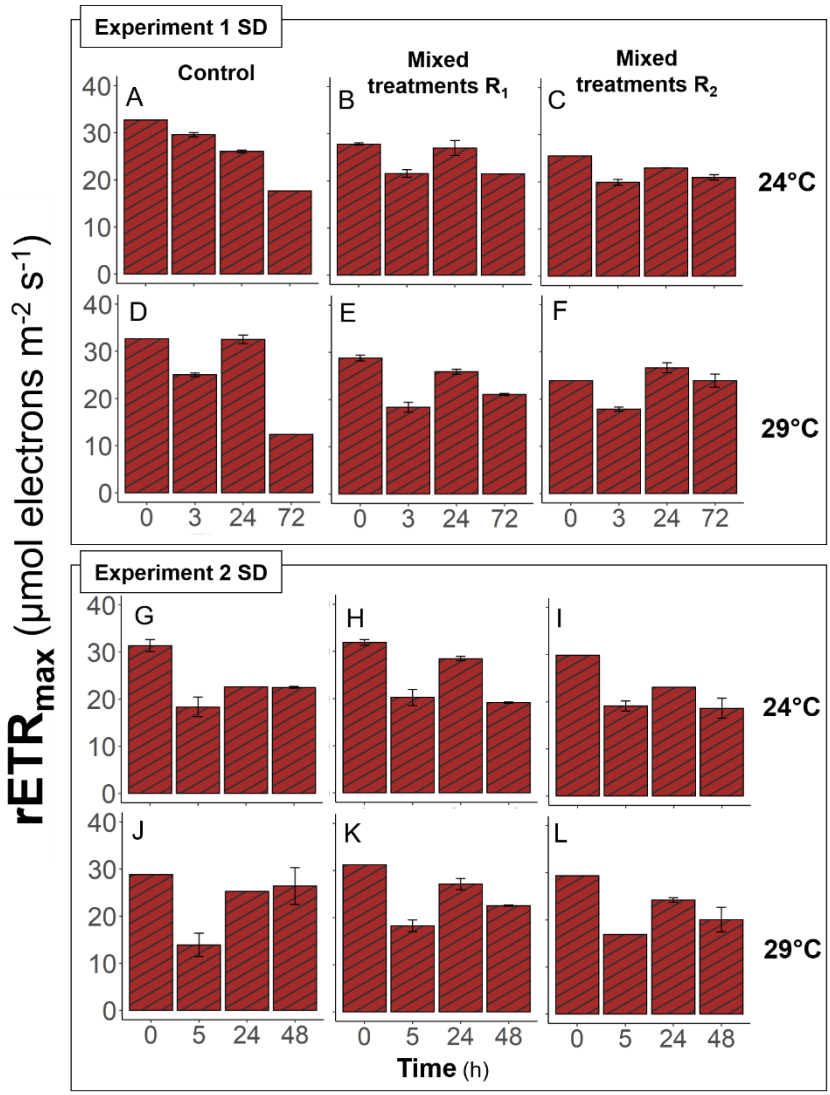

Figure 6.7. The maximum relative electron transfer rate, $rETR_{max}$, of *Karehia brevis* over time in Experiments 1 (A-F) and 2 (G-L). R_1, R_2, SD, and BD represent ratio 1, ratio 2, South Dock, and Bay Dock, respectively.

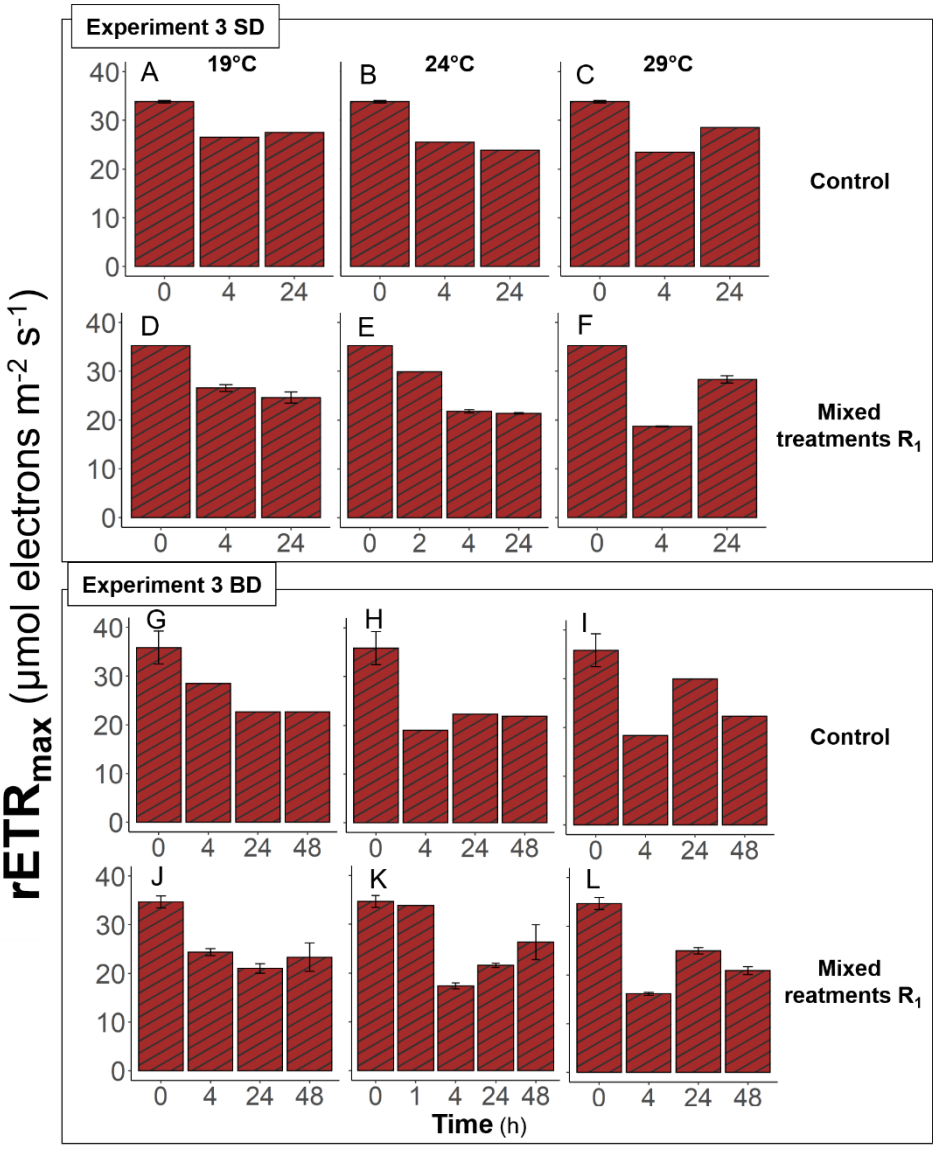

Figure 6.8. The maximum relative electron transfer rate, $rETR_{max}$, of *Karenia brevis* over time in Experiments 3 SD (A-F) and BD (G-L). R_1, R_2, SD, and BD represent ratio 1, ratio 2, South Dock, and Bay Dock, respectively.

Discussion

The short-term temperature-dependent mixotrophic and photosynthetic activities of natural *K. brevis* populations were examined here when cells were supplied with cultured *Synechococcus*. As hypothesized, the grazing rates of *K. brevis*

generally enhanced with rising temperatures and affected the photosynthetic rates of prey more at warmer temperatures.

Grazing on *Synechococcus* by natural *Karenia brevis* population

As consistent with previous culture experiments, natural populations of *K. brevis* could graze on *Synechococcus,* and the rates strongly depended on prey-to-predator ratios (Jeong et al., 2005; Glibert et al., 2009). Prey concentrations have been important factors that positively correlate with ingestion rates until saturation points (Frost, 1972). In addition, prey encounter rates could regulate the ingestion rates, thus showing a positive relationship between prey-to-predator ratios and feeding rates. However, Glibert et al. (2009) did not observe saturating responses in grazing until the prey:predator ratio (cell:cell) was 226:1. In this study, although the actual densities of prey and grazer were significantly different from Glibert et al. (2009), saturation responses were not observed up to 243:1 of prey-to-predator ratio (cell:cell) (Table 6.2), showing a linear relationship (R^2= 0.75, Eq.(1)). These findings suggest that *K. brevis* has greater ability to graze on *Synechococcus* possibly because of the small cell size of these picocyanobacterial (estimated spherical diameter [ESD] = ~ 1 μm).

Warming shifts *Karenia brevis* towards more phago-heterotrophic in a short-term

Several studies have revealed that mixotrophs became more heterotrophic with rising temperatures. Wilken et al. (2013) exhibited that grazing rates on bacterial prey by the mixotrophic chrysophyte *Ochromonas* sp. and showed that rates increased more

with temperature (13 – 33°C) than did photosynthetic electron transport rates. Mixotrophic dinoflagellate *Lepidodinium* sp. also showed enhanced ingestion rates on *Rhodomonas salina* with rising temperatures from 25°C, 28°C to 31°C (Liu et al., 2021, 2022). The dinoflagellate *Alexandrium pohangense* and *Gymnodinium smaydae* fed more on *Margalefidium polykrikoides* (15 – 30 °C) and *Heterocapsa rotundata* (10 – 32 °C), respectively, with increasing temperature (Lim et al., 2019; You et al., 2020). Furthermore, Lepori-Bui et al. (2022) found out that mixotrophs that were adapted to 18, 24, and 30°C (> 200 generations) evolved reduced photosynthesis but higher grazing ability with increasing temperature in general.

In this study, grazing responses of *K. brevis* on *Synechococcus* to increasing temperatures were consistent with previous studies even though our experiments were conducted with grazers not acclimated to specific temperatures (Fig. 6.4). However, unlike previous studies, increases in density or growth rates were not generally observed in this study (Fig. 6.3). Specifically, at warmer temperatures, the density tended to decrease more. This was possibly due to the fact that the mixotrophs were experiencing short-term stress when exposed to new environments (e.g., new temperatures). At warmer temperatures, respiration rates would also increase, as predicted by the metabolic theory of ecology; therefore, less energy would directed to synthesizing new biomass (Brown et al., 2004; Allen et al., 2005). In addition, hourly ingestion rates measured in the interval from $\leq T_3$-T_5 were mainly the highest at 24°C (e.g., the ambient temperature), and grazing was not observed in some cases (Table 6.3), implying stress responses of grazers to new environments.

The potential role of *Karenia brevis* grazing in the surface layer on the West Florida Shelf

Karenia brevis are subject to temperature fluctuations due to daylight surface aggregation behavior, and this surface layer might be the area of increased biological activities as well as nutrient cycling (Heil et al., 2014b). The surface layer is typically warmer than deeper depths unless significant upwelling existed. These results demonstrate the increased grazing behavior by *K. brevis* on *Synechococcus, a* ubiquitous picocyanobacteria found in the Gulf of Mexico (Paul et al., 2000; Wawrik et al., 2009), at ambient temperature + 5°C compared to ambient temperature - 5°C. Although no significant differences were found in $rETR_{max}$ values of grazers except in the experiment that lasted the longest (72 h) (Fig. 6.7 and 6.8), photosynthetic rates of prey were strongly regulated by the presence of grazer, especially at warmer temperatures in general (Fig. 6.5 and 6.6).

The undefined nanoflagellates could also contribute to increased grazing at warmer temperatures. They contributed < 0.5 % to ~4% at T_0 samples but increased to ~15% at 24°C and ~34% at 29°C in the final sampling points in one of treaments. Indeed, mixotrophic nanoflagellates are also predicted to be more heterotrophic with rising temperatures (e.g., Lepori-Bui et al., 2022). Nanoflagellates can be prey of *K. brevis* and grazer of *Synechococcus* at the same time, therefore, it is hard to distinguish their contribution to the total grazing. However, even short-term exposure of *K. brevis*-dominated bloom water to warmer temperatures enhanced the grazing pressure on prey.

Chapter 7: Summary and Conclusions

The primary goal of this study was to measure how autotrophic and mixotrophic metabolisms of *Karenia* spp., the toxic dinoflagellate that forms Florida Red Tide almost every year, respond to short-term changes of two major environmental factors, temperature and N forms and availability, using cultured and natural populations of *Karenia* spp. and to provide new physiological data for their parameterization to incorporate into a new mechanistic model of *K. brevis* nested in a hydrodynamic and biogeochemical framework on the WFS.

The cultured *K. mikimotoi*, maintained at 20°C, was exposed to 15, 20, 25, 30°C for 1 h after pulsing the cells with either ^{15}N-NO_3^-, ^{15}N-NH_4^+ or ^{15}N-urea with varying amounts (1, 5, 10, 20, 50 µM-N) (Chapter 2). When temperatures were not stressful, at 15-25°C, the values of fluorescence parameters for all N treatments were comparable. Furthermore, within a given light intensities, photosynthetic yields generally rose with increasing concentrations of all N forms, indicating that cells were dynamically balancing the "push" due to photon flux pressure with consumption in overall metabolism ("pull" due to demand). However, at 30°C, no such trends were found, and all fluorescence parameters declined significantly, but differential responses were observed: Cells enriched with urea exhibited a smaller decline in fluorescence parameters than cells pulsed with NO_3^- or NH_4^+, implying that urea might induce a photoprotective mechanism by increasing metabolic "pull". The enhanced incorporation of ^{15}N-urea at 30°C partly supports this notion.

The winter *K. brevis* coastal populations from the WFS, when ambient temperature was ~20°C, were exposed to similar treatments as culture experiments to investigate if the natural *Karenia* populations would exhibit similar photosynthetic responses to temperature and N forms (Chapter 3). Winter sampling (January 2021) was conducted during the early phase of 2020-2021 prolonged *K. brevis* blooms. Although the decline in fluorescence parameters due to thermal stress at 30°C was much less than culture work, the values of fluorescence parameters generally declined from 15°C to 30°C in controls, and those enriched with 10 µM-N of NO_3^- or NH_4^+ but not in cells enriched with urea.

Additional samplings were conducted during January 2021 in addition to coastal stations (winter populations) and during July 2021 (summer populations), and the rates of photosynthesis and N uptake of winter and summer populations in response to manipulations of temperature (15, 20, 25, 30°C or 15, 25, 30, 33°C) and N forms (^{15}N-NO_3^-, ^{15}N-NH_4^+, ^{15}N-urea) and amounts (0 – 50 µM-N) were compared (Chapter 4). The winter and summer populations showed different thermal preferences of photosynthesis at the same temperature, showing a capacity for thermal acclimation. Although bloom biomass was remarkably higher in summer blooms, they were stressed photosynthetically (e.g., lower $rETR_{max}$) and nutritionally (e.g., lower N uptake rates). When the summer cells were treated with urea, however, N uptake rates and total C and N $cell^{-1}$ were relatively higher than with the other N substrates, especially in warmer waters, showing differential thermal responses depending on N forms of this species.

The grazing ability of *K. brevis* on *Synechococcus* of different quantities and quality and *Rhodomonas* and how such grazing affects the predator and prey photophysiological responses were investigated (Chapter 5). In addition, cellular incorporation of ^{15}N-labeled *Synechococcus* into single *K. brevis* cells was confirmed by NanoSIMS analysis. No consistent patterns were observed in ingestion rates based on the different quality of *Synechococcus*, but ingestion rates were a function of prey-to-grazer ratios (R^2=0.76) as well as prey abundance (R^2=0.71) across all treatments. In addition, it was demonstrated that *K. brevis* could graze on *Rhodomonas*, implying that the spectrum of *K. brevis*' prey could be broader than previously thought. Furthermore, the growth and density-promoting effects of feeding on prey under higher inorganic nutrient availability conditions indicate the synergistic effects of phago-mixotrophy as a nutrient source.

Motivated by the metabolic theory of ecology, short-term thermal regulation of grazing and photosynthetic performance by natural *Karenia brevis* populations on *Synechococcus* was investigated (Chapter 6). The bloom waters of *Karenia brevis* were collected during the fall of 2022, and cultured *Synechococcus* were provided as prey. The treatments were incubated at ambient (24°C) and ambient temperature ± 5°C (19, 29°C). Ingestion rates were significantly regulated by the prey-to-grazer ratios ($p < 0.01$) and by temperatures ($p < 0.05$) to a lesser degree (R^2= 0.75). At each treatment, generally, the grazing coefficients (g), clearance rates, and ingestion rates were higher in warmer waters. In addition, the grazer effects on the photosynthetic performance of *Synechococcus* were higher in warmer temperatures, decreasing $rETR_{max}$ of *Synechococcus* more. These results suggest that grazing on

Synechococcus could directly regulate the density of *Synechococcus* populations but also indirectly reduce the photosynthetic performance of prey, especially at warmer temperatures.

This dissertation has demonstrated that increasing temperature effects on the metabolism of *Karenia* spp. are not linear due to complex mechanisms. The initial hypothesis, increasing temperature will enhance the metabolic rates (nutrient uptake, photosynthesis, mixotrophy, growth) of the dinoflagellate *Karenia* spp. and will do so to a greater extent with chemically reduced nitrogen and with heterotrophic process than autotrophic process, was largely born out through several laboratory and field experiments. However, the temperature and prey effects on the growth of *K. brevis* were not apparent in short-term experiments except when both prey and inorganic nutrients were available. The selective feeding on prey with different quality was not observed when tested with *Synechococcus*. In addition, the contribution of photosynthesis did not vary with temperature or presence of prey under the experimental setting of this dissertation. Therefore, future studies might consider

1) Longer-term effects of temperature on *Karenia* spp. to quantify better the relative contributions of photo-autotrophy and phago-mixotrophy as well as their impacts on the growth of this species to understand the fates of *Karenia* blooms under projected climate change conditions.
2) Optimal prey size and prey range of *Karenia* spp. to identify and quantify additional nutrient sources supporting *Karenia* blooms on the WFS. NanoSIMS analysis with potential prey would help distinguish if the prey was mainly grazed or disappeared due to other factors, such as allelopathy.

3) Effects of the nutritional history of prey on mixotrophy of *Karenia* spp. with larger cells than picoplankton as prey (e.g., *Rhodomonas*). Different qualify of prey might induce selective feeding and differences in the photophysiology of grazers.

References

Ahn, S.H., Glibert, P.M. (2022) Shining Light on photosynthesis in the harmful dinoflagellate *Karenia mikimotoi*-Responses to short-term changes in temperature, nitrogen form, and availability. Phycology 2:30-44.

Ahn, S.H., Glibert, P.M., Heil, C.A. (2022) Dynamic photo-physiological responses of the dinoflagellate *Karenia brevis* to short-term changes in temperature and nitrogen substrates, In: Band-Schmidt, C.J. and Rodríguez-Gómez, C.F. (eds.) (2022) Proceedings of the 19th International Conference on Harmful Algae, La Paz, B.C.S., Mexico. International Society for the Study of Harmful Algal Blooms. pp.52-57.

Aldrich, D.V. (1960) Physiology of the Florida red tide organism. In: Rounsefell, G.A., Skud, B.E. (eds.), Galveston Biology Fishery Research for the Year Ending June 30, 1960. U.S. Fish and Wildlife Service, Washington, DC, pp. 40-42.

Allen, A.E., Dupont, C.L., Oborník, M., Aleš, H., Adriano, N.-N., John, P.M., Zheng, H., Johnson, D.A., Hu, H., Fernie, A.R., Bowler, C. (2011) Evolution and metabolic significance of the urea cycle in photosynthetic diatoms. Nature 473:203-207.

Allen, A.P., Gillooly, J.F., Brown, J.H. (2005) Linking the global carbon cycle to individual metabolism. Funct. Ecol. 19:202-213.

Arar, E.J., Collins, G.B. (1997) *In vitro* Determination of chlorophyll *a* and phaeophytin *a* in marine and freshwater algae by fluorescence. Method 445, National Exposure Research Laboratory, EPA. Cincinnati, OH.

Beck, M.W., Altieri, A., Angelini, C., Burke, M.C., Chen, J., Chin, D.W., Gardiner, J., Hu, C., Hubbard, K.A., Liu, Y., Lopez, C., Medina, M., Morrison, E., Phlips, E.J., Raulerson, G.E., Scolaro, S., Sherwood, E.T., Tomasko, D., Weisberg, R.H., Whalen, J. (2022) Initial estuarine response to inorganic nutrient inputs from a legacy mining facility adjacent to Tampa Bay, Florida. Mar. Pollut. Bull. 178:113598.

Brand, L.E., Campbell, L., Brensnan, E. (2012) *Karenia*: The biology and ecology of a toxic genus. Harmful Algae 14:156-178

Brand, L.E., Compton, A. (2007) Long-term increase in *Karenia brevis* abundance along the Southwest Florida Coast. Harmful Algae 6:232-252.

Brawley, S.H., Johnson, L.E. (1992) Gemetogenesis, gametes and zygotes: An ecological perspective on sexual reproduction in the algae. Br. Phycol. J. 27(3): 233-253.

Bronk, D. A., Killberg-Thoreson, L., Sipler, R. E., Mullholland, M. R., Roberts, Q. N., Bernhardt, P. W., Garrett, M., O'Neil, J. M., Heil, C. A. (2014) Nitrogen uptake and regeneration (ammonium regeneration, nitrification and photoproduction) in waters of the West Florida Shelf prone to blooms of *Karenia brevis*. Harmful Algae 38:50-62

Brown, J.H., Gillooly, J.F., Allen, A.P. Savage, V.M., West, G.B. (2004) Toward a metabolic theory of ecology. Ecology 85:1771-1789.

Burkholder, J.M., Glibert, P.M., Skelton, H.M. (2008) Mixotrophy, a major mode of nutrition for harmful algal species in eutrophic waters. Harmful Algae 8:77-93.

Caron, D.A., Porter, K.G., Sanders, R.W. (1990) Carbon, nitrogen, and phosphorus budgets for the mixotrophic phytoflagellate *Poterioochromonas malhamensis* (Chrysophyceae) during bacterial ingestion. Limnol. Oceanogr. 35(2):433-443.

Chen, Y., Li, M., Glibert, P.M., Heil, C. (2023) Mu*r*Ky waters: Modeling the succession from *r* to K strategists (diatoms to dinoflagellates) following a nutrient spill from a mining facility in Florida. Limnol. Oceanogr.

Clayton, J.R., Ahmed, S.I. (1968) Detection of glutamate synthase (GOGAT) activity in phytoplankton: Evaluation of cofactors and assay optimization. Mar. Ecol. Prog. Ser. 32:115–122.

Corcoran, A.A., Richardson, B., Flewlling, L.J. (2014) Effects of nutrient-limiting supply ratios on toxin content of *Karenia brevis* grown in continuous culture. Harmful Algae 39:334-341.

Cuadrado, A., Bustons, A.D., Figueroa, R.I. (2019) Chromosomal markers in the genus *Karenia*: Towards an understanding of the evolution of the chromosomes, life cycle patterns and phylogenetic relationships in dinoflagellates. Sci. Rep. 9:3072

Dagenais-Bellefeuille, S., Morse, D. (2013) Putting N in dinoflagellates. Front. Microbiol. 4:369.

Dai, A.Q., Shi, X.Y., Ding, Y.Y., Tang, H.J., Wang, L.S., Wang, X.L. (2014) Effects of temperature on the growth and nitrate reductase activity of *Chaetoceros curvisetus* and *Karenia mikimotoi*. Prog. Biochem. Biophys. 41:896–9003.

Dekas, A.E., Parada, A.E., Mayali, X., Fuhrman, J.A., Wollard, J., Weber, P.K., Pett-Ridge, J. (2019) Characterizing chemoautotrophy and heterotrophy in marine archaea and bacteria with single-cell multi-isotope NanoSIP. Front. Microbiol. 10:2682.

Duan, S., Banger, K., Toor, G.S. (2021) Evidence of phosphate mining and agriculture influence on concentrations, forms, and ratios of nitrogen and phosphorus in a Florida River. Water 13(8):1074.

Eppley, R.W. (1972) Temperature and phytoplankton growth in the sea. Fish. Bull. 70:1063–1085.

Fan, C., Glibert, P.M., Alexander, J., Lomas, M.W. (2003) Characterization of urease activity in the three marine phytoplankton species, *Aureococcus anophagefferens, Prorocentrum minimum*, and *Thalassiosira weissflogii.* Mar. Biol. 142:949-958.

Frost, B.W. (1972) Effects of size and concentration of food particles on the feeding behavior of the marine planktonic copepod. Limnol. Oceanogr. 17(6):805-815.

Gao, Y., Smith, G.J., Alberte, R.S. (1983) Nitrate reductase from the marine diatom *Skeletonema costatum* (biochemical and immunological characterization). Plant Physiol. 103:1437-1445.

Garcia, N.S., Bonachela, J.A., Martiny, A.C. (2016) Interactions between growth-dependent changes in cell size, nutrient supply and cellular elemental stoichiometry of marine *Synechococcus*. The ISME J. 10:2715-2724.

Gentien, P. (1998) Bloom dynamics and ecophysiology of the *Gymnodinium mikimotoi* species complex. In: Anderson, D.M., Cembella, A.D., Gustaaf M.H. (eds.) Physiological Ecology of Harmful Algal Blooms, Springer, Berlin, pp.155-173.

Genty, B., Briantais, J., Baker, N.R. (1989) The relationship between the quantum yield of photosynthetic electron transport and quenching of chlorophyll fluorescence. Biochim. Biophys. Acta 990:87-92.

Glibert, P.M., Burkholder, J.M., Kana, T.M., Alexander, J., Skelton, H., Shilling, C. (2009) Grazing by *Karenia brevis* on *Synechococcus* enhances its growth rate and may help to sustain bloom. Aquat. Microb. Ecol. 55:17-30.

Glibert, P.M., Capone, D.G. (1993) Mineralization and assimilation in aquatic, sediment, and wetland systems. In: Knowles, R., Blackburn, T.H. (eds.) Nitrogen isotope techniques. Academic Press, pp.243-272.

Glibert, P.M., Harrison, J., Heil, C., Seitzinger, S. (2006) Escalating worldwide use of urea—A global change contributing to coastal eutrophication. Biogeochemistry 77:441-463.

Glibert, P.M., Middelburg, J.J., McClelland, J.W., Zanden, M.J.V. (2019) Stable isotope tracers: Enriching our perspectives and questions on sources, fates, rates, and pathways of major elements in aquatic systems. Limnol. Oceanogr. 64:950–981.

Glibert, P.M., Wilkerson, F.P., Dugdale, R.C., Raven, J.A., Dupont, C.L., Leavittm, P.R., Parker, A.E., Burkholder, J.M., Kana, T.M. (2016) Pluses and minuses of ammonium and nitrate uptake and assimilation by phytoplankton and implications for productivity and community composition, with emphasis on nitrogen-enriched conditions. Limnol. Oceanogr. 61:165-197.

Guillard, R.R. (1975) Culture of phytoplankton for feeding marine invertebrates. In: Smith, W.L., Chanley, M.H., (eds.) Culture of Marine Invertebrate Animals, Plenum Press: New York, NY, USA, pp.29–60.

Guillard, R.R.L., Hargraves, P.E. (1993) *Stichochrysisimmobilis* is a diatom, not a chrysophyte, Phycologia 32:234-236.

Haywood, A.J. Steidinger, K.A. Truby, E.W. Bergquist, P.R. Bergquist, P.L. Adamson, J. MacKenzie, L. (2004) Comparative morphology and molecular phylogenetic analysis of three new species of the genus *Karenia* (Dinophyceae) from New Zealand. J. Phycol. 40:165–179.

Heil, C.A., Amin, S.A., Glibert, P.M., Hubbard, K.A., Li, M., Martínez, J.M., Weisberg, R., Liu, Y., Sun, Y., (2022) Termination patterns of *Karenia brevis* blooms in the eastern Gulf of Mexico. In: Band-Schmidt, C.J. and Rodríguez-Gómez, C.F. (eds.). Proceedings of the 19th International Conference on Harmful Algae, La Paz, B.C.S., Mexico. International Society for the Study of Harmful Algal Blooms. pp.365.

Heil, C.A., Bronk, D.A., Mulholland, M.R., O'Neil, J.M., Bernhardt, P.W., Mursako, S., Havens, J.A., Vargo, G.A. (2014b) Influence of daylight surface aggregation behavior on nutrient cycling during a *Karenia brevis* (Davis) G. Hansen & Ø. Moestrup bloom: Migration to the surface as a nutrient acquisition strategy. Harmful Algae 38:86–94.

Heil, C.A., Dixon, L.K., Hall, E., Garrett, M., Lenes, J.M., O'Neil, J.M., Walsh, B.M., Bronk, D.A., Killberg-Thoreson, L., Hitchcock, G.L., Meyer, K.A., Mulholland, M.R., Procise, L., Kirkpatrick, G.J., Walsh, J.J., Weisberg, R.W. (2014a) Blooms of *Karenia brevis* (Davis) G. Hansen & Ø. Moestrup on the West Florida Shelf: Nutrient sources and potential management strategies based on a multi-year regional study. Harmful Algae 38:127-140.

Heil, C.A., Kerkhof, L.J., Schofield, O.M. (2013) *Trichodesmium*-derived dissolved organic matter is a source of nitrogen capable of supporting the growth of toxic red tide *Karenia brevis*. Mar. Ecol. Prog. Ser. 483:31-45

Heil, C.A., Mulholland, M.R., Bronk, D.A., Bernhardt, P., O'Neil., J.M. (2004). Bacterial and size fractionated primary production within a large *Karenia brevis* bloom on the west Florida shelf. In: Steidinger, K.A., Landsberg, J.H., Tomas, C.R., Vargo G.A. (eds.), Harmful Algae 2002. Florida Fish and Wildlife Conservation Commission, Florida Institute of Oceanography and Intergovernmental Oceanographic Commission of UNESCO, St. Petersberg, Florida, USA. pp.38-40.

Heil, C.A., Revilla, M., Glibert, P.M., Murasko, S. (2007) Nutrient quality drives differential phytoplankton community composition on the southwest Florida Shelf. Limnol. Oceanogr. 52(3):1067-1078.

Heinbokel, J.F. (1978) Studies on the functional role of Tintinnids in the Southern California Bight. I. Grazing and growth rates in laboratory cultures. Mar. Biol. 47:177-189.

Heisler, J., Glibert, P.M., Burkholder, J.M., Anderson, D.M., Cochlan, W., Dennison, W.C., Dortch, Q., Gobler, C.J., Heil, C.A., Humphries, E., Lewitus, A., Magnien, R., Marshall, H.G., Sellner, K., Stockwell, D.A., Stoecker, D.K., Suddleson, M. (2008) Eutrophication and harmful algal blooms: A scientific consensus. Harmful Algae 8:3-13.

Hendrickson, L., Furbank, R.T., Chow, W.S. (2004) A simple alternative approach to assessing the fate of absorbed light energy using chlorophyll fluorescence. Photosynth. Res. 82:73-81.

Hikosaka, K., Ishikawa, K., Borjigidal, A., Muller, O., Onoda, Y. (2006) Temperature acclimation of photosynthesis: Mechanisms involved in the changes in temperature dependence of photosynthetic rate. J. Exp. Bot. 57:291–302.

Holm-Hansen, O., Lorenzen, C.J., Holmes, R.W., Strickland, J.D.H. (1965) Fluorometric determination of Chlorophyll. ICES J. Mar. Sci. 30(1):3-15.

Huang, K., Feng, Q., Zhang, Y., Ou, L., Cen, J., Lu, S., Qi, Y. (2020) Comparative uptake and assimilation of nitrate, ammonium, and urea by dinoflagellate *Karenia mikimotoi* and diatom *Skeletonema costatum* s.l. in the coastal waters of the East China Sea. Mar. Pollut. Bull. 155:111200.

Jeong, H.J., Park, J.Y., Nho, J.H., Park, M.O., Ha, J.H., Seong, K.A., Jeng, C., Seong, C.N., Lee, K.Y., Yih, W.H. (2005) Feeding by red-tide dinoflagellates on the cyanobacterium *Synechococcus*. Aquat. Microb. Ecol. 41:131-143.

Johnson, M.D. (2015) Inducible mixotrophy in the dinoflagellate *Prorocentrum minimum*. J. Eukaryot. Microbiol. 62:431-443.

Kamiyama, T., Arima, S. (2001) Feeding characteristics of two tintinnid ciliate species on phytoplankton including harmful species: effects of prey size on ingestion rates and selectivity. J. Exp. Mar. Biol. Ecol. 257: 281-296.

Kana, T.M., Geider, R.J., Critchley, C. (1997) Regulation of photosynthetic pigments in micro-algae by multiple environmental factors: A dynamic balance hypothesis. New Phytol. 137:629-638.

Killberg-Thoreson, L., Mulholland, M. R., Heil, C. A., Sanderson, M. P., O'Neil, J. M., Bronk, D. A. (2014) Nitrogen uptake kinetics in field populations and cultured strains of *Kareniabrevis*. Harmful Algae 38:73-85

Klughammer, C., Schreiber, U. (2008) Complementary PS II quantum yields calculated from simple fluorescence parameters measured by PAM fluorometry and the saturation pulse method. PAM Appl Notes 1:27–35

Kramer, D.M. Johnson, G. Kiirats, O. Edwards, G.E. (2004) New fluorescence parameters for the determination of Q_A redox state and excitation energy fluxes. Photosynth. Res.79:209–218.

Kristiansen, S. (1983) The temperature optimum of the nitrate reductase assay for marine phytoplankton. Limnol. Oceanogr. 28(4):776-780.

Kubanek, J., Hicks, M.K., Naar, J., Villareal, T.A. (2005) Does the red tide dinoflagellate *Karenia brevis* use alleopathy to outcompete other phytoplankton? Limnol. Oceanogr. 50(3):883-895

Kusek, K.M., Vargo, G., Steidinger, K. (1999) *Gymnodinium breve* in the field, in the lab, and in the newspaper: A scientific and journalistic analysis of Florida red tides. Contr. Mar. Sci. 34:1-229.

Lenes, J.M., Heil, C.A. (2010) A historical analysis of the potential nutrient supply from the N_2 fixing marine cyanobacterium *Trichodesmium* spp. to *Karenia brevis* blooms in the eastern Gulf of Mexico. J. Plankton Res. 32(10):1421-1431.

Lepori-Bui, M., Paight, C., Eberhard, E., Mertz, C.M., Moeller, H.V. (2022) Evidence for evolutionary adaptation of mixotrophic nanoflagellates to warmer temperatures. Glob. Change. Biol. 28:7094-7107.

Li, A., Stoecker, D.K., Adolf, J.E. (1999) Feeding, pigmentation, photosynthesis and growth of the mixotrophic dinoflagellate *Gyrodinium galatheanum*. Aquat. Microb. Ecol. 19(2):163-176.

Li, X., Yan, T., Yu, R., Zhou, M. (2019) A review of *karenia mikimotoi*: Bloom events, physiology, toxicity and toxic mechanism. Harmful Algae 90:101702.

Lin, C.-H., Accoroni, S., Glibert, P.M. (2017) *Karlodinium veneficum* feeding responses and effects on larvae of the eastern oyster *Crassostrea virginica* under variable nitrogen:phosphorus stoichiometry. Aquat. Microb. Ecol. 79:101-114.

Lin, C.-H., Flynn, K., Glibert, P. M. (2018) Simulating effects of variable stoichiometry and temperature on mixotrophy in the harmful dinoflagellate *Karlodinium veneficum*. Front. Mar. Sci. 5:320.

Lim, A.S., Jeong, H.J., Ok, J.H., You, J.H., Kang, H.C., Kim, S.J. (2019) Effects of light intensity and temperature on growth and ingestion rates of the mixotrophic dinoflagellate *Alexandrium pohangense*. Mar. Biol. 166:98.

Liu, K., Ng, H.Y.-T., Gao, Z., Liu, H. (2022) Selective feeding of a mixotrophic dinoflagellate (*Lepidodinium* sp.) in response to experimental warming and inorganic nutrient imbalance. Front. Microbiol. 13:805306.

Liu, K., Ng, H.Y.-T., Zhang, S., Liu, H. (2021) Effects of temperature on a mixotrophic dinoflagellate (*Lepidodinium* sp.) under different nutritional strategies. Mar. Ecol. Prog. Ser. 678:37-49.

Lomas, M. W., Glibert, P. M. (1999a) Temperature regulation of nitrate uptake: A novel hypothesis about nitrate uptake and reduction in cool-water diatoms. Limnol. Oceanog. 44:556-572.

Lomas, M.W.; Glibert, P.M. (1999b) Interactions between NH_4^+ and NO_3^- uptake and assimilation: Comparison of diatoms and dinoflagellates at several growth temperatures. Mar. Biol. 133:541–551.

Lundgren, V.M., Glibert, P.M., Granéli, E., Vidyarathna, N.K., Fiori, E., Ou, L., Flynn, K.J., Mitra, A., Stoecker, D.K., Hanse, P.J. (2016) Metabolic and physiological changes in *Prymesium parvum* when grown under, and grazing on prey of, variable nitrogen:phosphrous stoichiometry. Harmful Algae 55:1-12.

Magaña, H.A., Villareal, T.A. (2006) The effect of environmental factors on the growth rate of *Karenia brevis* (Davis) G. Hansen and Moestrup. Harmful Algae 5:192-198.

Marañón, E., Lorenzo, M.P., Cermeño, P., Mouriño-Carballido, B. (2018) Nutrient limitation suppresses the temperature dependence of phytoplankton metabolic rates. ISME J.12:1836–1845.

Martín-Cereceda, M., Williams, R.A.J., Novarino, G. (2008) Easy visualization of the protist *Oxyrrhis marina* Grazing on a live fluorescently labelled heterotrophic nanoflagellate. Curr. Microbiol. 57(1):45-50.

Maxwell, K., Johnson, G. (2000) Chlorophyll fluorescence-a practical guide. J. Exp. Bot. 51:659–668.

Morey, J.S., Monroe, E.A., Kinney, A.L., Beal, M., Johnson, J.G., Hitchcock, G.L., Van D., Frances, M. (2011) Transcriptomic response of the red tide dinoflagellate, *Karenia brevis*, to nitrogen and phosphorus depletion and addition. BMC Genomics 12:346.

Morrison, E.S., Phlips E., Badylak, S., Chappel, A.R., Altieri, A.H., Osborne, T.Z., Tomasko, D., Beck, M.W., Sherwood, E. (2023) The response of Tampa Bay to a legacy mining nutrient release in the year following the event. Front. Ecol. Evol. 11:1144778.

Murchie, E.H., Lawson, T. (2013) Chlorophyll fluorescence analysis: A guide to good practice and understanding some new applications. J. Exp. Bot. 64:3983–3998.

Ok, J.H., Jeong, H.J., Lim, A.S., Kang, H.C., You, J.H., Park, S.A., Eom, S.H. (2023) Lack of mixotrophy in three Karenia species and the prey spectrum of *Karenia mikimotoi* (Gymnodiniales, Dinophyceae). Algae 38(1):39-55.

Padfield, D., Yvon-Durocher, G., Buckling, A., Jennings, S., Yvon-Durocher, G. (2015) Rapid evolution of metabolic traits explains thermal adaptation in phytoplankton. Ecol. Lett. 19:133–142.

Paul, J.H., Alfreider, A., Kang, J.B., Stokes, R.A., Griffin, D., Campbell, L., Ornolfsdottir, E. (2000) Form IA *rbcL* transcript associated with a low salinity/high chlorophyll plume ('Green River') in the eastern Gulf of Mexico. Mar. Ecol. Prog. Ser.198:1-8.

Peers, G., Truong, T.B., Ostendorf, E., Busch, A., Elrad, D., Grossman, A.R., Hippler, M., Niyogi, K.K. (2009) An ancient light-harvesting protein is critical for the regulation of algal photosynthesis. Nature 462:518–521.

Perozoni, F., Beghini, G., Cazzaniga, S., Ballottari, M. (2020) *Clamydomonas reinhardtii* LHCSR1 and LHCSR3 proteins involved in photoprotective non-photochemical quenching have different quenching efficiency and different carotenoid affinity. Sci. Rep. 10:21957.

Persson, A., Smith, B.C., Alix, J.H., Li, Y., Holohan, B.A., Wikfors, G.H. (2021) Differences in specific mass density between dinoflagellate life stages and

relevance to accumulation by hydrodynamic process. J. Phycol. 57:1492-1503.

Platt, T., Gallegos, C.L., Harrison, W.G. (1980) Photoinhibition of photosynthesis in natural assemblages of marine phytoplankton. J. Mar. Res. 38:687–701.

Poulin, R.X., Hogan, S., Poulson-Ellestad, K.L., Brown, E., Fernández, F.M., Kubanek, J. (2018) *Karenia brevis* allelopathy compromises the lipidome, membrane integrity, and photosynthesis of competitors. Sci. Rep. 8:9572

Poulson-Ellestad, K, Mcmillan, E., Montoya, J.P., Kubanek, J. (2014) Are offshore phytoplankton susceptible to *Karenia brevis* allelopathy? J. Plankt. Res. 36(5):1344-1356

R Core Team, 2022. R: A language and environment for statistical computing. R Foundation and Statistical Computing, Vienne, Austria. http://www.R-project.org/

Ras, M., Steyer, J., Bernard, O. (2013) Temperature effect on microalgae: A crucial factor for outdoor production. Rev. Environ. Sci. Bio. 12:153-164

Schreiber, U., Bilger, W., Neubauer, C. (1994) Chlorophyll fluorescence as a non-intrusive indicator for rapid assessment of in vivo photosynthesis. In: Schulze, E., Caldwell, M.M., (eds.) Ecophysiology of Photosynthesis, Springer, Berlin/Heidelberg, Germany, pp.49– 70.

Shen, A., Ma, Z., Jiang, K., Li, D. (2016) Effects of temperature on growth, photophysiology, Rubisco gene expression in *Prorocentrum donghaiense* and *Karenia mikimotoi*. Ocean Sci. J. 51:581-589

Shen, A., Yuan, X., Liu, G., Li, D. (2014) Growth interactions between the bloom - forming dinoflagellates *Prorocentrum donghaiense* and *Karenia mikimotoi* under different temperature. Thalassas 30(2):33-45.

Shi, X., Xiao, Y., Liu, L., Xie, Y., Ma, R. (2021) Transcriptome responses of the dinoflagellate *Karenia mikimotoi* driven by nitrogen deficiency. Harmful Algae 103:101977

Sinclair, G., Kamykowski D., Glibert, P. M. (2009) Growth, uptake, and assimilation of ammonium, nitrate, and urea, by three strains of *Karenia brevis* grown under low light. Harmful Algae 8:770-780.

Sipler, R.E., Bronk, D.A., Seitzinger, S.P., Lauck, R.J., McGuinness, L.R., Kirkpatrick, G.J., Heil, C.A., Kerkhof, L.J., Schofield, O.M. (2013) *Trichodesmium*-derived dissolved organic matter is a source of nitrogen capable of supporting the growth of toxic red tide *Karenia brevis*. Mar. Ecol. Prog. Ser. 483:31-45.

Smalley, G.W., Coats, D.W., Stoecker, D.K. (2003) Feeding in the mixotrophic dinoflagellate *Ceratium furca* is influenced by intracellular nutrient concentrations. Mar. Ecol. Prog. Ser. 262:137-151.

Solomon, C.M., Alexander, J.A., Glibert, P.M. (2007) Measuring urease activity in aquatic environmental samples. Limnol. Oceanogr. 5:280-288.

Solomon, C.M., Collier, J.L., Berg, G.M., Glibert, P.M. (2010) Role of urea in microbial metabolism in aquatic systems: a biochemical and molecular review. Aquat. Microb. Ecol. 59:67-88.

Stoecker, D., Hansen, P., Caron, D.A., Mitra, A. (2017) Mixotrophy in the Marine plankton. Annu. Rev. Mar. Sci. 9(1):311-335.

Thomas, M.K., Aranguren-Gassis, M., Kremer, C.T., Gould, M.R., Anderson, K., Klausmeier, C.A., Litchman, E. (2017) Temperature-nutrient interactions exacerbate sensitivity to warming in phytoplankton. Glob. Change. Biol. 23: 3269–3280.

Turley, B.D., Karnauskas, M., Campbell, M.D., Hanisko, D.S. (2022) Relationship between blooms of *Karenia brevis* and hypoxia across the West Florida Shelf. Harmful Algae 114:102223.

Vargo, G.A. (2009) A brief summary of the physiology and ecology of *Karenia brevis* Davis (G. Hansenand Moestrup comb. nov.) red tides on the West Florida Shelf and of hypotheses posed for their initiation, growth, maintenance, and termination. Harmful Algae 8:573-584.

Wawrik, B., Callaghan, A.V. and Bronk, D.A. (2009) Use of inorganic and organic nitrogen by *Synechococcus* spp. and diatoms on the West Florida Shelf as measured using stable isotope probing. Appl. Environ. Microb. 75(21):6662-6670.

Weisberg, R.H., He, R. (2003) Local and deep-ocean forcing contributions to anomalous water properties on the West Florida Shelf. J. Geophys Res. Oceans 108:3184.

Weisberg, R.H., Zheng, L., Liu, Y., Lembke, C., Lenes, J.M., Walsh, J.J. (2014) Why no red tide was observed on the West Florida Continental Shelf in 2010. Harmful Algae 38:119–216.

Wilken, S., Huisman, J., Naus-Wiezer, S., van Donk, E. (2013) Mixotrophic organisms become more heterotrophic with rising temperature. Ecol. Lett. 16:225-233

Wilson, W.B. (1955) Laboratory studies of *Gymnodinium brevis*. Address to American Association for the Advancement of Science, pp.14.

Witt, F.G., Stöhr, C., Ullrich, W.R. (1999) Soluble and membrane-associated nitrate reductase in the dinoflagellate *Peridinium gatunense*. New Phytol. 142:27-34.

You, J.H., Jeong, H.J., Lim, A.S., Ok, J.H., Kang, H.C. (2020) Effects of irradiance and temperature on the growth and feeding of the obligate mixotrophic dinoflagellate *Gymnodinium smaydae*. Mar. Biol. 167:64.

Zhang, F., Li, M., Glibert, P.M., Ahn, S.H. (2021) A three-dimensional mechanistic model of *Prorocentrum minimum* blooms in eutrophic Chesapeake Bay. Sci. Total Environ. 769:144528.

Zhang, Q., Rencheng, Y., Jiangjing, S., Tian, Y., Yunfeng, W., Mingjiang, Z. (2011) Will harmful dinoflagellate *Karenia mikimotoi* grow phagotrophically? Chin. J. Oceanol. Limn. 29:849-859.

Zhang, Q., Song, J., Yu, R., Yan, T., Wang, Y., Kong, F., Zhou, M. (2013) Roles of mixotrophy in blooms of different dinoflagellates: Implications from the growth experiment. Harmful Algae 30:10-26.